n9

MSC-TA-R-67-3

NATIONAL AERONAUTICS AND SPACE ADMINISTRATION

INTERIM REPORT

MANNED SPACE FLIGHT EXPERIMENTS

GEMINI XII MISSION

November, 11-15, 1966

SCIENCE AND APPLICATIONS DIRECTORATE

MANNED SPACECRAFT CENTER

HOUSTON, TEXAS

August 1967

INTERIM REPORT

MANNED SPACEFLIGHT EXPERIMENTS

GEMINI XII MISSION

November, 11 - 15, 1966

Prepared by: Mission and Data Management Office
Science and Applications Directorate

Approved by:

for Wilmot N. Hess
Director
Science and Applications Directorate

NATIONAL AERONAUTICS AND SPACE ADMINISTRATION
Manned Spacecraft Center
Houston, Texas
August 1967

CONTENTS

TABLES

FIGURES

INTERIM REPORT

MANNED SPACE FLIGHT EXPERIMENTS

GEMINI XII MISSION

INTRODUCTION

This compilation of papers constitutes an interim report on the results of manned space flight experiments conducted on the Gemini XII mission. Manned space flight experiments conducted on earlier flights have been published in similar interim reports which are available on request from the Mission and Data Management Office, Science and Applications Directorate, Code TF2, Houston, Texas.

The Gemini Agena Target Vehicle was launched at 2:07:58 p.m. eastern standard time and the Gemini XII spacecraft was launched at 3:46:33 p.m. eastern standard time on November 11, 1966. The splashdown of the spacecraft was at 95 hours 34 minutes 30 seconds ground elapsed time (g.e.t.) on November 15, 1966.

Fourteen scientific or technological experiments were planned for the Gemini XII mission. During the second standup extravehicular activity (EVA), the pilot performed an additional nonscheduled activity — taking ultraviolet photography of predicted dust clouds within the earth's upper atmosphere. Table I lists, in alphanumeric order, the 14 experiments performed and shows the experiment title, sponsoring agency, principal investigator, and qualitative success met during this mission. The actual schedule of experiment operations is shown in table II and was reconstructed from the preflight plans, real-time flight plan, onboard voice tapes, mission notes, crew flight logs, and technical and scientific debriefings.

Preliminary analyses of available photographic and telemetry data indicate that the fundamental objectives were obtained for 11 of the 14 scheduled experiments. The S010 Agena Micrometeorite Collection experiment was opened by the pilot during umbilical EVA; however, it will probably not be retrieved because reentry of the target vehicle is estimated to occur prior to Apollo earth orbital missions. The S029 Libration Regions Photography and S051 Daytime Sodium Cloud experiments were successfully operationally completed. Because of camera malfunctions, the exposures obtained were not of usable quality for scientific analysis.

Each experiment scheduled for the Gemini XII mission is described in the sections that follow. Success or failure of each experiment is so indicated. Detailed analyses and evaluation of the data require more time to reach definitive conclusions. Additional scientific or technological reports will be published as appropriate.

TABLE I.- EXPERIMENTS ON GEMINI XII

Experiment number	Experiment title	Principal Investigator	Sponsor	Data obtained	Completion of planned objectives
D010	Ion-Sensing Attitude Control	Air Force Cambridge Research Laboratory, Hanscom AFB, Massachusetts	Department of the Air Force, Detachment 2, Space Systems Division (AFSC)	Seven periods of useful data	Completed
M405	Triaxis Magnetometer	NASA Manned Spacecraft Center (MSC), Space Sciences Division	NASA/MSC	Data available during all revolutions	Completed
M408	Beta Spectrometer	NASA Manned Spacecraft Center, Space Sciences Division	NASA/MSC	One 5-minute period of useful data	Partial
M409	Bremsstrahlung Spectrometer	NASA Manned Spacecraft Center, Space Sciences Division	NASA/MSC	Data available during all revolutions	Completed
S003	Frog Egg Growth	NASA Ames Research Center, Moffett Field, California	NASA Office of Space Sciences and Applications (OSSA)	Ten frog eggs, five tadpoles	Completed
S005	Synoptic Terrain Photography	NASA Goddard Space Flight Center	NASA/OSSA	160 frames of photographic data	Completed
S006	Synoptic Weather Photography	U.S. Weather Bureau, National Weather Satellite Center	NASA/OSSA	200 frames of photographic data	Completed
S010	Agena Micrometeorite Collection	Dudley Observatory Albany, New York	NASA/OSSA	None	Substantial[a]

[a]Package deployed but probably will not be recovered.

TABLE I.- EXPERIMENTS ON GEMINI XII - Concluded

Experiment number	Experiment title	Principal Investigator	Sponsor	Data obtained	Completion of planned objectives
S011	Airglow Horizon Photography	U.S. Naval Research Laboratory, Washington, D.C.	NASA/OSSA	23 good photographs	Substantial
S012	Micrometeorite Collection	Dudley Observatory, Albany, New York	NASA/OSSA	Data package recovered	Completed
S013	Ultraviolet Astronomical Camera	Dearborn Observatory, Northwestern University	NASA/OSSA	25 frames of film	Substantial
S029	Libration Regions Photography	U.S. Geological Center, Flagstaff, Arizona	NASA/OSSA	Two photographs only (camera malfunction)	Flight operations completed
S051	Daytime Sodium Clouds	CNES-France	NASA/OSSA	None (camera malfunction)	Flight operations completed
T002	Manual Navigation Sightings	NASA Ames Research Center, Moffett Field, California	NASA/OSSA	5 sightings, 13 measurements	Completed
Objects of opportunity (formerly S064)	Ultraviolet Atmospheric Dust Photography	Dudley Observatory Albany, New York	NASA/OSSA	None (camera malfunction)	Flight operations completed

TABLE II.- FINAL EXPERIMENT FLIGHT PLAN FOR GEMINI XII

Experiment title	Priority	Activation time, g.e.t., hr:min	Revolution	Condition	Remarks
D010 Ion-Sensing Attitude Control	1	67:20	42	Mode A	Mode A is equipment extension and activation
		67:48	42	Mode E, photo emission effects	All four temperature parameters stabilized during the mission
		69:30	43	Mode B, roll attitude study	Sensors were used for platform alignment; good results were obtained
		69:55	43	Mode B	No degrading effects caused by thruster firings
		71:20	44	Mode C, pitch attitude study	
		72:20	45	Mode D, yaw attitude study	
		73:20	46	Mode E	
		76:30	47	Mode F, random data accumulation	
		89:40	55	Mode G, translation thruster effects	
		92:49	57/58	Equipment off	
M405 Triaxis Magnetometer	12	4:57	3/4	Boom extended; equipment turned on	Orbits of particular interest were those passing through the South Atlantic Anomaly region
		14:44	9	Equipment off	Sensors performed satisfactorily throughout the mission
		27:05 to 30:15	17 to 19	Equipment on	
		51:07 to 60:30	32 to 37	Equipment on	
		75:00 to 84:45	47 to 52	Equipment on	

TABLE II.- FINAL EXPERIMENT FLIGHT PLAN FOR GEMINI XII - Continued

Experiment title	Priority	Activation time, g.e.t., hr:min	Revolution	Condition	Remarks
M408 Beta Spectrometer	13	Same as M405 5:00 to 5:20 28:50 to 29:10 54:00 to 54:20	 4 18 33	South Atlantic Anomaly passes	Attitude control was provided; data for revolution 4 showed good correlation with M405 data Approximately 5 minutes of useful data were obtained during revolution 4. Equipment failed during remainder of mission.
M409 Bremsstrahlung Spectrometer	14	Same as M405		Sensors on during same periods as M405	Data from revolutions 4, 17, 18, 19, 32, and 33 showed sensors functioned normally Quick-look data showed useful results throughout mission
S003 Frog Egg Growth	2	41:44 85:10 96:00	24 53 End	Unit no. 1 fixed Unit no. 2 fixed Recovery	Frog egg compartment no. 1 was actuated (fixed) by flight crew Temperature stabilized at 72° F during mission Five live tadpoles retrieved
S005 Synoptic Terrain Photography	9	Varied		Targets of opportunity	Approximately 160 useful 70-mm pictures taken; most are of Texas and Mexico
S006 Synoptic Weather Photography	10	Varied		Targets of opportunity	The crew confirmed that weather photographs were taken during stateside passes Jet stream clouds photographed over Red Sea on successive passes Approximately 200 pictures were taken

TABLE II.- FINAL EXPERIMENT FLIGHT PLAN FOR GEMINI XII - Continued

Experiment title	Priority	Activation time, g.e.t., hr:min	Revolution	Condition	Remarks
S010 Agena Micrometeorite Collection	4	43:11	27	Pilot opened S010 hardware during umbilical EVA	S010 package not recoverable due to limited Agena lifetime
S011 Airglow Horizon Photography	6	24:13	15	Red filter used for sunset exposures; red, green and no filter used during night pass	23 of 36 planned photographs were obtained
		25:13	16	Yellow filter used	
		70:45	44	Yellow filter used	
S012 Micrometeorite Collection	3	8:05	5	Opened during crew sleep period by ground commands	Total exposure time was 6 hours 20 minutes. Retrieval was accomplished during the first standup EVA
		14:29	9	Closed from MCC-H	
		20:26	13	First standup EVA	
S013 Ultraviolet Astronomical Camera	5	19:38 to 20:10	12/13	Standup EVA	25 exposures were taken with useful information
		21:13 to 22:00	13/14		Gamma Velorum star field sequence not accomplished
					Sirius ultraviolet spectrum excellent
S029 Libration Regions Photography	7	27:13	18	Anticipated L_5 regions photographed	Six exposures taken during each sequence
		73:45	47	L_5 region photographed	10 of 12 photographs unusable (overexposed)
					Two photographs obtained, both of poor quality

TABLE II.- FINAL EXPERIMENT FLIGHT PLAN FOR GEMINI XII - Concluded

Experiment title	Priority	Activation time, g.e.t., hr:min	Revolution	Condition	Remarks
S051 Daytime Sodium Cloud	8	62:41:48	40	Controlled attitude over Hammaguir, Algeria	A total of 20 frames exposed
		64:16:49	41		All photographs overexposed due to camera malfunction
T002 Manual Navigation Sightings	11	63:06 to 63:45	40	Betelgeuse/Rigel	Approximately 14 measurements obtained on each sequence
		75:15 to 75:43	48	Betelgeuse/Rigel	Both deviation and bias errors below 10 arc seconds
		85:45	54	Betelgeuse/Bellatrix	
		87:15 to 87:40	55	Betelgeuse/Bellatrix	
		88:45 to 89:10	56	Betelgeuse/Rigel	
Objects of Opportunity	None	67:00	42	Photographs of atmospheric dust cloud taken prior to sunrise	42 frames exposed All photographs fogged by static electricity

1. EXPERIMENT D010, ION-SENSING ATTITUDE CONTROL

By R. C. Sagalyn and M. Smiddy
Air Force Cambridge Research Laboratories

SUMMARY

An attitude sensing system using ambient positive ions has been developed and successfully flown on the Gemini XII mission. The outputs of two planar electrostatic analyzers mounted symmetrically about the appropriate axis are combined to directly give pitch and yaw angles. Comparisons of the experiment flight results with those obtained with the onboard inertial guidance system show that the average values over the angular range of $\pm 20^\circ$ for which the ion-sensing system was designed, are in agreement. The results have provided a unique description of the distribution of charged particles in the wake of the spacecraft and supplied information on the motion of the neutral winds and earth's rotation relative to the mean motion of charged particles in the upper atmosphere.

OBJECTIVES

The principal objective of the D010 Ion-Sensing Attitude Control experiment was to investigate the feasibility of an attitude control system using environmental positive ions and an electrostatic detection system to measure spacecraft pitch and yaw. A secondary objective was to measure the spatial and temporal variations of ambient positively charged particles along the orbital path of the Gemini spacecraft.

THEORY

In the altitude range from 100 kilometers to 10 earth radii, positive ions and electrons produced primarily through photoionization by the sun exist in equal concentrations. The number density varies greatly in space and with time; for example, the charge density reaches a maximum of the order of 10^6 particles/cc in the vicinity of the earth's F ionization region maximum at approximately 350 kilometers and decreases to approximately 100 particles/cc at about 10 earth radii. There are also great variations in the number densities on the day and night side of the earth, in the vicinity of the geomagnetic equator, and in the lower ionosphere below approximately 1000 kilometers. Very rapid increases in ion and electron concentrations occur at sunrise due to photoionization an and dissociation of the neutral atmosphere constituents. More gradual decreases in density occur at local sunset when recombination and diffusion become important. This is illustrated in figure 1-1 which gives the results of positive ion measurements obtained with spherical electrostatic analyzers on a Discoverer satellite as a minimum interference experiment. The average energy of the charged particles varies from about 0.01 electron volt at 100 kilometers to approximately 0.4 electron volt at 10 earth radii. The kinetic temperature of the charged particles in the altitude range covered by the Gemini spacecraft varies from approximately 250° Kelvin to about 3000° Kelvin. It has been demonstrated by the authors and other experimenters that the charged particles in the upper atmosphere have an essentially Maxwellian velocity distribution. The average thermal velocity of the particles is then given by the relation

$$v = \left(\frac{8kT}{\pi\ m}\right)^{1/2} \tag{1}$$

where

k = Boltzmann constant

T = temperature in degrees Kelvin

m = mass in grams

v = thermal velocity in centimeters per seconds

When representative values for temperature and mass of the positive ions are substituted in equation (1), positive ion random thermal velocity varies between 0.8 and 1 kilometer per second over the altitude range of the Gemini spacecraft orbit. (Satellites orbiting in the upper ionosphere have varying average velocities depending upon the nature of the orbit. Typical velocities vary between 7 kilometers per second and 11 kilometers per second.) The spacecraft velocity is therefore approximately 10 times greater than the average thermal velocity of the positive ions. Relative to the spacecraft, the positive ions possess negligible velocity. The situation is very different for electrons since their average mass is approximately 10^4 times less than that of the ions. Applying equation (1) the average electron velocity is about 30 times greater than a spacecraft velocity. That positive ions may be considered stationary with respect to the spacecraft velocity is fundamental to the operation on the ion attitude sensing system.

EQUIPMENT

Two planar electrostatic analyzers with a sensor configuration as indicated in figure 1-2 were utilized in this experiment.

When the ratio of the satellite velocity to the random velocity of the ions is greater than or equal to 2 and with grid and collector voltage as indicated in figure 1-2, the current i to the collector of a planar electrostatic analyzer is given by

$$i = ANe\ |V|\ f(v)\ \alpha \qquad (2)$$

where

A = aperture area

N = charged particle density

$f(v)$ = a function of the vehicle potential with respect to the undisturbed plasma

α = experimentally determined transmission factor for the grid electrodes

e = particle charge

Under the experimental conditions discussed, the ions may be considered fixed and the magnitude of the velocity $|V|$ is equal to $v_s \cos\theta$, where v_s is the spacecraft velocity and θ is the angle between the direction of motion of the vehicle and normal to the plane of the sensor. Equation (2) then becomes

$$i = ANev_s \cos\theta\ f(v)\ \alpha \qquad (3)$$

It is seen from equation (3) that the planar sensor current is highly dependent on its orientation with respect to the direction of motion. For example, for the yaw measurement, two identical sensors are alined at 45° with respect to the plane of zero yaw. An identical sensor system, mounted symmetrically about the zero pitch plane, is used for the measurement of pitch angles. These two independent systems are mounted on booms approximately 3 feet in length which are located in the aft section of the spacecraft. They are extended on command by the astronaut at the appropriate time after orbital injection is accomplished. The location of the booms and sensors on Gemini XII spacecraft is shown in figure 1-3. The location of the sensors and the boom lengths are set to minimize the influence of spacecraft wake, contamination, and space charge effects.

The principle of operation of the experiment may be understood by considering first the measurement of pitch. Except for the change in alinement as indicated above, the analysis of the yaw measurement is identical. With two sensors alined symmetrically about the pitch axis as shown in figure 1-2, the current to the collector of each sensor is given by

$$i_1 = Nev_s \alpha A \cos(45 - \theta) \tag{4}$$

$$i_2 = Nev_s \alpha A \cos(45 + \theta) \tag{5}$$

where

i_1 = current to sensor 1

i_2 = current to sensor 2

θ = pitch angle (in degrees)

Solving equations (4) and (5) for θ,

$$\tan\theta = \frac{i_1 - i_2}{i_1 + i_2} \tag{6}$$

For θ less than or equal to 20°, tangent θ is equal to θ in radians.

From equation (6) it is seen that the output of the sensors may be displayed on a meter calibrated directly in degrees, and that changes in charge density N or satellite velocity v_s do not affect the angular measurement.

A block diagram of the pitch or yaw system is shown in figure 1-4. The output of each sensor is amplified by two electrometers. In order to obtain the desired accuracy over the current range 10^{-6} to 10^{-11} amperes, linear amplifiers with range switching covering five current decades are employed. The outputs of the electrometers are then electronically added, subtracted, integrated, and compared. The final output tangent θ, referred to as the compared output, is indicated on a meter in the crew station and transmitted by the telemetry to ground stations.

Sensor system characteristics are as follows for each of the two systems:

Weight (including electronics and sensors), lb	7
Power (at 28 V), watts	3.5
Electronics response time, millisecond.	<1
Dimensions, inch	11 by 6.5 by 6
Angular measurement range, degree	±20

In order to fully evaluate the experimental system, to obtain information on the ambient ion densities and on the distribution of positive ions in the wake of the vehicle, the direct outputs of the electrometers, the range analog indicator, and calibrate monitors are also transmitted through telemetry. These latter outputs would not be required in an operational system. It should be noted that while the D010 experiment was designed for precise pitch and yaw angular measurements over the range $\pm 20^\circ$, there is no basic limitation to the magnitude of the angle to be measured. The required resolution, response time, and so forth, vary with the specific application of the system. A simple engineering modification of the ratio circuits would be involved for varying systems requirements.

PROCEDURES

Six principal modes of operation excluding mode A (Equipment Activation) were requested for the mission and four were accomplished. These were as follows:

(a) Mode B, Roll Attitude Study: This procedure consisted of rolling the spacecraft through 720° at a rate of approximately 3 deg/sec while holding the spacecraft pitch and yaw constant at zero.

(b) Mode C, Pitch Attitude Study: This procedure consisted of maintaining a fixed yaw and roll attitude, then varying the pitch angle through a specified angular range at a rate of approximately 0.1 deg/sec. This rate was specified to insure good comparison of the experiment results with the Inertial Guidance System. The rate of 0.1 deg/sec was determined by the telemetry bandwidth available for the experiment.

(c) Mode D, Yaw Attitude Study: This procedure consisted of maintaining a fixed pitch and roll position, then varying the yaw angle through a specified angular range of 0 to 360° at a rate of approximately 0.1 deg/sec.

(d) Mode E, Photo Emission Effects and Ambient Data Accumulation: The equipment measured effects of the sun on the ion environment. The measurements were scheduled before, during, and after the sunrise phase of the vehicle orbit.

(e) Mode F, Random Data Accumulation: The ion-sensor switch was left in this mode while the spacecraft was in drifting flight.

(f) Mode G, Translation Thruster Effects: The spacecraft OAMS thrusters were fired to observe the degrading effects on the sensors accuracy.

RESULTS

The D010 experiment was initially activated at 67 hours 20 minutes g.e.t. and remained on for approximately 15 hours of which 1 hour was in mode B, approximately 30 minutes in mode C, 30 minutes in mode D, 2 hours in mode E, 8 hours in mode F, and 1 hour in mode G.

The D010 experimental equipment operated extremely well throughout the activation period. Over the angular range for which the ion attitude experiment was designed, both the pitch and yaw measurements on the Gemini XII spacecraft and the inertial guidance results were within the experimental error of both systems. The postflight analysis showed that the pitch angle results agree within $\pm 0.5^\circ$. Comparison of yaw angles over the same angular range indicates an agreement within $\pm 1.5^\circ$. It should be noted that the inertial guidance system has an accuracy in yaw of the order of $\pm 2^\circ$.

An example of the simultaneous measurements of the ion yaw sensor output and the inertial yaw data during a controlled maneuver is shown in figure 1-5. The magnitudes of the angles at given times agree within the errors of the systems. The inertial yaw measurement accuracy for the Gemini spacecraft is approximately $\pm 2^\circ$ and the ion yaw measurement accuracy is $\pm 1/4^\circ$. The inertial data shown illustrate characteristics which introduce difficulties in the manual control of the spacecraft; when the yaw angle is varied, a telemetry lag in the response time of approximately 8 seconds occurs and the steplike variations cause jumps of 1-1/2°. The addition of an ion yaw sensor would then be a significant improvement over existing attitude measurement systems. Also, the fast response of the ion attitude sensing system will be of importance in conserving thruster fuel when precise angular positioning is desired.

During controlled maneuvers on this mission, the ion attitude sensors operated both in forward and in the reverse direction. Ion attitude measurements could therefore be obtained from 0° to 360°. It was anticipated that thruster firings, specifically thrusters 14 and 16, might adversely affect the ion sensors. These thrusters are fired in the direction of either the pitch or yaw sensors. The firings do change the attitude of the vehicle which was confirmed by the inertial results. The firings also change the charge density for a period of 2 seconds. However, the density changes do not affect the angular measurement and no deterioration of the ion sensors is observed.

An example of the variation of positive ion density obtained during a complete spacecraft revolution is illustrated in figure 1-6. The large variations in charge density from 10^3 to 10^6 per cubic centimeter on a given orbit are due largely to changes in photoionization on the night and day side of the earth. The calculations of the charge densities from simultaneous outputs of the electrometers using either the inertial or ion attitude angles are in agreement which is consistent with the Gemini X D010 experiment results.

From the postflight analysis of the experimental results, the dependence of ion angular measurements on latitude was determined. In the case of Gemini XII, the geographic latitude range was approximately ±30°. Any periodic variation in $\Delta\phi$, the difference between the inertial and ion attitude ion measurements, over this latitude range would indicate variations in the mean ion drift motions in the F region, along the spacecraft trajectory. Only angular (pitch or yaw) measurements obtained over the range ±20° were selected for the analysis, at 5° intervals. The results as indicated in figure 1-7 giving latitude vs $\Delta\phi$, do not show a significant dependence on geographic latitude (±30°). The result implies a negligible influence of ion drift motion on latitude over the geographic region investigated. A detailed discussion of the significance of these results is the basis for a separate scientific report.

CONCLUSIONS

The results of the D010 experiment show that it is possible to measure pitch and yaw angles to within a fraction of a degree (based on the results obtained during 45 hours of operation). During this period specific maneuvers were carried out to determine the effects of photo-emission currents, the effect of pitch and roll on yaw maneuvers, the effect of yaw and roll on pitch maneuvers, et cetera. They also demonstrated the degree to which the flight crew could control the motion of the spacecraft. The results showed that the firing of lateral thrusters directly into the sensors did not effect the operation for more than a fraction of a second. The response time of the D010 ion attitude system was found to be much more rapid than the inertial guidance system (milliseconds compared to seconds).

The flight results also showed that the use of the ion attitude sensing system could considerably reduce the time required for special maneuvers, such as docking, maneuvering, photography, and reentry. During Gemini XII, for example, the flight crew was able to reduce the time to aline the inertial platform from 40 minutes to approximately 5 minutes, using the ion pitch and yaw sensors as a reference. The yaw sensing part of the system is particularly valuable because no other instrument exists which can directly give spacecraft yaw. One of the flight crew indicated that he observed a transient in the ion sensor indicator for a fraction of a second when certain thrusters were turned on. This could not be detected in the real-time transmitted data nor in the tape-recorder playback. The latter data are played back at the rate of once per second. A transient could be due to current surges or ground loops in the electrical circuits resulting from varying spacecraft potential or to transients in the power ground lines at the time of firing. Proper filtering could be introduced in future ion attitude systems.

The Gemini results indicate that the use of a horizon detector together with pitch and yaw sensors would give a complete description of the spacecraft position and attitude. Furthermore, with the addition of a servosystem the unit could be used to provide a complete automatic attitude control system. It would be applicable from the lowest satellite altitudes up to at least 10 earth radii. In addition, results showed that by transmitting output voltages from the individual electrometers, the charge density along trajectory of the satellite could be determined. This could be very useful in determining phenomena which occur in manned or unmanned space flights. If a sweep voltage were periodically applied to the appropriate grids of the sensor, the spacecraft potential with respect to the undisturbed environment could be measured. Since spacecraft potential has been of interest in manned space flights, this type of measurement could easily be incorporated. The measurement of spacecraft potential is incorporated in unmanned satellite experiments where the properties of thermal charged particles are studied.

The Gemini D101 results also showed no significant systematic change in the ion drift motion with latitude over the range of $\pm 30^\circ$ (Gemini spacecraft latitudes). This demonstrates that for precision attitude determination, a mean ion drift motion is not needed as a correction to the measurement. The analysis of D010 data is continuing in order to determine other characteristics of the ionosphere and the sensing equipment.

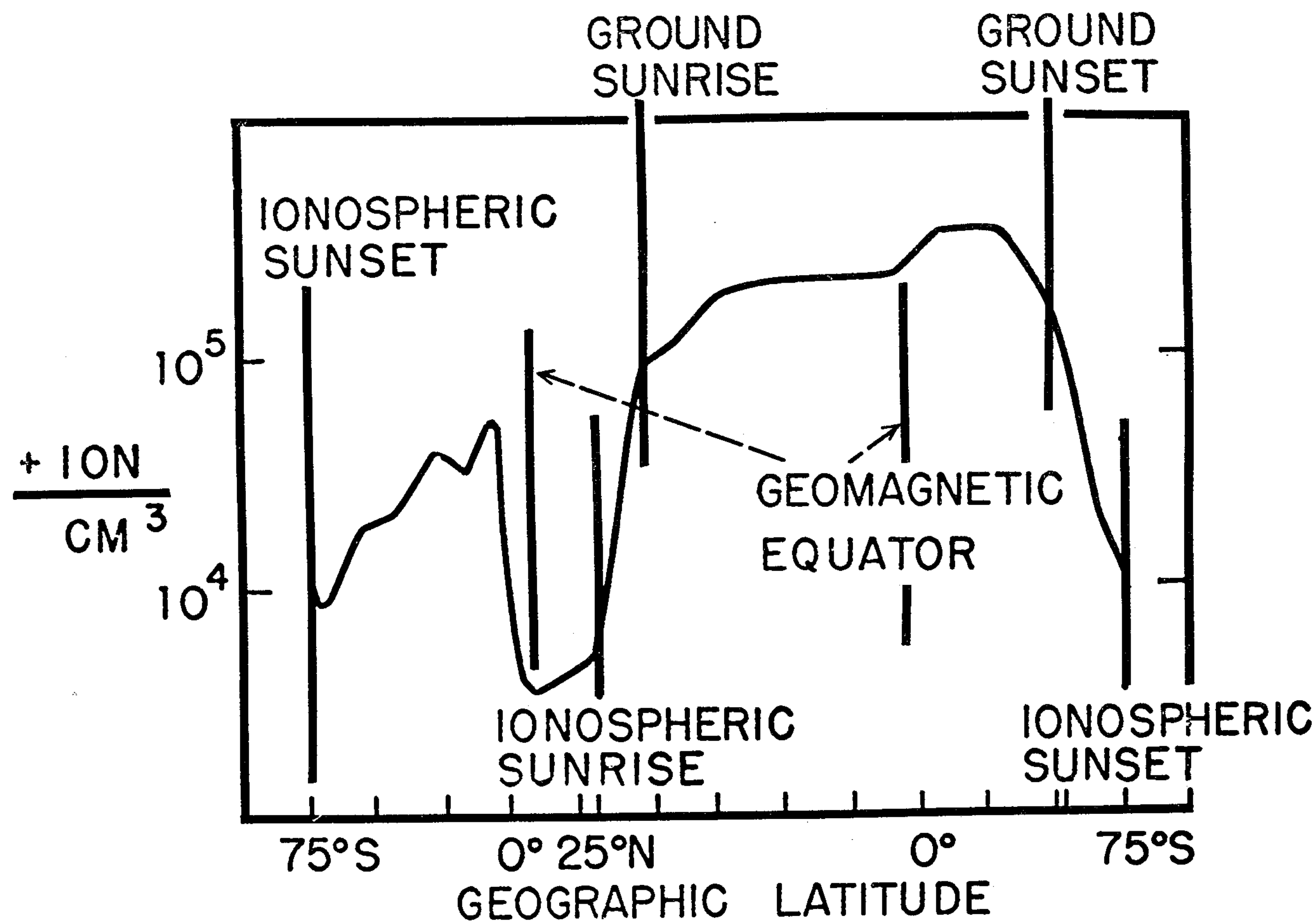

Figure 1-1. - Variation of positive ions in the earth F region during one spacecraft revolution.

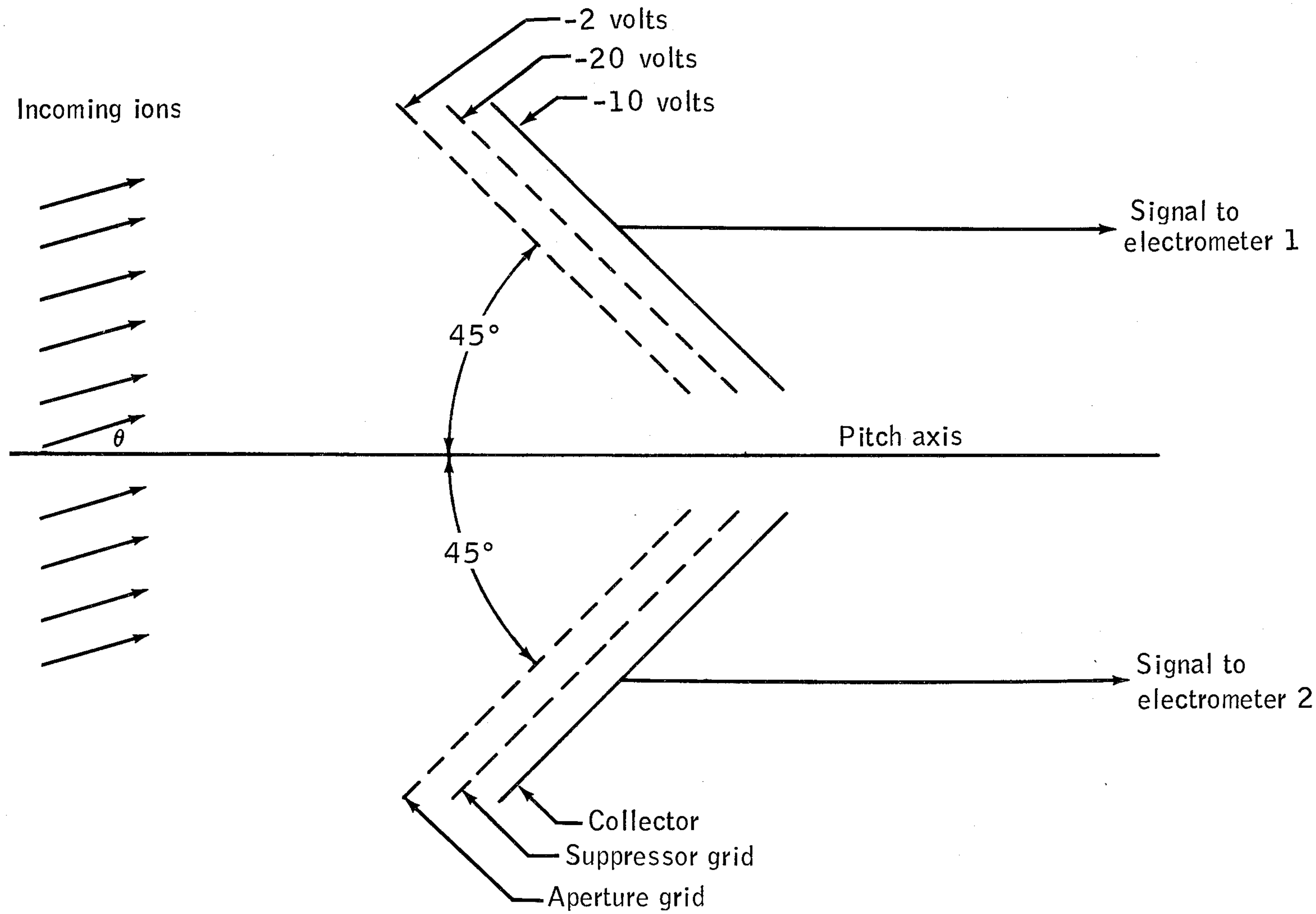

Figure 1-2. - Experiment D010, ion-sensing configuration.

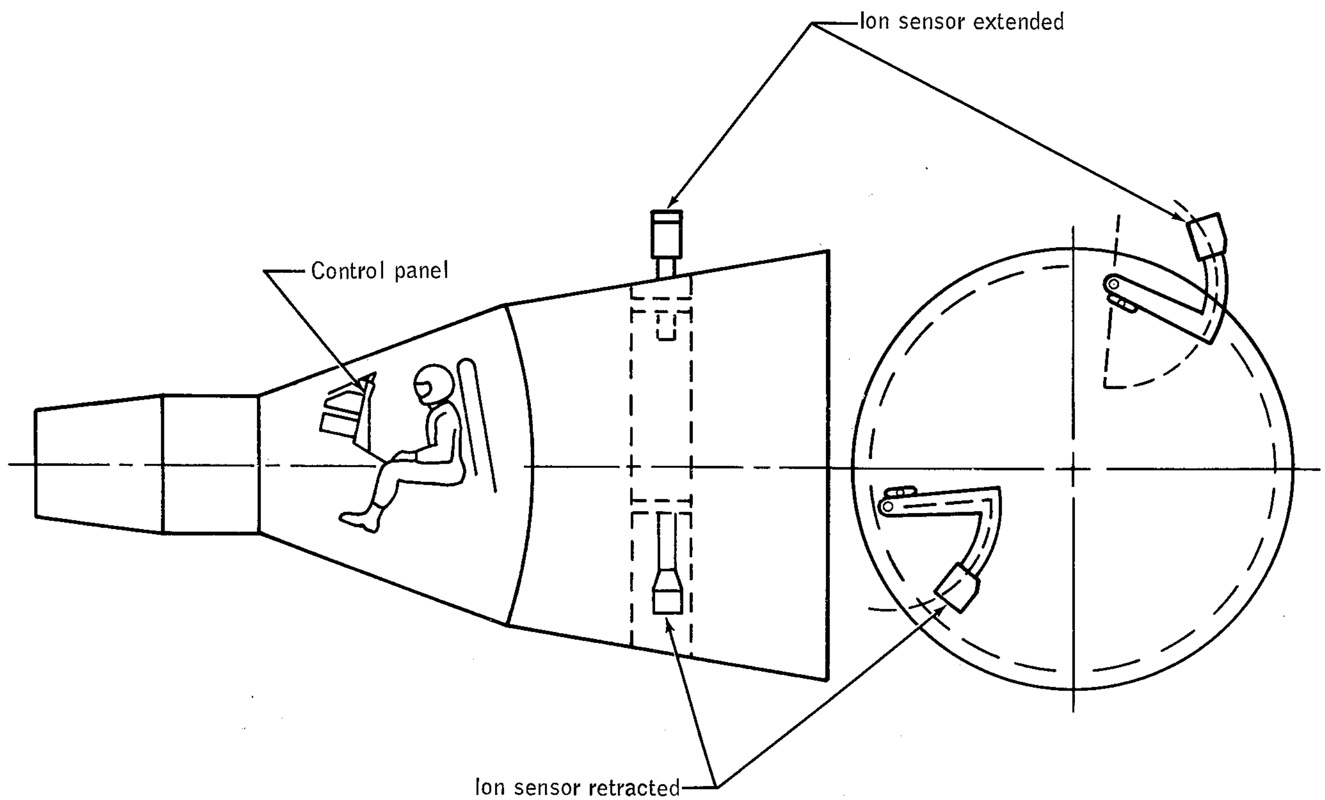

Figure 1-3. - Experiment D010, location of equipment.

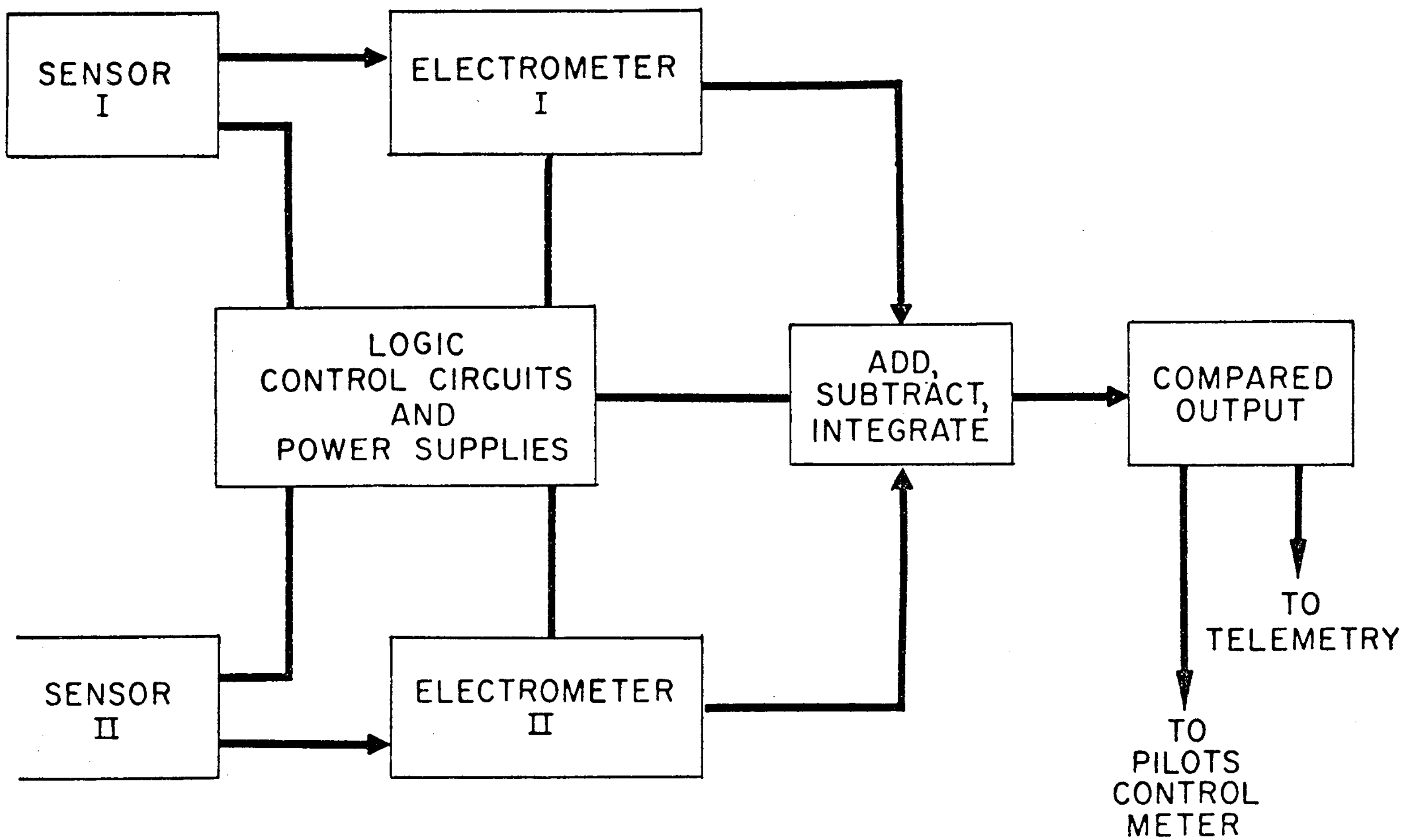

Figure 1-4. - Block diagram of ion yaw/pitch sensing system.

NASA-S-67-302 JAN 6

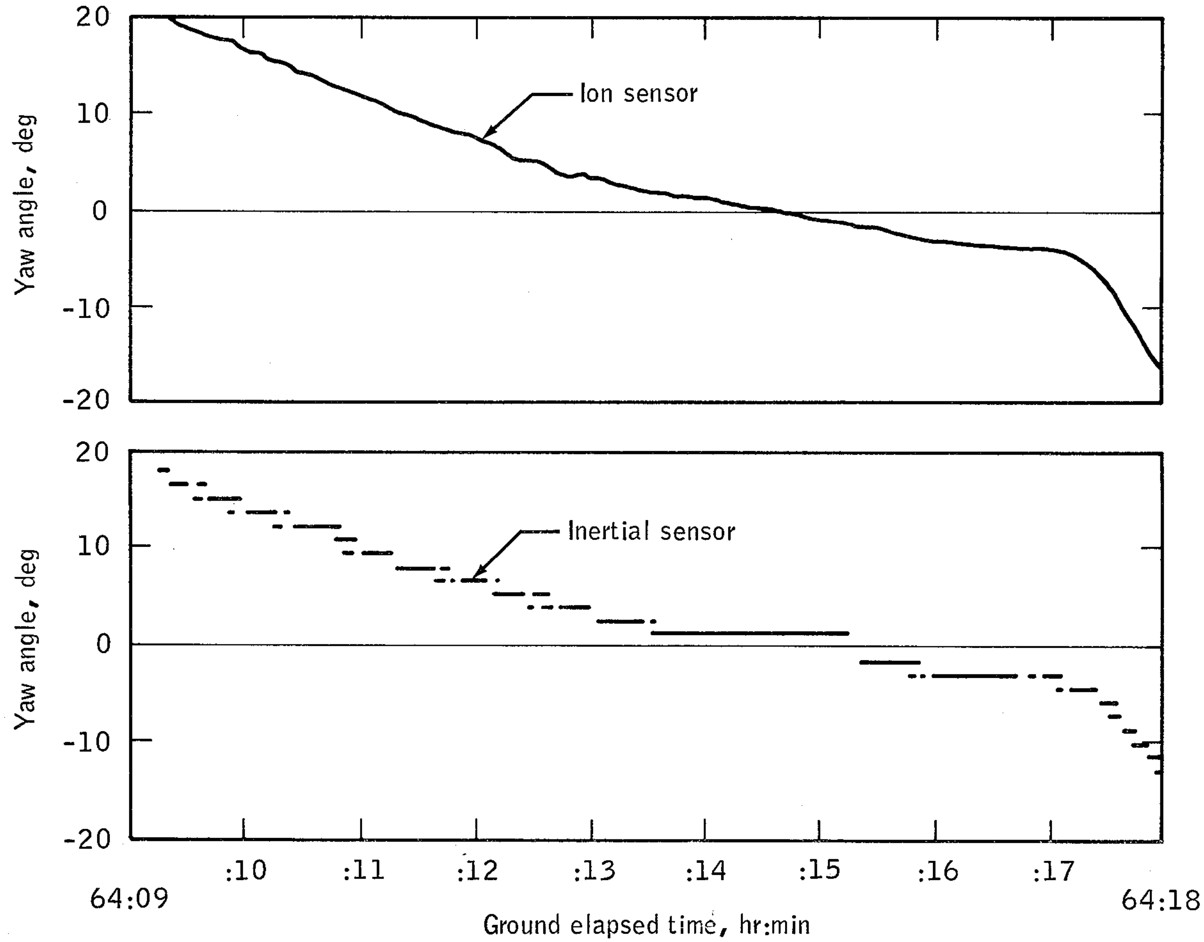

Figure 1-5. - Comparison of spacecraft inertial sensor and D010 ion sensor measurements.

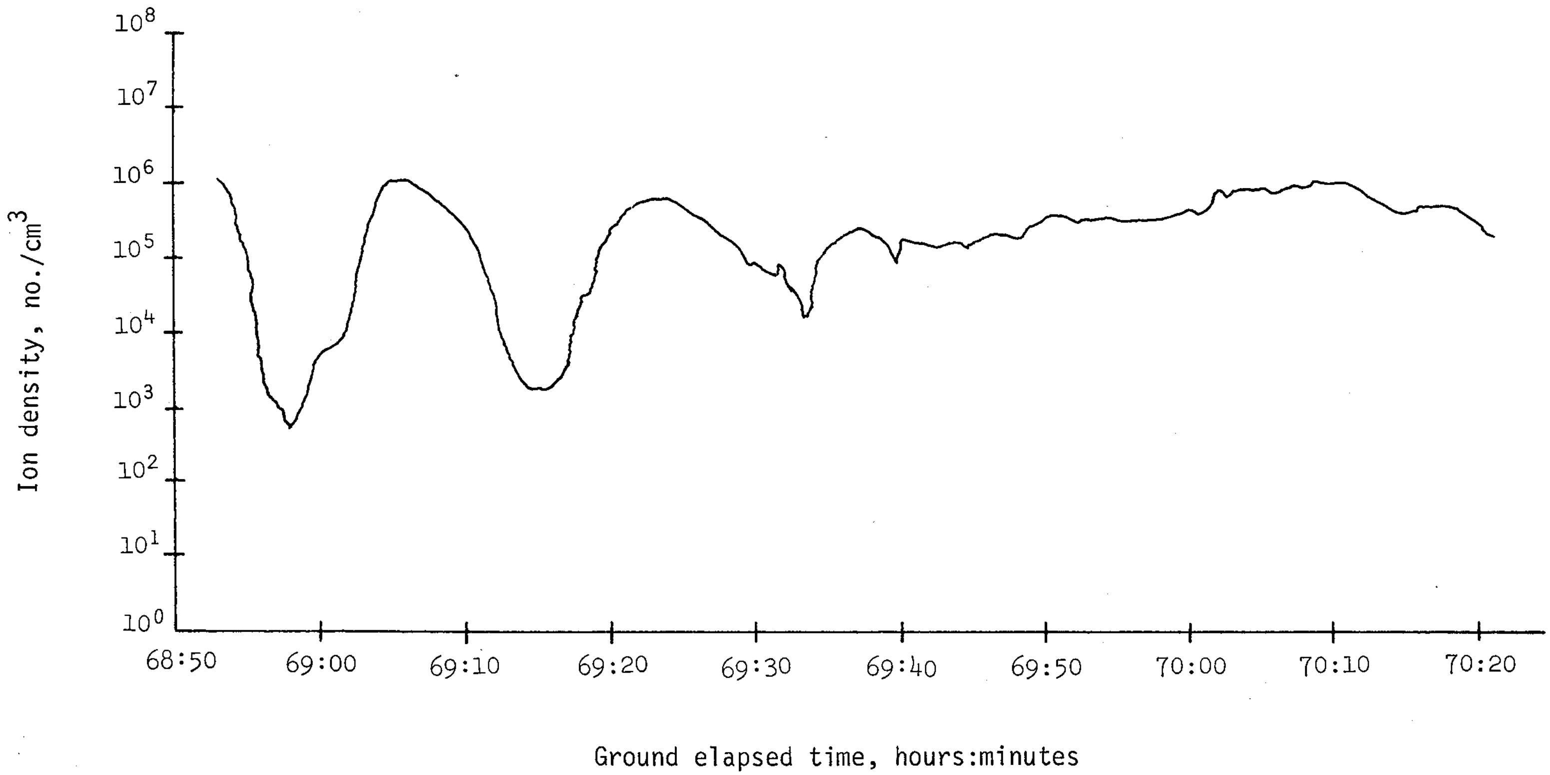

Figure 1-6. - Ion density versus time from launch, one revolution of Gemini XII spacecraft.

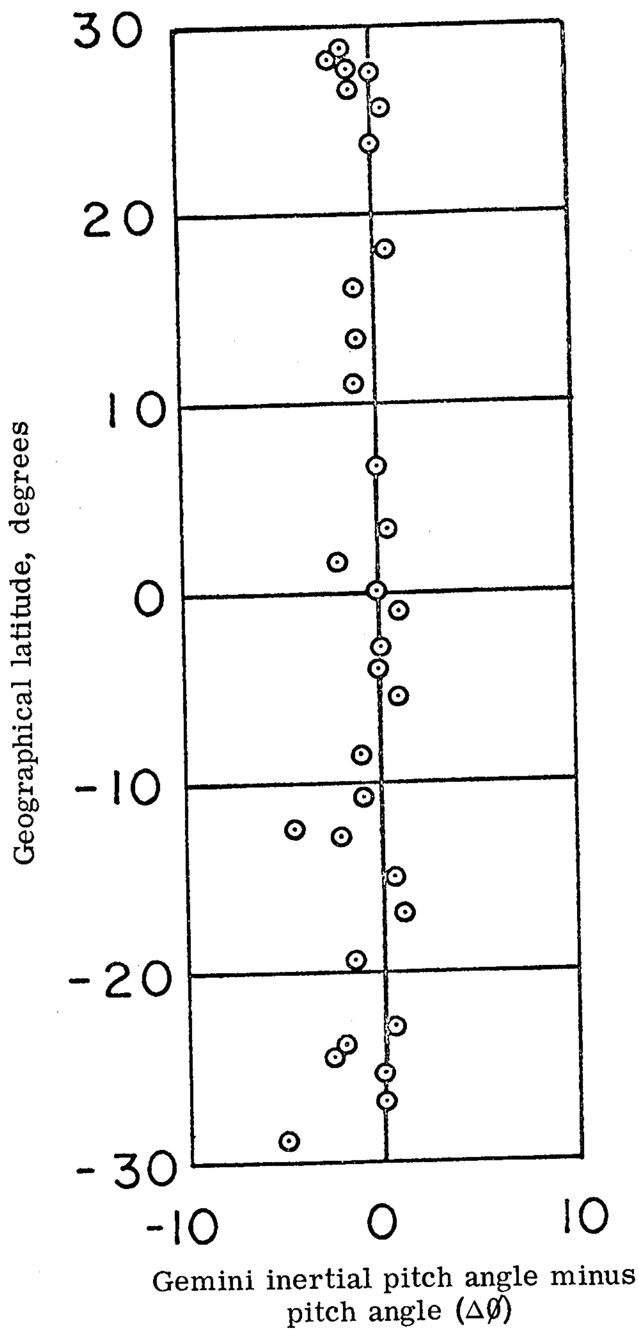

Figure 1-7. - Geographical latitude versus $\Delta\phi$.

2. EXPERIMENT M405, TRIAXIS MAGNETOMETER

By William Dan Womack
NASA Manned Spacecraft Center

SUMMARY

The Triaxis Magnetometer experiment was used to determine the direction and magnitude of the geomagnetic field with respect to the M408 Beta Spectrometer experiment (section 2). The inflight experimental telemetry data indicated that the equipment functioned as designed and provided information throughout the mission.

The magnitudes of the geomagnetic fields measured during the Gemini XII mission compared favorably with the theoretical calculated magnetic field magnitudes.

OBJECTIVE

Knowledge of the magnetic field magnitude and direction is most important for evaluation of charged particle measurements, especially where directional instrumentation is used. Due to the directionality of charged particles with magnetic field lines, the measurement of those particles becomes impossible when employing a directional measuring instrument without determining the direction of the magnetic field line.

The objective of the M405 Triaxis Magnetometer experiment was to determine the magnitude and direction of the earth's geomagnetic field in the South Atlantic Anomaly regions to support the M408 experiment. The M408 experiment used a directional beta spectrometer with a half-angle of 15° flown on Gemini Titan XII (GT-12) spacecraft to determine the flux of charged particles incident on the exterior of the spacecraft.

EQUIPMENT

The experimental equipment consisted of the triaxis magnetometer and an extendible boom.

The triaxis magnetometer was a flux-gate variety which included an electronic package, a sensor unit, and an interconnecting cable (fig. 2-1).

The electronic package contained a dc-to-dc converter and three electronic subassemblies which supplied the necessary sensor-drive voltages, detected and transformed the vector field ac second-harmonic signals, and converted them to a 0- to 5-volt analog dc signal.

The sensor unit contains three identical second-harmonic sensors. Each sensor contains a high permeable core material driven into saturation by a 15-kc signal. When an external field is applied the second harmonic signal on the secondary winding is picked off, filtered, amplified, and converted into an analog voltage.

The three sensor probes are mounted orthogonally in one package to measure vector components H_x, H_y, and H_z of the magnetic field. By measuring the vector components, the direction and total field could be calculated the following equations.

$$H_t = \sqrt{H_x^2 + H_y^2 + H_z^2}$$

$$\Theta_x = \cos^{-1}\left(\frac{H_x}{H_t}\right)$$

$$\Theta_y = \cos^{-1}\left(\frac{H_y}{H_t}\right)$$

$$\Theta_z = \cos^{-1}\left(\frac{H_z}{H_t}\right)$$

where

H_t is the total field; H_x, H_y, and H_z are vector components of the field; and Θ_x, Θ_y, and Θ_z are the component angles measured from their respective axes.

If the location of the sensor unit with respect to the spacecraft is known, the direction of the field with respect to the spacecraft can be calculated.

The boom, spring-loaded and telescopic, extends the sensor unit approximately 42 inches from the spacecraft for attenuating any residual magnetic field produced by electrical cables, instrumentation, or material within the area of the sensor assembly. The boom was fabricated from titanium tubes, loaded with a beryllium-copper spring, and actuated with pyrotechnics during sustainer engine cutoff (SECO).

PROCEDURE

The equipment was turned on by the flight crew at 4:57:33 g.e.t. and was turned off at 14:44:20 g.e.t. It was turned on again at 27:15, 51:6, and 75:5 g.e.t. The total experimental ON time was approximately 32 hours.

The magnetometer and the beta spectrometer were scheduled to operate for at least 10 revolutions while the spacecraft passed over the region bounded approximately by 30° east longitude and 60° west longitude, and by 15° and 55° south latitude. In addition, the equipment was to be operated for a period of at least 15 minutes while the spacecraft was not within this region.

RESULTS

Data obtained from the experiment hardware while passing through the South Atlantic Anomaly were played back by telemetry at the Hawaii tracking station for on-site evaluation in support of the M408 Beta Spectrometer experiment requirements. The data indicated that the equipment functioned as designed and provided information throughout the mission.

The data shown in this portion of the report are not conclusive and are given as an example of the type of data which may be of interest to the scientific community. All computations made on the data to obtain direction of the magnetic field where referenced to the beta spectrometer (experiment M408) only, as described in the purpose of this experiment. Other computation and analysis would have to be made before direction of the magnetic field could be determined with respect to any other portion of the spacecraft or the earth.

An example of data obtained through an anomaly pass is presented in figure 2-2. For a typical pass, these data illustrate relative values of the total beta spectrometer count rate and the angle made with respect to the center line of the spectrometer detector. The figure shows the earth's magnetic field angle alpha in degrees as a function of ground elapsed time. The data shown were measured during a crew sleep period. Analysis is continuing as computer-determined computations become available.

Figure 2-3 represents a pictorial view of the magnitude of the geomagnetic fields as measured during revolution 10 of the Gemini XII mission compared to the theoretical calculated magnetic field magnitude by Dr. C. E. McIlwain's computer codes (ref. 1). The pattern formed by the data points of the measured field can be explained by the random sample rate of the telemetry system and the accuracy of the flight hardware. If the measured field were interpolated to acquire a smooth curve, the comparison of the measured field and theoretical field would agree favorably. The trend illustrated by this figure seems to hold throughout all data which have been analyzed.

REFERENCE

1. McIlwain, Carl E.: Coordinates for Mapping the Distribution of Magnetically Trapped Particles. J. Geophys. Res., vol. 66, no. 11, Nov. 1961, pp. 3681-3691.

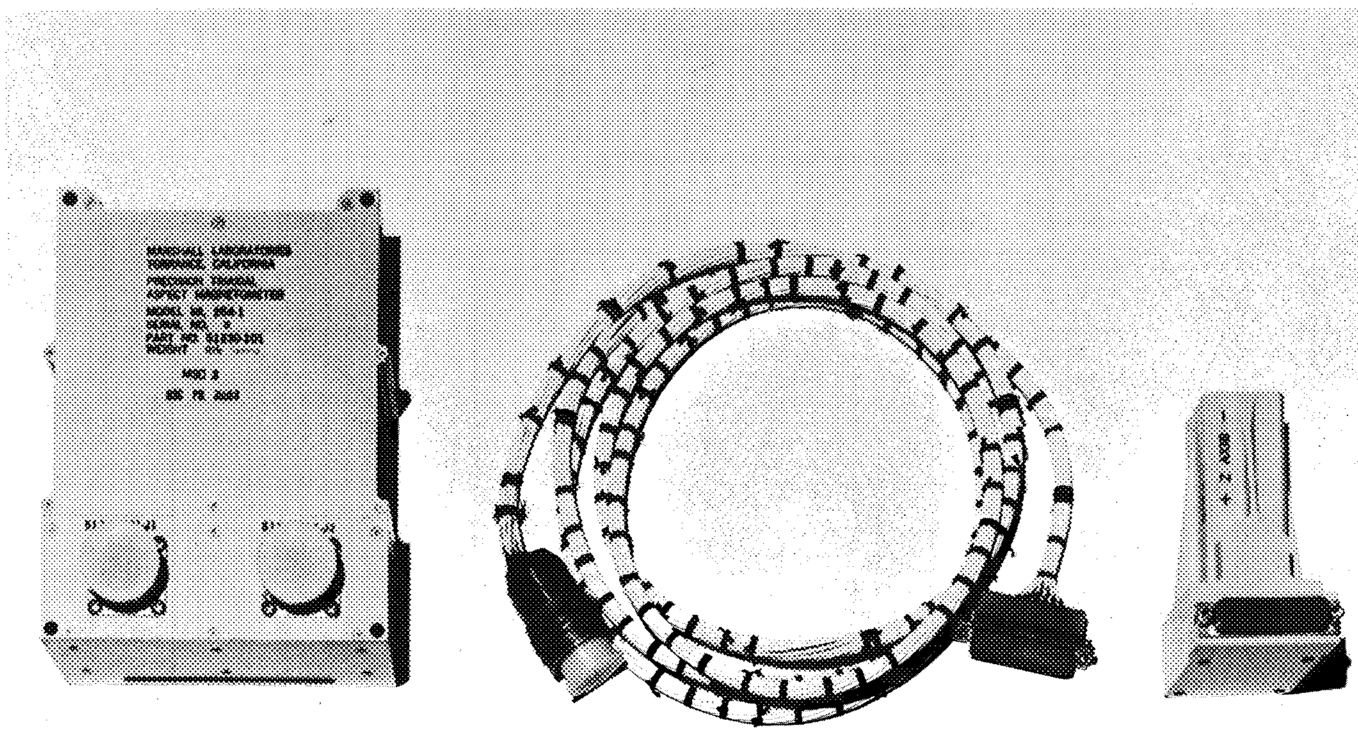

Figure 2-1. - Experiment M408, equipment.

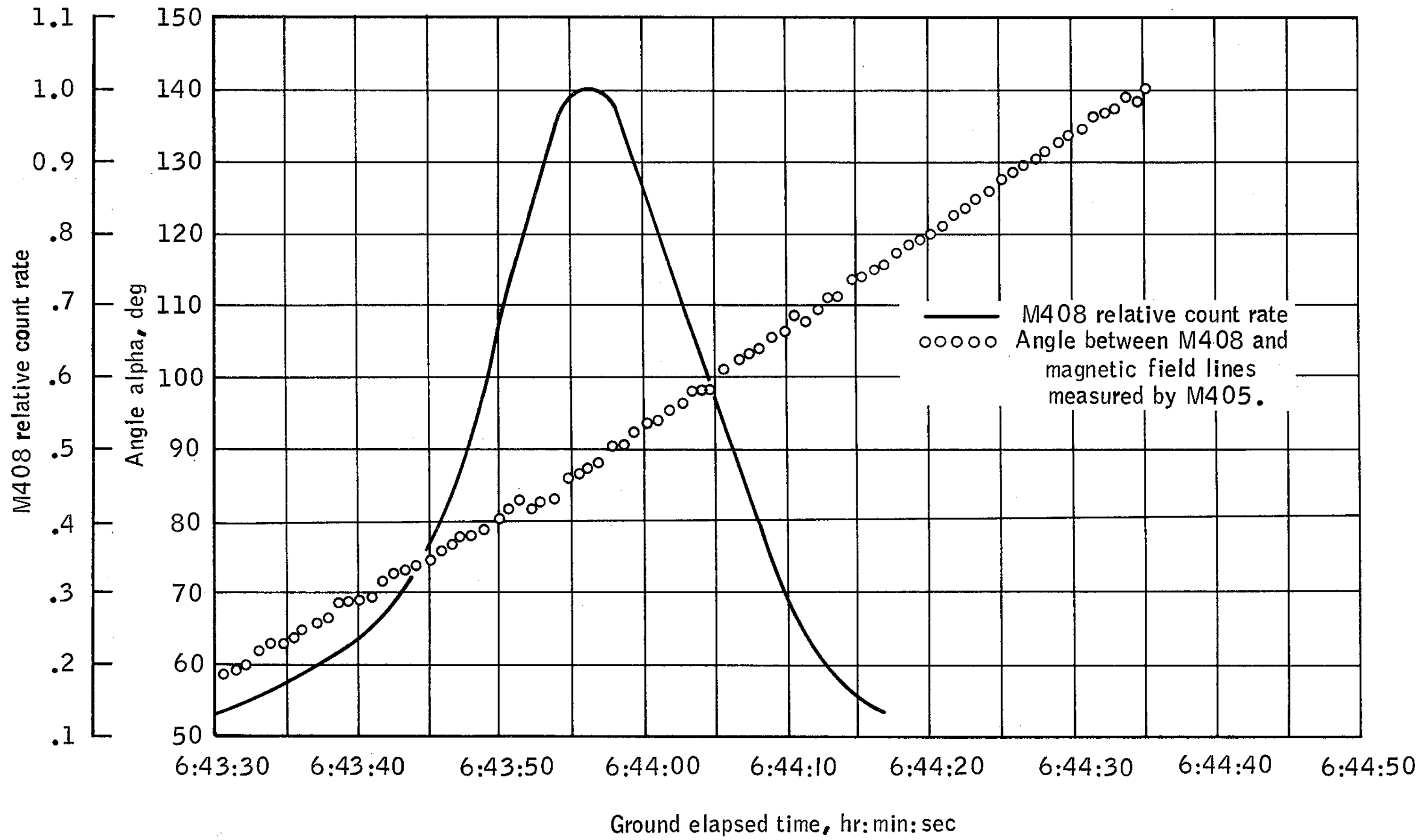

Figure 2-2. - Experiment M408, triaxis magnetometer response.

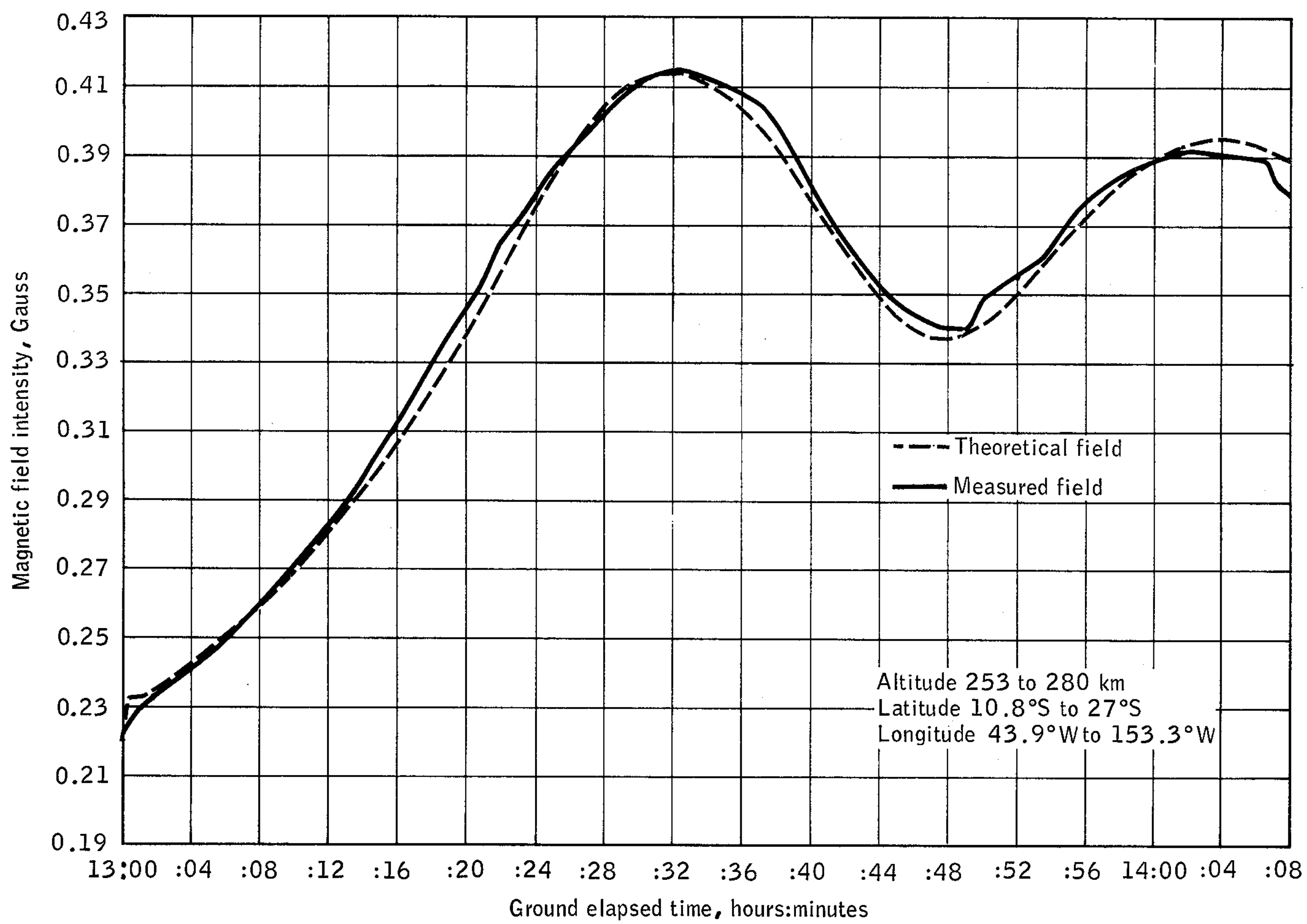

Figure 2-3. - Comparison of the magnitude of measured geomagnetic fields with theoretical magnetic field magnitude.

3. EXPERIMENT M408, BETA SPECTROMETER

By James R. Marbach
Manned Spacecraft Center

SUMMARY

The Beta Spectrometer Experiment was one of three measurements conducted on the Gemini XII Mission in support of programs within the Radiation and Fields Branch, Manned Spacecraft Center. Data were obtained on three revolutions through the South Atlantic Anomaly region. Representative electron spectra show apparent decay of the artificially-injected electrons from the Starfish high-altitude nuclear test of July 1962 to such low levels that "natural" trapped electrons are becoming detectable.

OBJECTIVE

The principal objective of the M408 experiment was to provide a measurement of the electron flux and energy distribution exterior to the spacecraft as it passed through the region of the South Atlantic Anomaly off the eastern coast of South America. This region is known to contain the only significant ionizing radiation encountered on typical Gemini missions. These flux-energy spectra are needed to verify radiation-dose computational techniques being developed within the Radiation and Fields Branch.

EQUIPMENT

The beta spectrometer is similar in function to the proton-electron spectrometer of experiment M404, flown on previous Gemini missions; however, it is quite different in design. The beta spectrometer consists of two containers, one housing the detector and analyzer system, and the other the data processing system. The total weight is approximately 16 pounds. Power consumption is about 5.5 watts at 28 volts dc. All data are processed in digital form and are relayed via Gemini pulse code modulation (PCM) telemetry system. Figure 3-1 is a photograph of the completed assembly.

Particles are detected by solid-state detectors in a dE/dx, total E arrangement providing seven channels of flux information over the energy bands of 0.41 to 0.67, 0.67 to 1.0, 1.0 to 1.22, 1.22 to 2.00, 2.00 to 2.88, 2.88 to 3.63, and 3.63 to 4.61 MeV.

Figure 3-2 is a cross section of the detector/analyzer system. The total E detector is a stack of four lithium-drifted silicon detectors providing a total active region approximately 1 cm in depth. The outputs of all four detectors are connected in parallel to a common amplifier and pulse shaper. The dE/dx detector is a 60-micron surface barrier and functions solely as an anticoincidence device in conjunction with the total E detector to discriminate against protons. To minimize the probability of electrons being scattered out of the dE/dx detector and completely (or partially) missing the total E detector, the two are physically mounted as close to each other as practical. This requires that mass shielding be used for collimation. As indicated in figure 3-2, lead spacers are arranged to provide a solid angle aperture of approximately 0.25 steradian (half-angle approximately 15°). To eliminate analysis of particles entering the total E detector from a direction other than through the collimator, the rear and sides of the detector assembly are surrounded with plastic scintillator (NE102). This third detector is viewed by an RCA 4460 photomultiplier (pm) tube, the output of which feeds an anticoincidence circuit similar to that of the dE/dx detector. Additional aluminum acts as both support and a shield to minimize anticoincidence rate (and subsequent dead-time) around the plastic and pm tube assembly. The aluminized Mylar and aluminum housing surrounds the silicon detectors and serves as an electromagnetic shield to minimize noise in the detector outputs.

The effect of the combination of shielding and coincidence circuitry can be summarized as follows:

(1) All particles entering the instrument through any other portion other than the entrance aperture are either stopped in shielding or rejected by anticoincidence as they enter the plastic scintillator.

(2) Protons of $E < 2$ MeV entering the aperture are completely stopped in the front detector.

(3) Protons of $0.2 < E < 20$ MeV will deposit greater than 200 keV in the front detector. The threshold for coincidence rejection is adjusted to 200 keV and these particles are not analyzed.

(4) Protons with $E > 5.5$ MeV will deposit more than 4.6 MeV in the total E detector and will be out of the range of the PHA and rejected on that basis.

(5) Protons with $E > 70$ MeV will penetrate both silicon detectors and enter the plastic coincidence scintillator for rejection.

(6) Electrons of $E < 410$ keV and of $4.6 < E < 10$ MeV will deposit energies in the total E detector that are outside the range of the PHA.

(7) Electrons of $E > 10$ MeV will penetrate to the scintillator for rejection.

(8) Electrons of $0.41 \geq E \leq 4.6$ MeV will be analyzed.

A block diagram of the detector/analyzer system is shown in figure 3-3.

Pulses from either the dE/dx, total E, or scintillator detector are routed into essentially identical charge-sensitive amplifiers. The amplified and shaped pulses from the dE/dx and scintillator detectors are fed into level discriminators which are adjusted to equivalent energy deposited of 200 keV and 100 keV, respectively. When an incoming pulse exceeds the threshold level, the discriminator triggers and remains latched on for approximately 0.7 microsecond. The two discriminator outputs are then routed through a complementary AND gate to a strobe control circuit.

The strobe pulse feeds an AND gate together with the inhibit/enable logic discriminator outputs. Its function is to hold the analyzer storage input closed to an analyzed pulse from the total E detector until the inhibit circuits have enough time to present an output should they have one.

Firing time of the strobe is adjusted to occur sufficiently down on the decay slope of the pulse to allow the latest and shortest, as well as the earliest and shortest, inhibit pulses to be recognized.

Figure 3-4 is a simplified block diagram of the pulse height analyzer. The amplified and shaped signals from the total E detector are applied to eight voltage-to-current converters, each of which feeds a tunnel diode discriminator. Each discriminator is adjustable, to allow flexibility of the selected energy thresholds of about 50 percent of its nominal levels. The first and eighth discriminators serve to define the energy window of the analyzer. The discriminators are similar in operation to the inhibit logic discriminators, that is, they detect a level and then latch on for approximately 0.7 microsecond. The ninth circuit in the diagram is a dE/dt-to-I converter which operates the previously mentioned strobe.

To obtain differential rather than integral spectra, interconnecting logic circuitry is provided between each discriminator output after strobe interrogation. As each discriminator fires, it inhibits the output of its next lower neighbor, leaving a pulse present on the highest energy line actuated.

A pulse that has been interrogated and accepted by the strobe circuit then feeds a one-shot multivibrator which is connected to the data processing package.

Data pulses from the one-shot multivibrators at the output of each of the seven energy channels are routed directly to the digital data processing system. Each channel is routed through a gate which is controlled by the time-base generator to control sampling time. When the gate is opened, pulses are fed into seven parallel, 14-bit scaler accumulators. After the preset sampling has occurred, the gate is closed and the information in the accumulators is shifted in parallel into seven 14-bit shift registers. The registers are connected to seven parallel-sampled, bilevel PCM telemetry channels. Each time the telemetry (TM) channels are sampled the next register bit is shifted for readout. Sampling rate is 10 per second so that 1.4 seconds are required to read out each seven channel spectrum. Immediately after the accumulated data are transferred, the input gates are opened to begin another sample. In this way data are accumulated and read out at the same time.

Figure 3-5 is a block diagram of the program control circuitry. All sequences are slaved to a 10-per-second gate pulse that is obtained from the PCM telemetry system. If it is assumed initially that the index pulse is set and the counters in the control circuitry are at zero, the sequencing can be traced as follows: A sync pulse enters the N/14 counter. The falling edge of this pulse triggers the N/14 counter one step and flips the index signal off. The index signal is routed to an eighth bilevel TM channel that is sampled in parallel with the seven energy channels. Its function is to define the first register bit being sampled. Simultaneously, this first sync pulse sends a shift command to all registers. The second to thirteenth sync pulses advance the N/14 counter and shift the register leaving them cleared. The N/14 counter, now filled, sends a pulse to a three-position sequencer. This sequencer consists of six cascaded one-shot multivibrators. After a 75-microsecond delay, a pulse appears at terminal 1 of the sequencer, resets the N/14 counter and the index flip-flop, and transfers data from the accumulators into the now depleted registers. After another 75-microsecond delay, a pulse appears at terminal 2 of the sequencer which resets all accumulators. After a third 75-microsecond delay, a pulse appears at terminal 3 of the sequencer initiating the time-base for controlling the input gates to the accumulators. This completes the cycle and the next sequence can begin.

The time-base generator works as follows. The pulse from terminal 3 of the sequencer opens the input gates to the accumulators and simultaneously gates a 100-kc crystal-controlled square wave oscillator into a 17-bit scaler. After 2^{17} pulses, the time-base flip-flop is toggled, closing the input gates to accumulators and the oscillator gate to the scaler. The circuit will now wait until a pulse from the sequencer reinitiates the cycle. The accumulator gates are open in the scaler for 131 075 ± 15 counts which corresponds to 1.31057 ± 0.00015 seconds. Stability is better than 3 parts per 13 000 over the temperature range of -65° to +170° F or ±0.102 percent.

It should be noted that although the output registers require 1.4 seconds to be sampled, the accumulators are filled for 1.31 seconds. The difference is to allow for time required to transfer the accumulator information into the output registers.

To assure that the silicon semiconductor detectors are maintained at room temperature or below (the noise figure improves with decreasing temperature), an evaporative cooling device is incorporated into the detector/analyzer. Water, stored in the cylindrical reservoir on the top of the assembly in the left of figure 3-1, is fed to two identical evaporators mounted to the side of the detector subassembly. The evaporators consist of ceramic disks which allow the water to evaporate through to the vacuum maintained inside the instrument during orbit. The water is sealed inside the reservoir in a polyethylene bag which leaves approximately half of the tank for air which is sealed at atmospheric pressure. During orbit, the 1-atmosphere pressure differential between the inside of the tank and the vacuum outside forces the water to the ceramic evaporators where it slowly bleeds out and evaporates, absorbing the heat of vaporization. The bleed rate is adjusted to approximately 5 grams per hour total, which will maintain the detectors at room temperature or lower for 4 hours with the equipment mounting structure temperature at 120° F.

PROCEDURE

The experimental equipment on GT-12 was located in the retrograde section of the spacecraft adapter. The detector/analyzer was mounted on the adapter ring structure and had an unobstructed view of the exterior environment through a hole in the spacecraft skin. The hole was covered with a half-hinged door to protect the instrument during the launch phase of the mission. It was automatically jettisoned during spacecraft separation from the booster.

Operation of the equipment during the flight was accomplished by means of a toggle switch on the control console of the pilot, who turned on the instrument after orbit insertion and left it on throughout the mission until just prior to retrofire.

To obtain information on the directionality of the electron radiation encountered, it was necessary that the instrument see as many different directions in space as possible. Since the radiation is concentrated in the relatively small South Atlantic Anomaly region at Gemini altitudes and is known to be trapped in the geomagnetic field, it was important that the instrument be made to look at several angles with respect to the magnetic field while in this area. To accomplish this part of the experiment, the crew was requested to execute a slow roll maneuver while in the South Atlantic Anomaly which would rotate the instrument about the magnetic field lines. This maneuver sweeps the experimental sensors through the normal to the field twice for every 360-degree roll of the spacecraft. In addition to providing directionality information, this would also assure several data points taken while the instrument is normal to the magnetic field direction where the electron intensity is known to be greatest.

RESULTS

A preliminary analysis has been performed on select data obtained during the first 4 hours of instrument operation. Figure 3-6 is a plot of count-rate versus energy as observed at McIlwain coordinates (ref. 1) of $L = 1.25$ and $B = 0.22$. This particular spatial location has been chosen for first analysis since considerable data from other measurements is available for comparison. The data plotted are not corrected for background and backscatter but are representative of the general shape of the spectrum.

Above approximately 1.2 MeV, the spectrum is seen to closely resemble the decayed fission spectrum as predicted by atmospheric scattering theory (ref. 2). The departure from the predicted spectral shape below this energy suggests a source of electrons separate from the Starfish explosion present at the time of the measurement. Similar measurements have seen this effect but not as pronounced as these data indicate (refs. 3 and 4). It is possible that the Gemini XII measurements were made at a time when the fission electrons have sufficiently decayed to allow pronounced visualization of a superimposed spectrum of "natural" Van Allen electrons. A further refinement of the data is necessary to establish the approximate shape of this superimposed spectrum and detailed studies of geomagnetic activity and other possible affecting phenomena must be conducted in order to speculate on the true source of these electrons. Results of these efforts will be published in appropriate journals as the results become available.

REFERENCES

1. Mc Ilwain, Carl E.: Coordinates for mapping the Distribution of Magnetically Trapped Particles. J. Geophys. Res., Vol. 66, No. 11, Nov. 1961, 3681-3691.

2. Walt, M.: The Effects of Atmospheric Collisions on Geomagnetically Trapped Electrons. J. Geophys. Res., Vol. 69, 3947, 1964b.

3. Imhof, W. L.; and Smith, R. V.: Energy Spectrum of Electrons at Low Altitudes. J. Geophys. Res., Vol. 70, 2129, 1965c.

4. Reagan, J. B.; et al: Final Report on Contract NAS 9-1587. J. Geophys. Res., Vol. 70, 2129, 1965c.

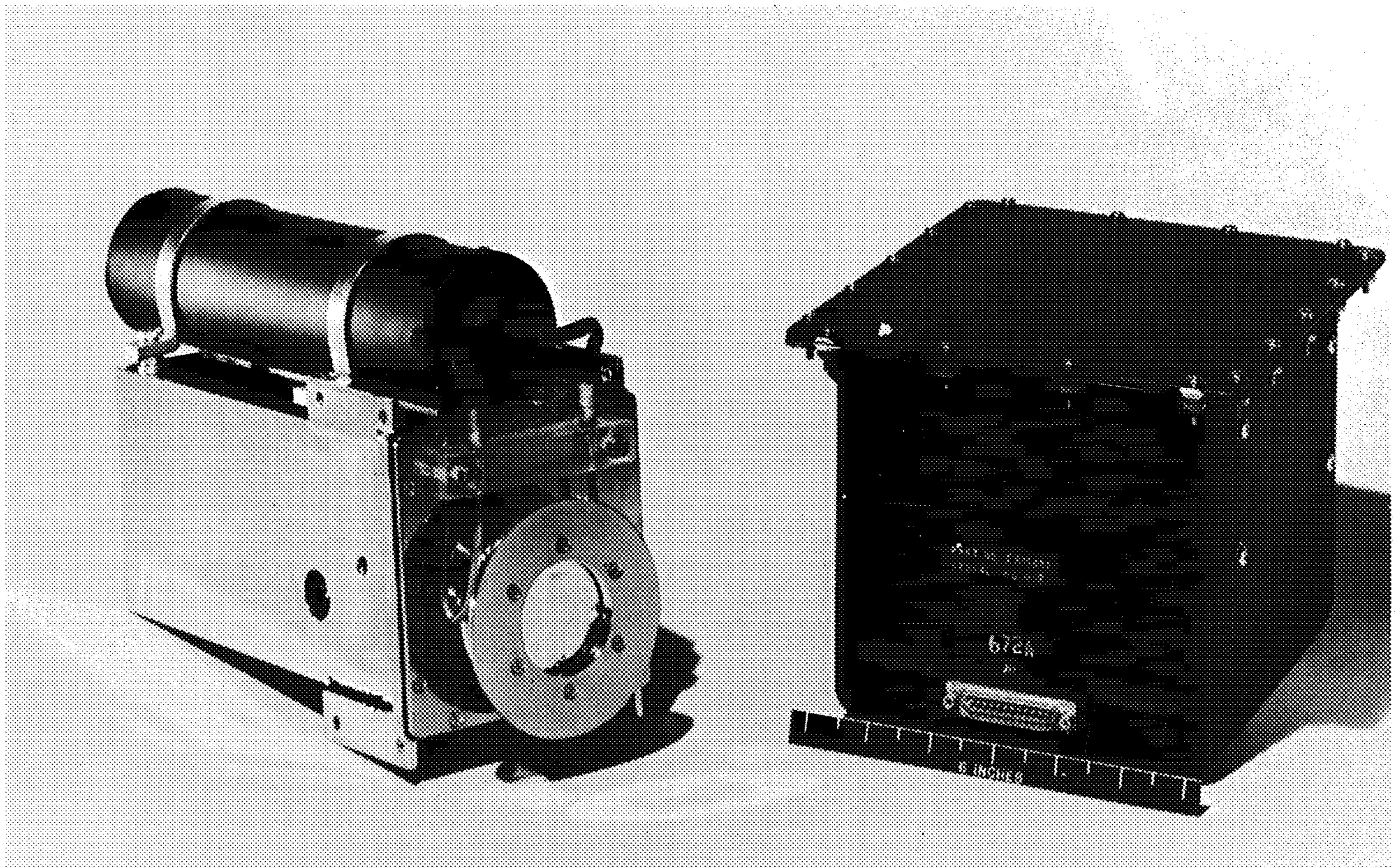

Figure 3-1. - Beta spectometer.

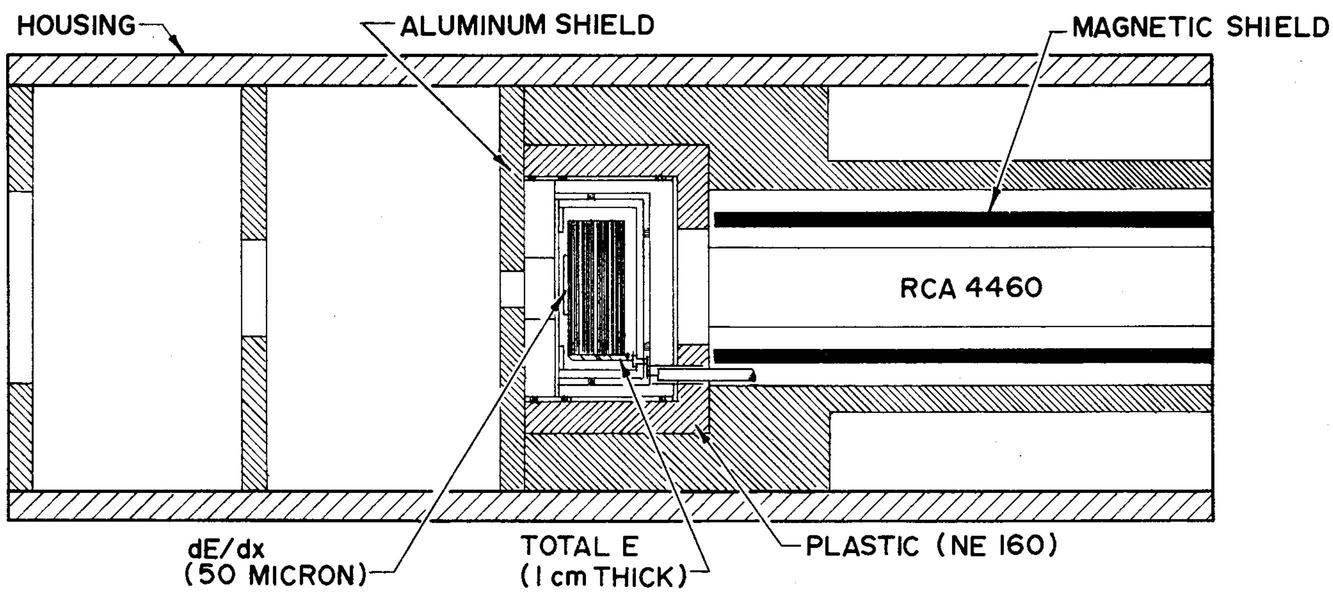

Figure 3-2. - Electron detector cross section.

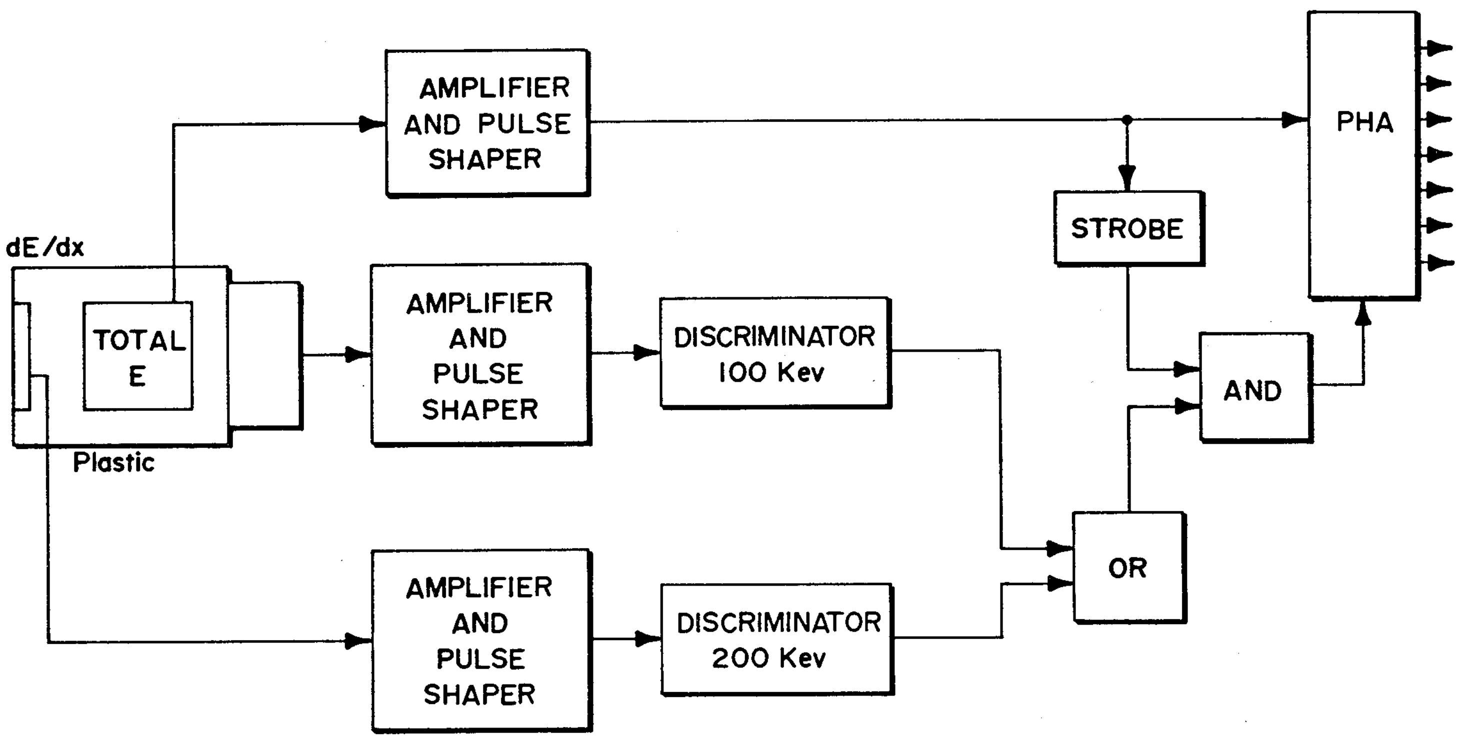

Figure 3-3. - Detector/analyzer block diagram.

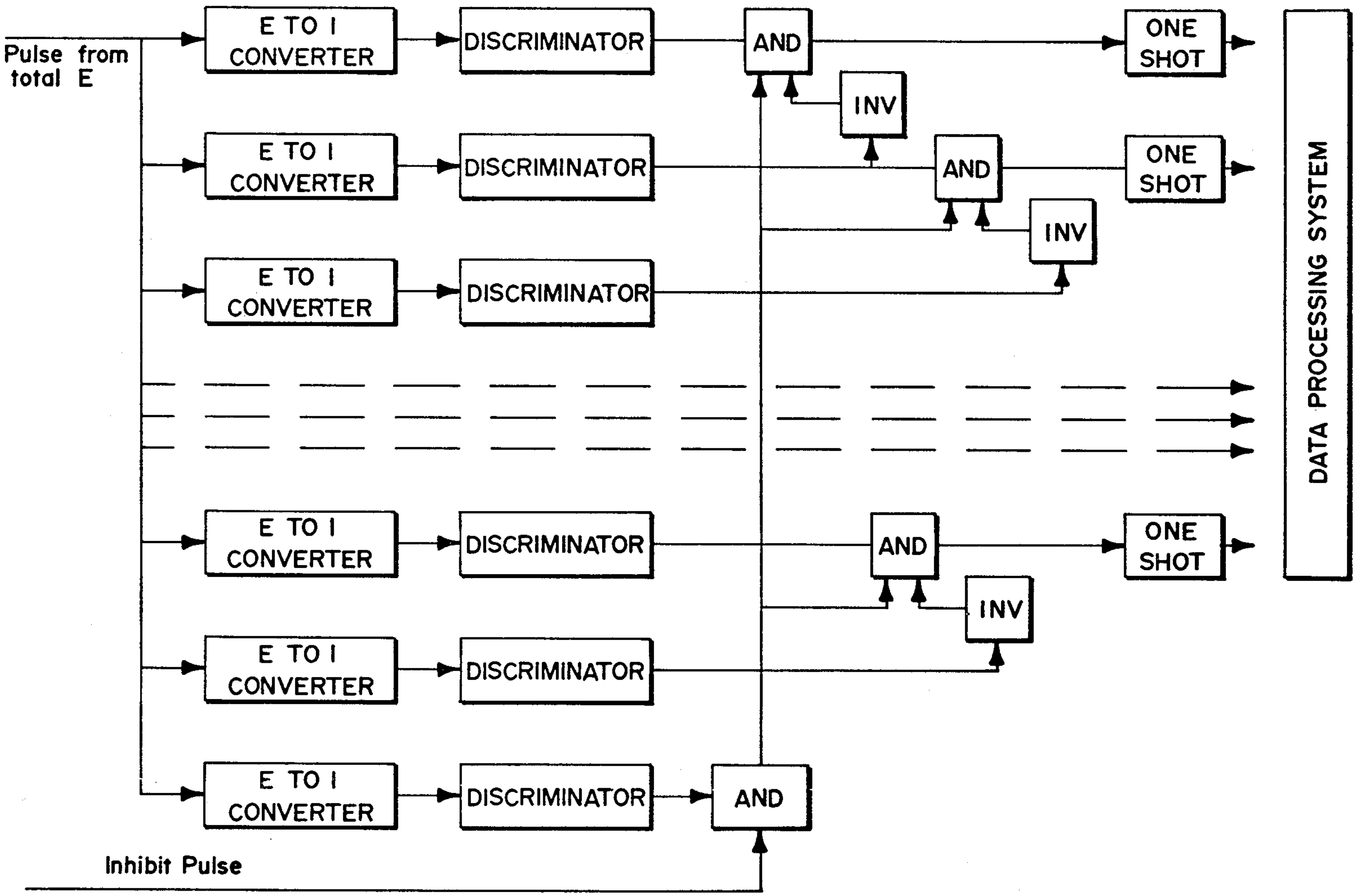

Figure 3-4. - Pulse height analyzer.

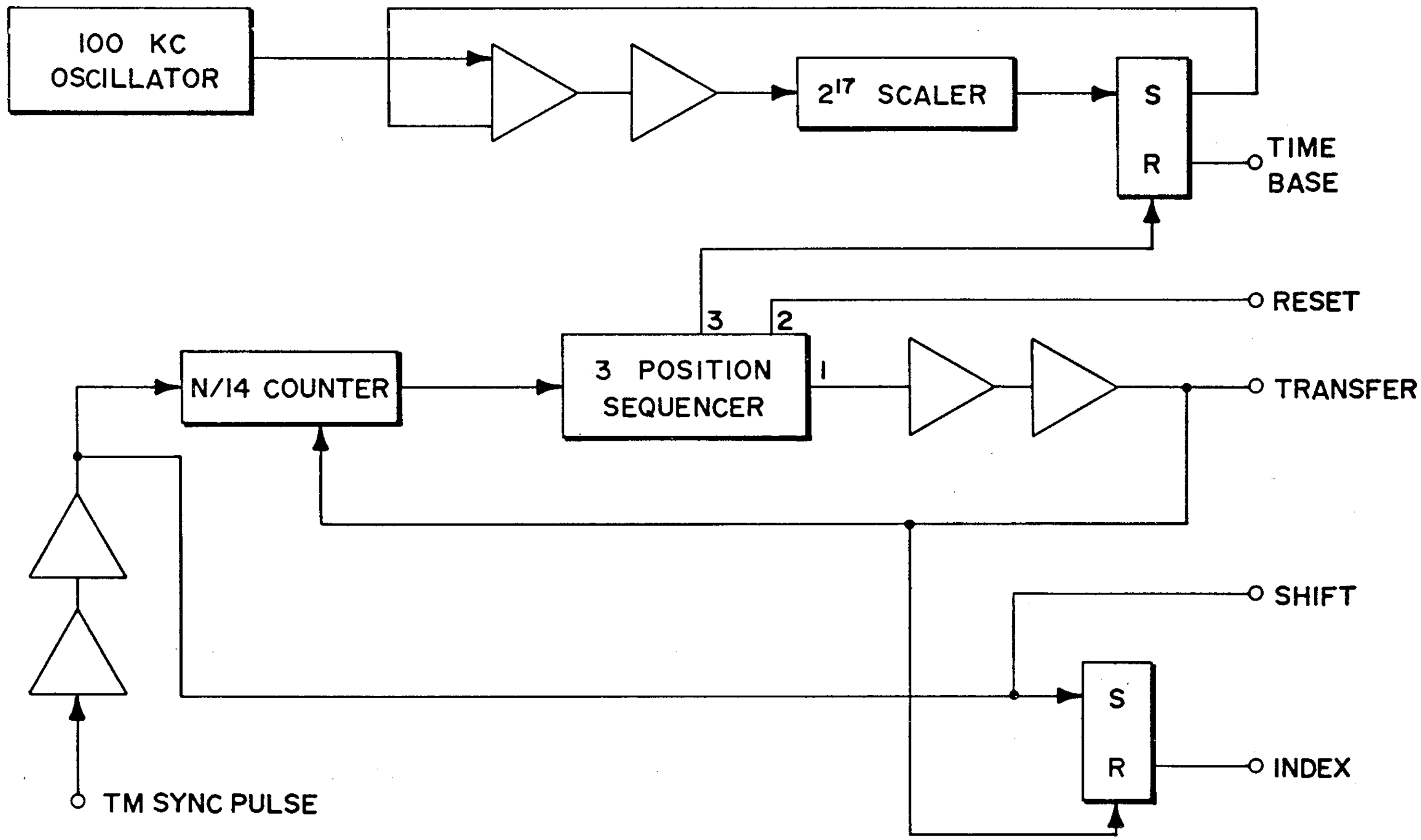

Figure 3-5. - Program control circuitry.

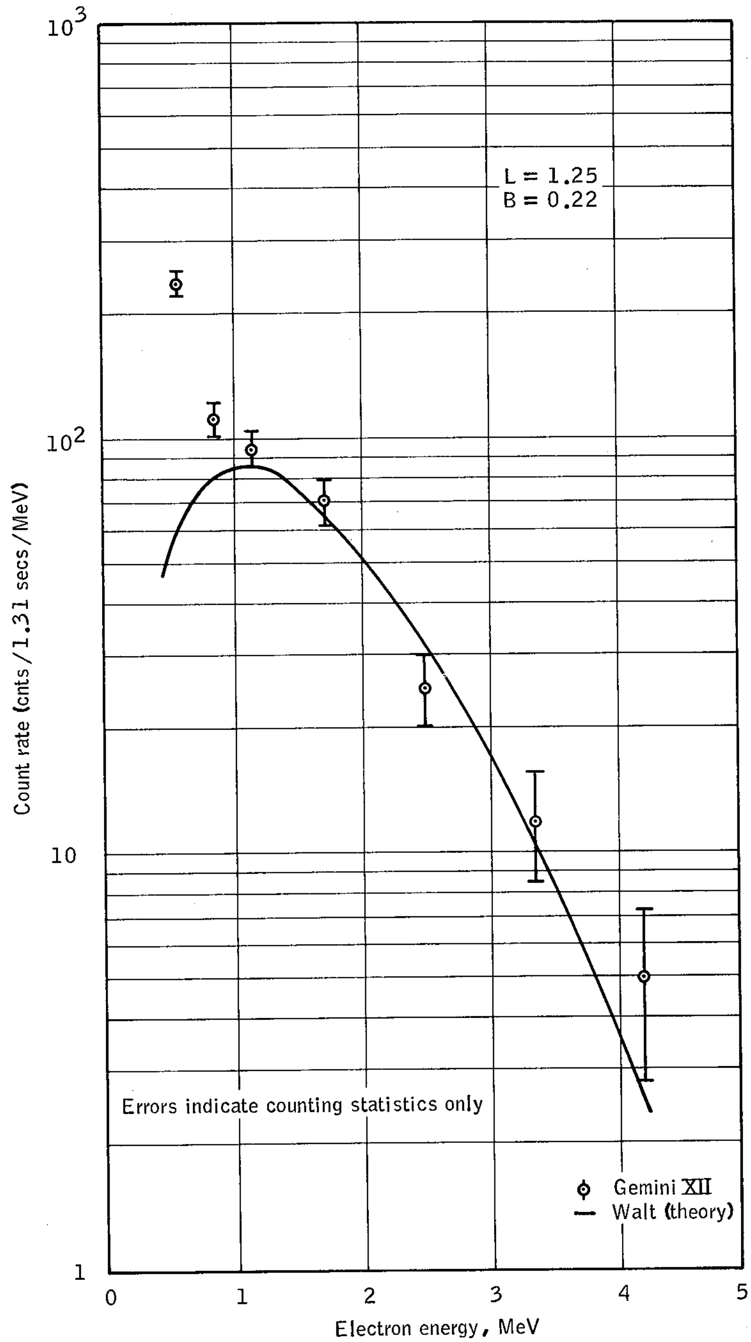

Figure 3-6. - Theoretical and measured countrate versus electron engery spectra at McIlwain coordinates of L = 1.25 and B = 0.22.

4. EXPERIMENT M409, BREMSSTRAHLUNG SPECTROMETER

By Reed S. Lindsey, Jr.
NASA Manned Spacecraft Center

SUMMARY

Preliminary analysis of data from the Gemini XII mission indicates that the spectrometer functioned as expected. Interior bremsstrahlung and electron relative countrate-time spectra are presented for the sixth Gemini revolution during the mission. In addition, uncorrected bremsstrahlung and electron relative flux-energy spectra for the same are also presented.

OBJECTIVE

The objectives of this experiment were to gain information for compution the flux-energy spectra of bremsstrahlung inside the Gemini spacecraft and to determine if energetic electrons are able to penetrate the vehicle walls. These spectra will be compared with computer-predicted bremsstrahlung spectra using data from the Beta Spectrometer (M408) experiment also flown on this mission.

Secondary gamma rays produced in the spacecraft during the Gemini mission trapped electrons were not expected to reach biologically significant levels. On long-duration missions which may be flown in high trapped-electron flux environments biological significant levels could exist. Calculations of bremsstrahlung radiation involve uncertainties due to the small amount of data available on cross-section interaction and the complex, heterogeneous makeup of the spacecraft. The bremsstrahlung detector specifically was designed to give a time-differentiated measurement of the electron-induced gamma rays over a large section of the vehicle.

EQUIPMENT

The spectrometer, figure 4-1, consists of two parts; the detector and the data processor. The detector and the data processor together weigh about 8 pounds and require 6 watts of electrical power. The detector unit is fastened to the command pilot's spacecraft hatch and oriented to measure the flux and energy of penetrating electrons. The data processor was located behind the command pilot's seat. An 8-foot cable provides electrical coupling between the two parts of the spectrometer.

The detector unit (fig. 4-2) was conceived, designed and constructed by the Ling Temco Vought Research Center. Basically, it consists of a 0.040-inch thick, 0.40-inch diameter Pilot-B plastic scintillator coupled to the top of a 0.50-inch thick, 0.750-inch diameter CsI (Tl) scintillator viewed by an RCA 4460 photomultiplier tube. The anode signal is fed through a shorted 10-nsec delay line to a high speed amplifier. The amplifier drives two high speed discriminators adjusted for acceptable energy deposition in the plastic scintillator. Since bremsstrahlung, in the energy region of interest, does not appreciably interact with the thin plastic while electrons do, an effective means of discrimination between the two types is available. The two discriminators effectively operate as a timing single channel analyzer for electrons between 200 keV and 4000 keV. Signals below the lower level discriminator are assumed to be due to bremsstrahlung. Those within the discriminator window are assumed to be due to interesting electrons and, those above the upper level detector are assumed to be due to cosmic rays, protons, or lower energy electrons. Digital gating signals derived from logic circuitry after the high speed discriminators route the linear signal to the proper analog to digital converter in the data processor.

The detector unit also includes a phototype high-voltage power supply and low-voltage power supplies for the amplifiers, discriminators, and logic circuits. The unit is sealed in a dry nitrogen atmosphere to allow proper operation of high voltage components under exterior vacuum conditions.

The last dynode signal drives a linear amplifier which in turn drives the data processor amplifier through the interconnecting cable.

The data processor (fig. 4-3) is a modification of the Bremsstrahlung Spectrometer flown on the Gemini X mission. It consists of two linear amplifiers, two analog-to-digital converters, two sets of five scalers each, necessary control logic, and power supplies.

Digital control signals from the detector unit allow operation of only one analog-to-digital converter at a time. The necessary dynamic energy range is covered by two linear amplifiers having gains of approximately 1 and 4. The analog-to-digital converters are of the parallel tunnel diode type. One extra channel is used to inhibit strobing of the analog-to-digital converters if the linear signal is too large as in the case of cosmic rays or energetic protons which can penetrate the detector from any direction. Data from the analog-to-digital converters are recorded by ten scalers and shifted serially to the telemetry under control of the telemetry sync pulse. Readout rate is 10 channels-per-second. Since the telemetry word is 8-bits long (256 events) and the scalers are a maximum of 12-bits long, a data compression technique is used. The five most significant digits of a scaler's information and three bits to locate their position in the 12-bit scaler are presented to the telemetry.

Power supplies for the analog and digital circuitry and noise filters are located in the data processor.

PROCEDURES

The flight crew turned the equipment on and off four times during the mission for a total ON time of approximately 32 hours. About 5 hours of this time was within the geographic anomaly areas of interest.

RESULTS

Preliminary analysis of data obtained during the Gemini XII mission indicates that electrons do penetrate the spacecraft wall, a condition which was previously doubted. Spacecraft interior-electron and bremsstrahlung integral-countrate-time spectra for Gemini revolution 6 are shown in figure 4-4. A strong correlation exists between the two general spectra, a correlation previously anticipated. Data reduction has not progressed to the point of relating absolute ordinates. Figure 4-5 is an uncorrected electron countrate-energy distribution. The anomolous increased number in the highest energy spectrometer channel is an unexplained occurrance. Figure 4-6 is an uncorrected bremsstrahlung countrate-energy distribution and is within reasonable estimation of such distributions.

Data reduction is continuing to complete analysis and evaluation necessary for obtaining the experimental objectives.

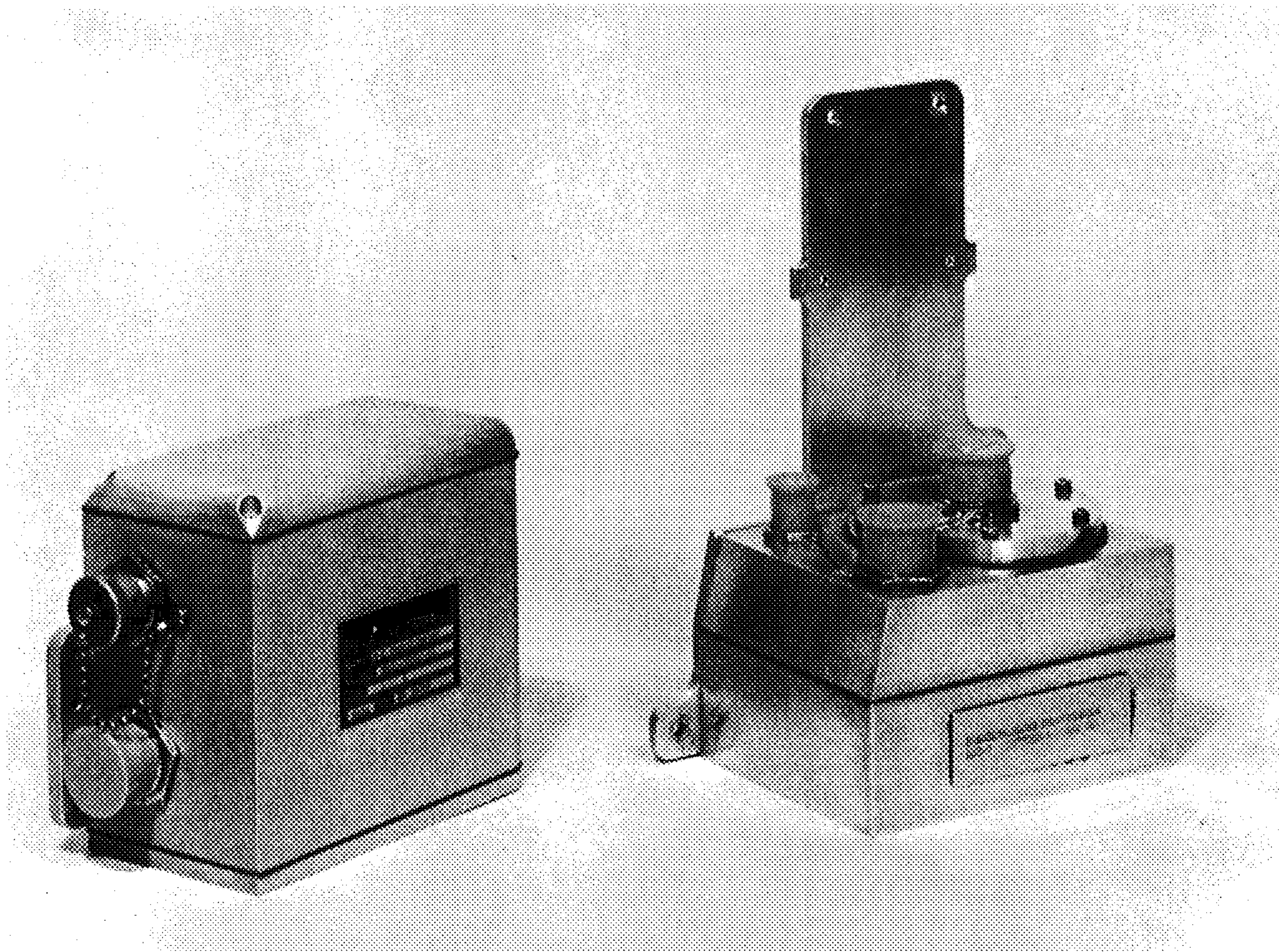

Figure 4-1. - Bremstralung spectrometer.

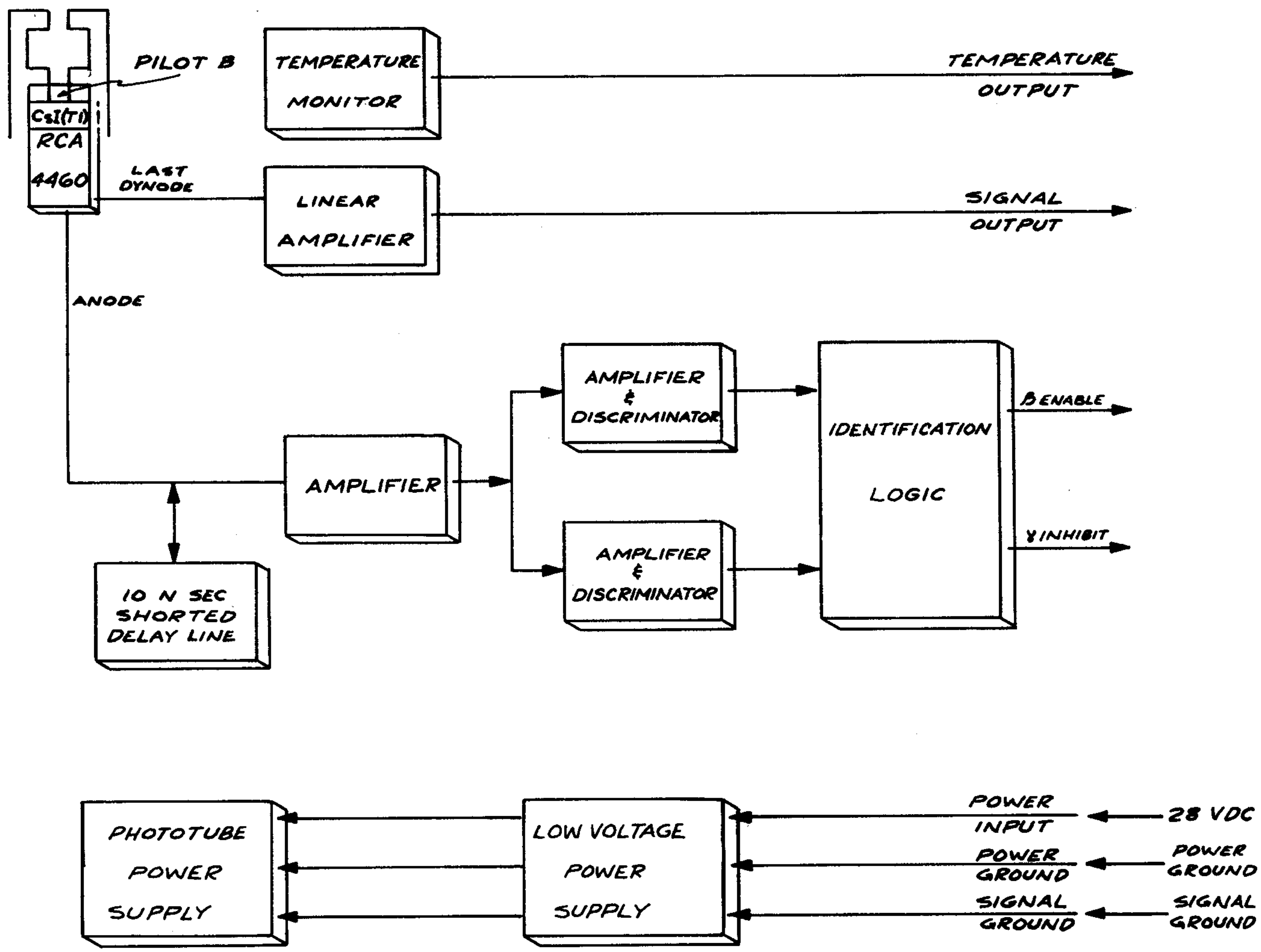

Figure 4-2.- Beta - bremsstrahlung spectrometer detector unit.

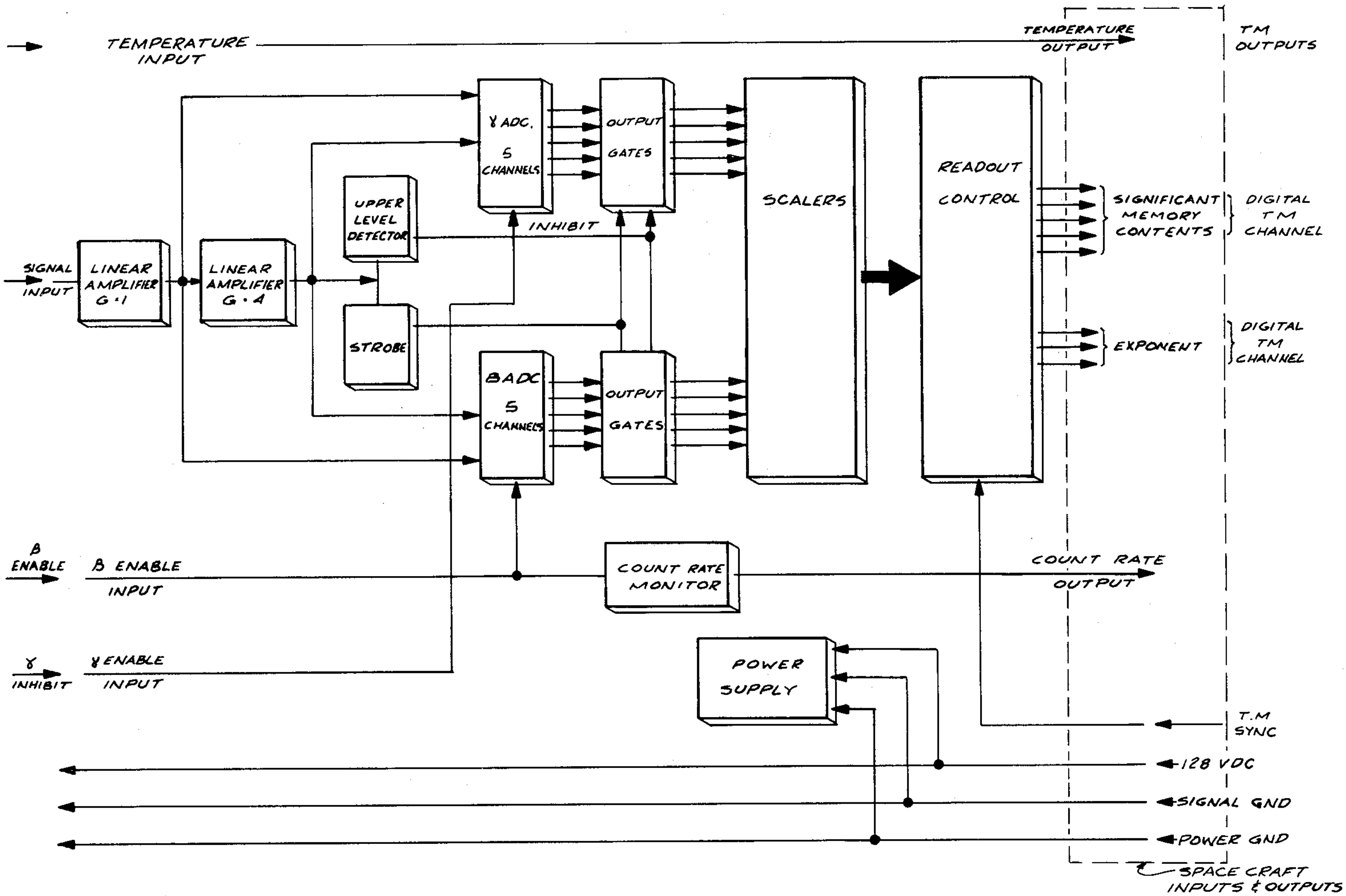

Figure 4-3. - Beta - bremsstrahlung spectrometer data processor.

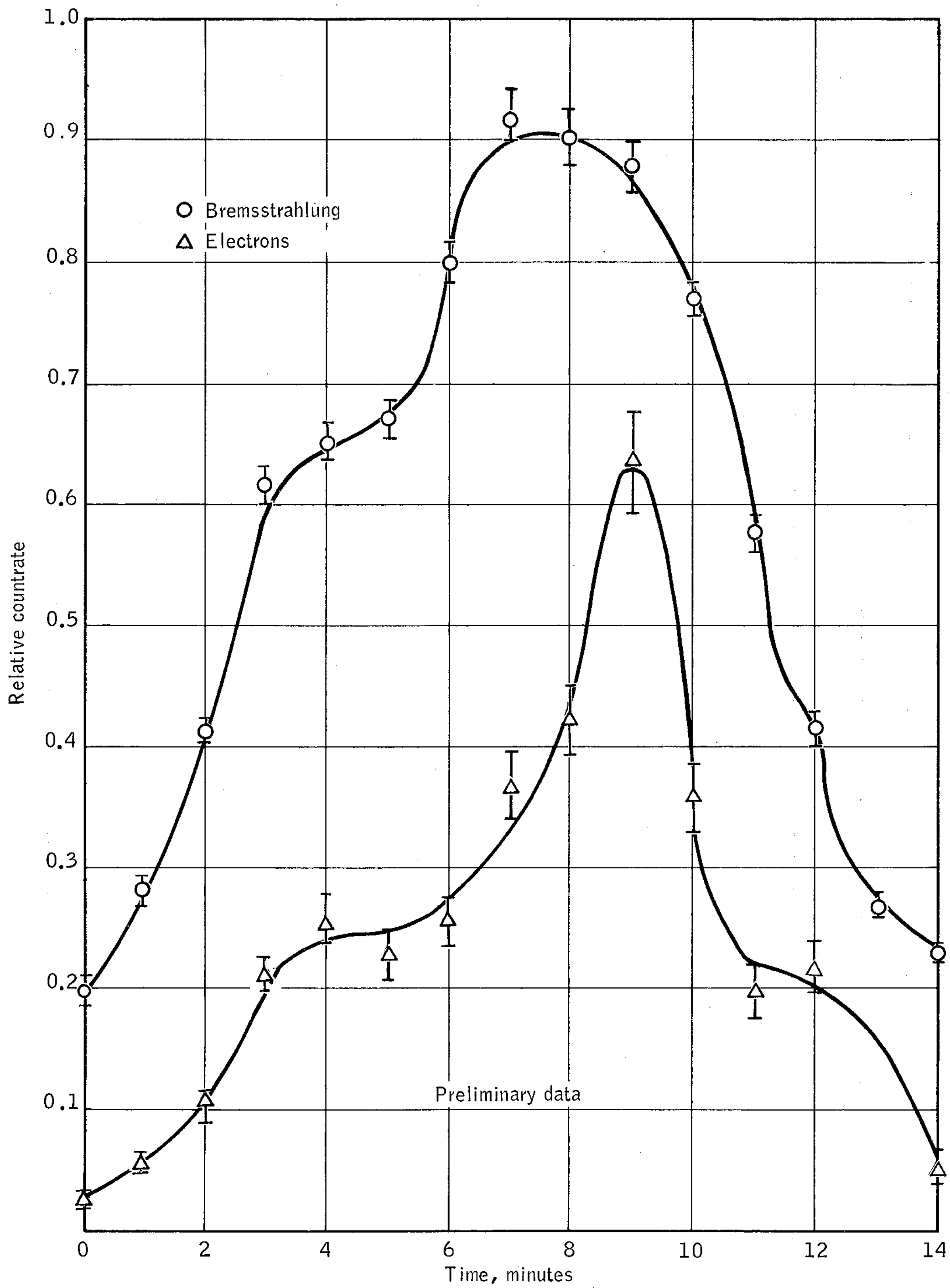

Figure 4-4. - Relative integral countrate - time spectra, revolution 6.

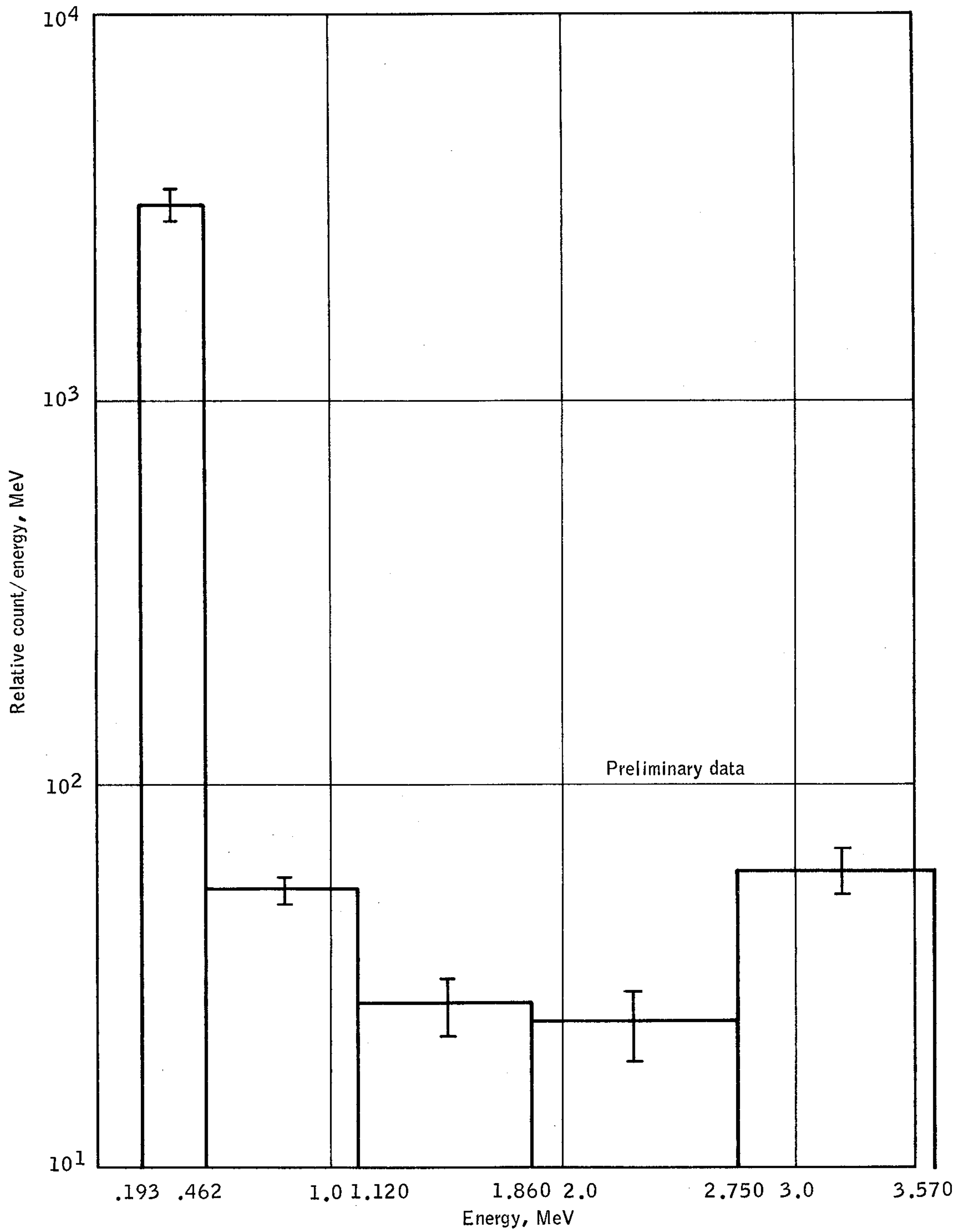

Figure 4-5. - Uncorrected electron relative count - energy distribution, revolution 6.

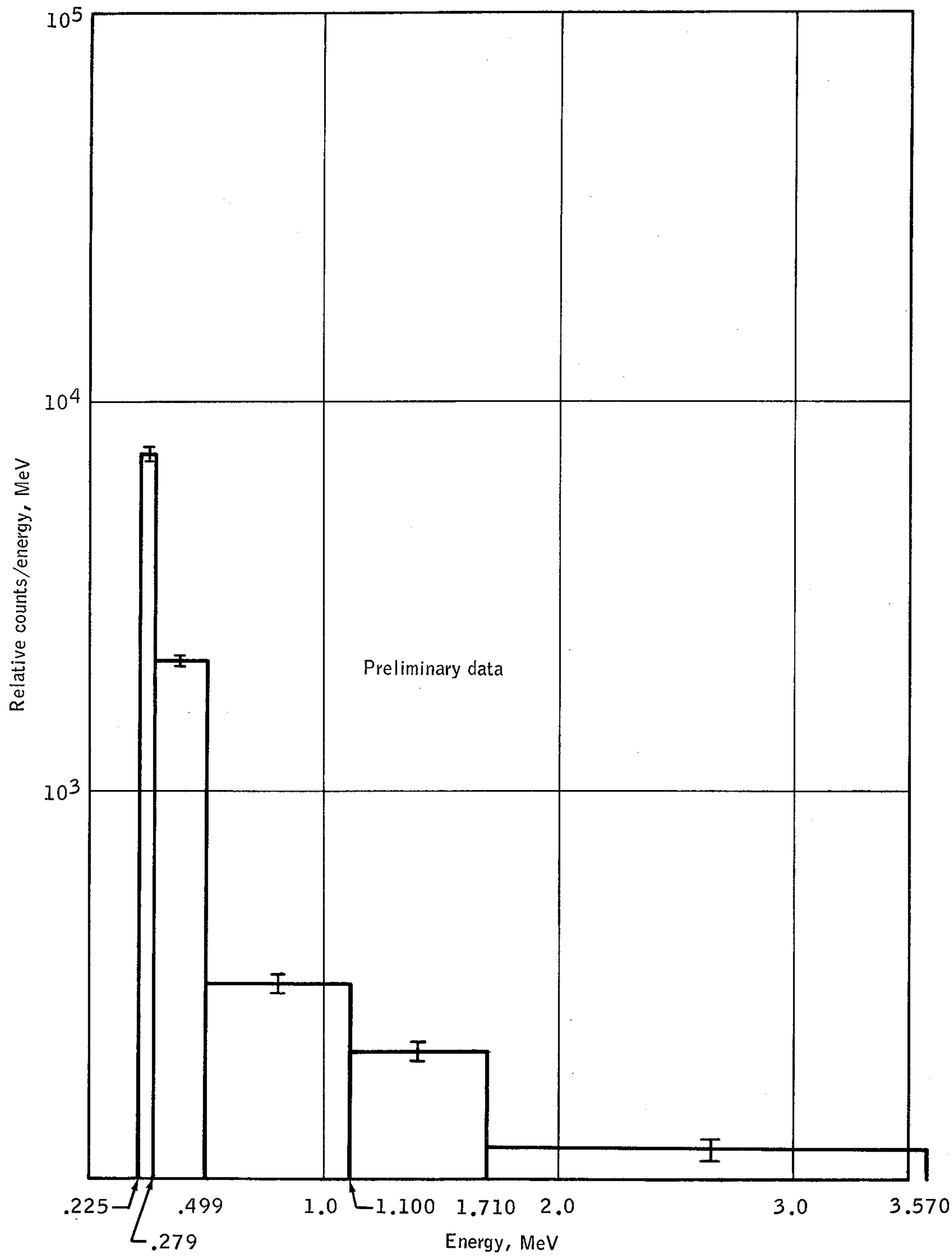

Figure 4-6. - Uncorrected bremsstrahlung relative count - energy distribution, revolution 6.

5. EXPERIMENT S003, FROG GROWTH

By R. S. Young and J. W. Tremor
NASA-Ames Research Center

SUMMARY

Fertilized frog eggs were flown in the Gemini vehicle, recovered and studied for evidence of abnormalities due to the relative absence of gravity. The egg cell divisions and subsequent differentiation were normal when compared to ground controls. The experiment will be repeated where fertilization can be accomplished during zero-g flight conditions.

OBJECTIVE

The objective of the S003 experiment was to determine the effect of weightlessness on the ability of a fertilized frog egg to divide normally and to differentiate and form a normal embryo. This experiment was first attempted on the Gemini VIII mission, and was only partially completed because of the early termination of that mission.

EQUIPMENT

The experiment was contained in one package mounted on the right-hand hatch of the Gemini vehicle. The package had four experimental chambers containing frog eggs in water, with a partitioned section containing a fixative (5-percent formalin). The entire package was insulated and contained a temperature control system for both heating and cooling to maintain an experiment temperature of approximately 70° F at all times during the mission including extravehicular activity. Electrical power was obtained from the spacecraft electrical system. The experiment was actuated by two handles on the outside of the package. These handles and a toggle switch for the heating element were manipulated by the pilot, either by ground-control request or according to a predetermined schedule. Identical equipment was used and controlled on the ground during these same time sequences. Figure 5-1 shows the experiment equipment assembled and figure 5-2 shows the hardware partially disassembled.

PROCEDURES

Eggs were obtained from several dozen female frogs (Rana pipiens) by injection of frog pituitary glands approximately 48 hours prior to launch, in order to induce ovulation at the desired time. The best of these eggs (from two females) were selected for flight and fertilized by immersion in a sperm suspension made by macerating frog testes in pond water. The fertilized eggs were then removed to a cold room (43° F) and placed in approximately 10 cc of pond water in each of the four experimental chambers. The formalin fixative was placed behind leak-proof partitions in three of the four chambers. The fourth chamber had water instead of formalin. Each chamber received 5 eggs, so that a total of 20 eggs was flown. Two sets of control experiments were set up in identical equipment on the ground. The first control was to be conducted simultaneously with the flight experiment. The second control was delayed approximately 2 hours so that changes in temperature experienced by the flight experiment could be duplicated more precisely than in the simultaneous control. Since telemetered temperatures were not received continuously, such a delayed control was necessary to duplicate the actual flight environment.

The flight experiment was installed in the spacecraft approximately 2-1/2 hours prior to launch. The fertilized eggs were kept at approximately 43° to retard the first cell division of the eggs until spacecraft installation. This precooling of the eggs was sufficient to retard first cleavage until the zero-g phase of the flight. At 41 hours g.e.t., the pilot was scheduled to turn the first handle on the experimental package to inject the formalin fixative into two of the four egg chambers. This would kill the eggs in these two chambers and preserve them for microscopic study after recovery. A second handle was scheduled to be actuated at 85 hours g.e.t. to fix the eggs in one of the remaining two chambers. The last chamber was unfixed and those embryos were recovered alive. All eggs and embryos were studied after recovery for gross morphological abnormalities in cleavage planes and differentiation. Histological examination and electron microscopy was also accomplished.

RESULTS

Successful early cleavage stages were attained during the Gemini VIII mission. Because of the short duration of this flight, the later cleavage and developmental stages were not obtained. This was the reason for repeating the experiment during the Gemini XII mission. Postflight analysis of the results from this mission indicate that all phases of the experiment were performed as scheduled with good results. The desired later cleavage and embryonic stages were obtained to complete the experiment successfully.

The experiment package maintained temperatures between 66° and 74° F throughout the mission, stabilizing at approximately 72° F. Although this temperature was 4° F above the expected average, it was well below the maximum allowable of 80° F. The temperature history is shown in figure 5-3. The experiment package toggle switch to turn on the internal heater was actuated at 17:41:55 g.e.t., to assure proper experiment temperatures during extravehicular activities. The first handle actuation was accomplished at 41:43:40 g.e.t. to release the formalin and fix the eggs in two of the egg chambers. The second handle actuation, performed at 85:10:22 g.e.t. to fix the eggs in the third chamber, completed the flight crew's participation in this experiment.

The 10 embryos in the 40-hour fixation chambers appeared to be morphologically normal when compared with the ground-control experiments. No abnormalities were detected by gross observation in either the flight or ground-control embryos. Figures 5-4, 5-5, and 5-6 are ground-control embryos fixed at 2 hours, 47 hours, and 100 hours, respectively. Figure 5-7 is a flight embryo fixed at 41 hours. The five embryos fixed at 85 hours g.e.t. were well developed and morphologically normal tadpoles. The five embryos which were not fixed were found to be well developed, live, swimming tadpoles when the experiment package was opened onboard the prime recovery ship (fig. 5-8). Three of these embryos were morphologically normal and two were abnormal. However, the abnormalities were not inconsistent with the ground-control embryos and they cannot be ascribed to development under a zero-g environment at this time. The five live tadpoles died several hours after their recovery and were fixed for histological sectioning. The reasons for their deaths have not been determined. Embryo specimens were sectioned for histological study. Again, all such studies indicated normal development (figs. 5-9 and 5-10).

CONCLUSIONS

In spite of the fact that the frog egg is known to orient itself with respect to gravity during its very early development, a gravitational field apparently is not necessary for the egg to divide normally. This was a preliminary conclusion reached after the Gemini VIII mission. It can now be concluded that gravity is not necessary for differentiation and morphological changes in the later stages of embryonic development. Whether the frog egg will divide and develop normally if it is also fertilized under zero-g conditions so that it never becomes oriented with respect to gravity is still an unanswered question. It is hoped that this question can be answered on later orbital missions.

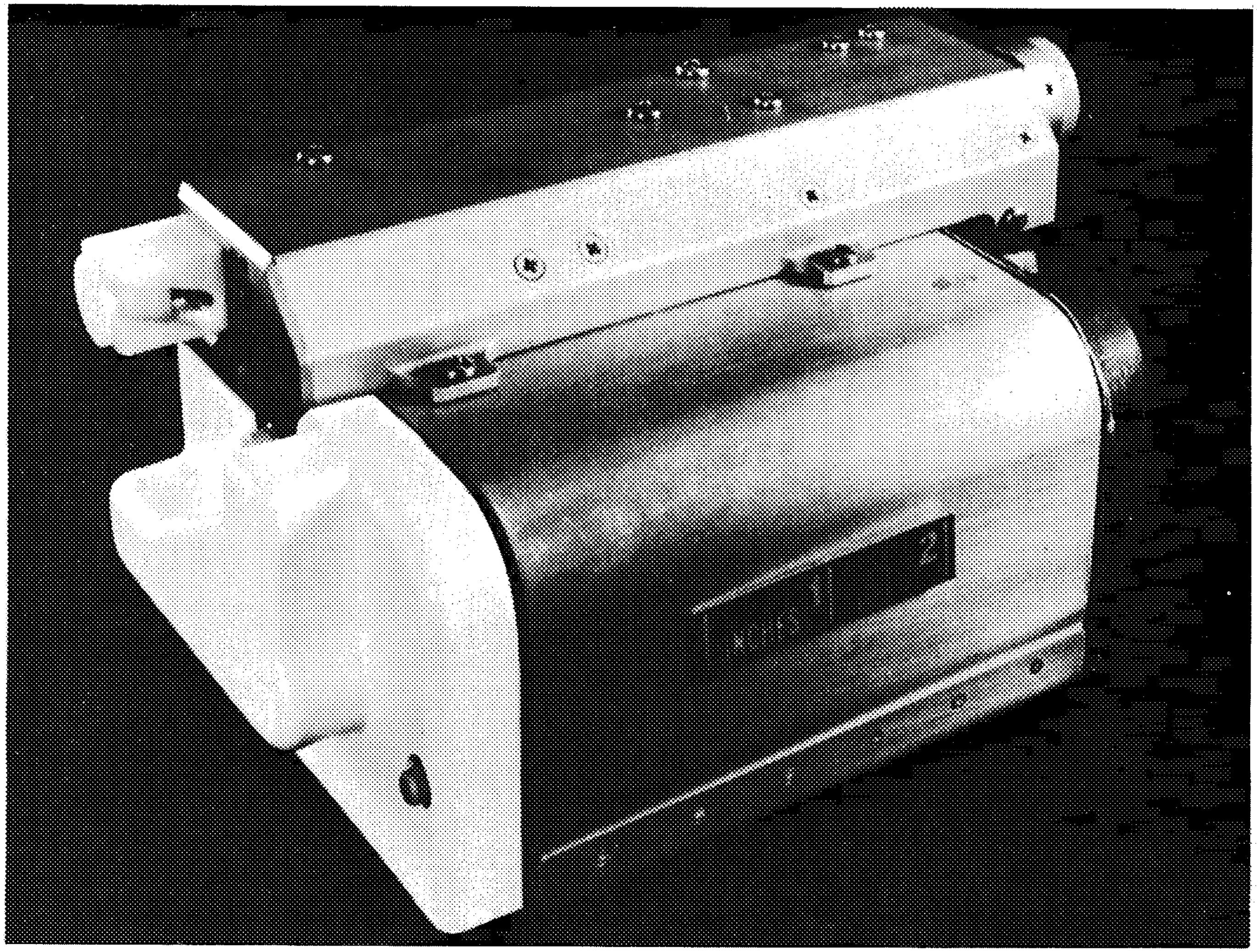

Figure 5-1. - Flight hardware intact.

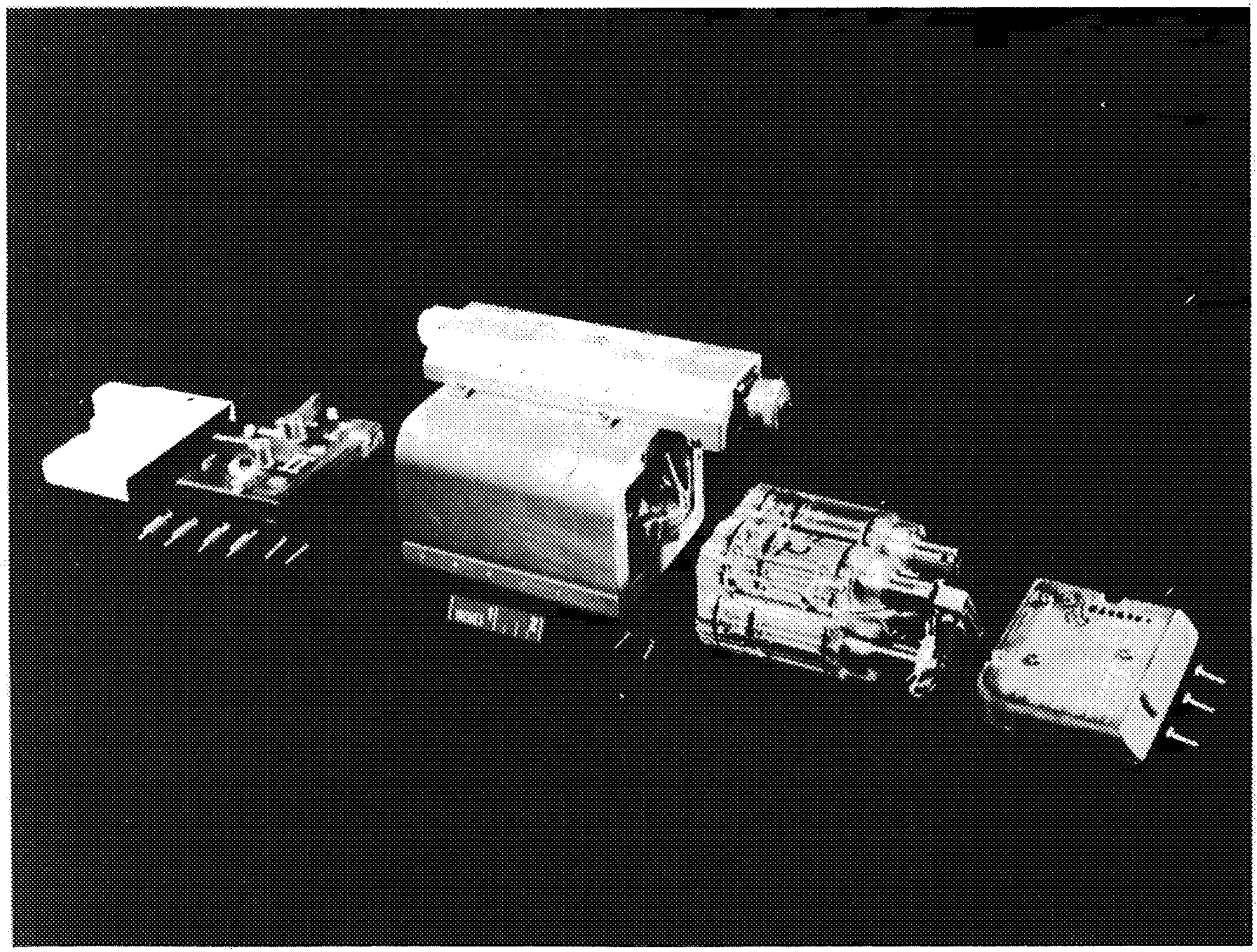

Figure 5-2. - Flight hardware partially disassembled.

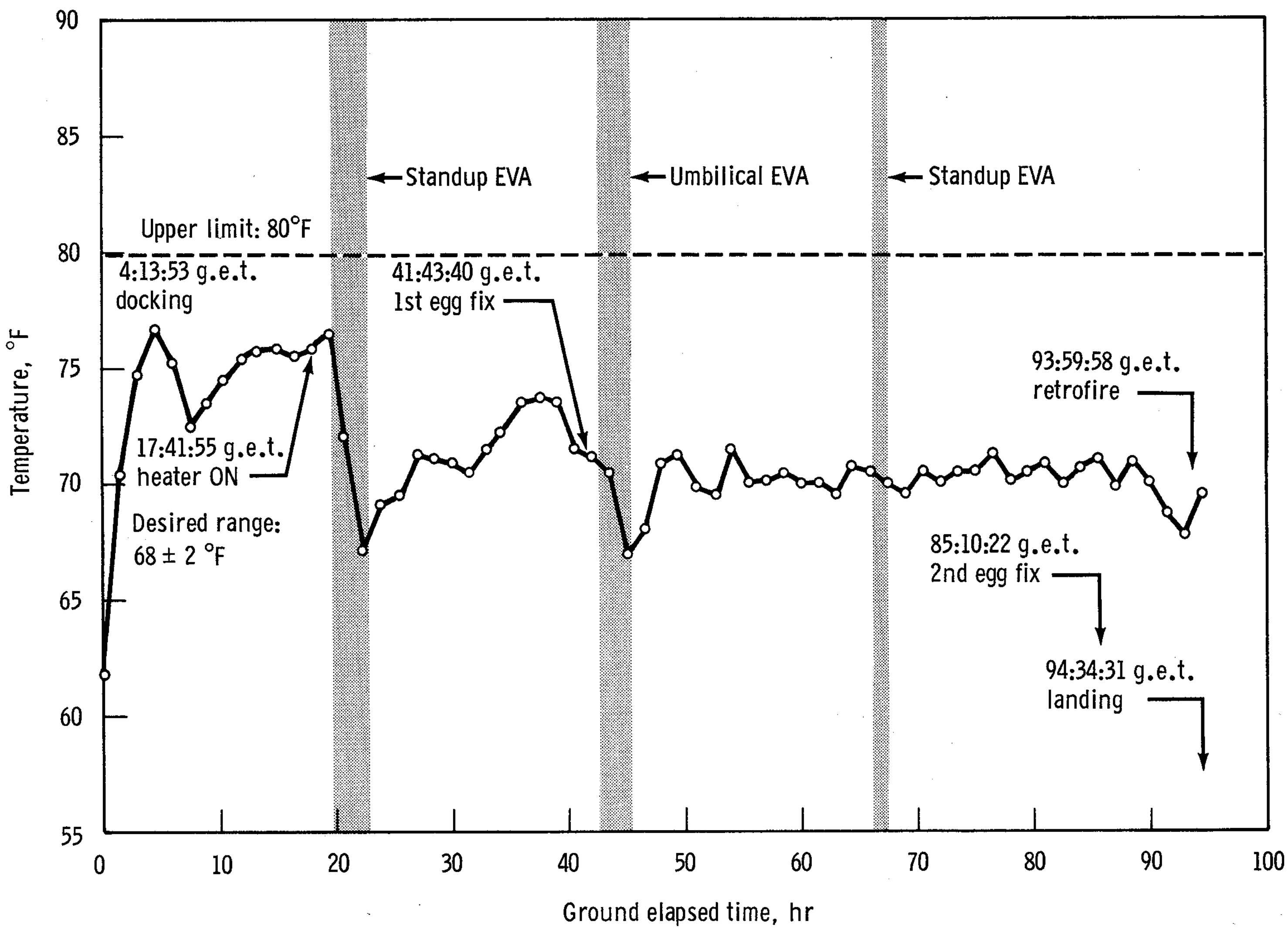

Figure 5-3. - Experiment S003, frog egg package internal temperatures.

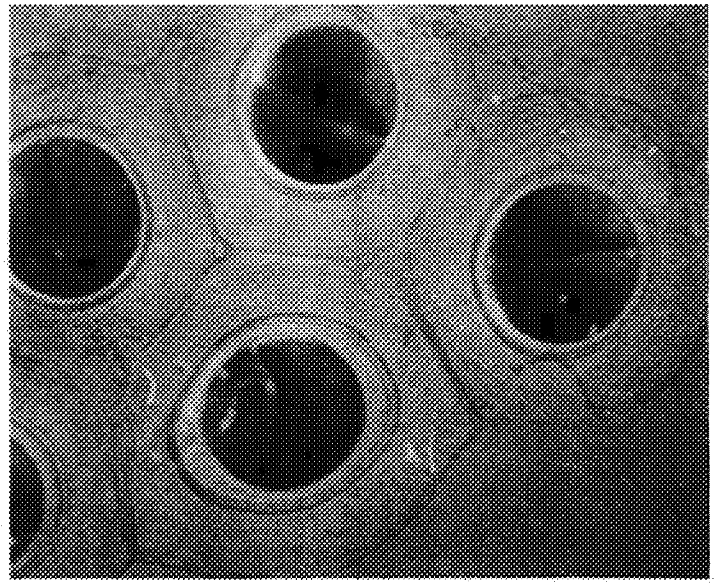

Figure 5-4. - Control embryo (2 hours).

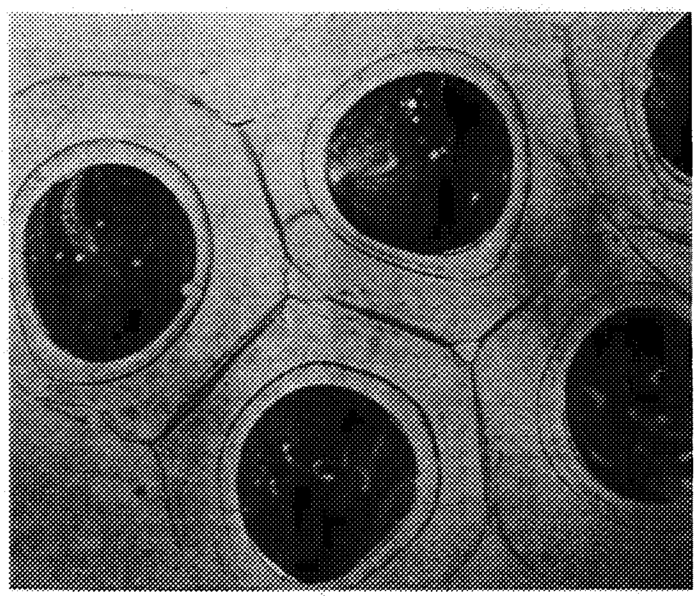

Figure 5-5. - Control embryo (47 hours).

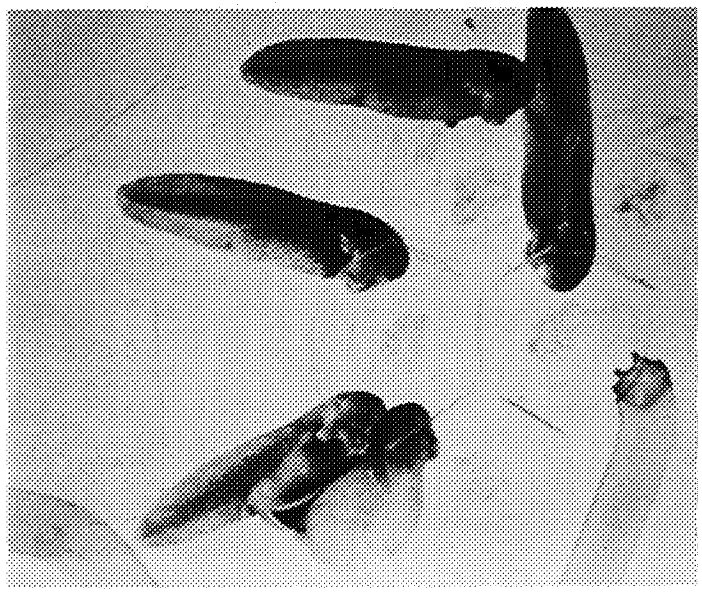

Figure 5-6. - Control embryo (100 hours).

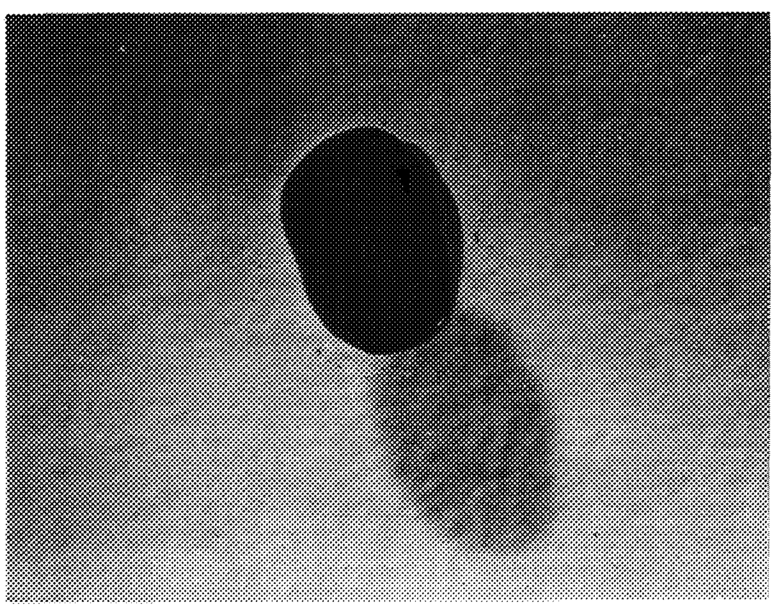

Figure 5-7. - Flight embryo (41 hours).

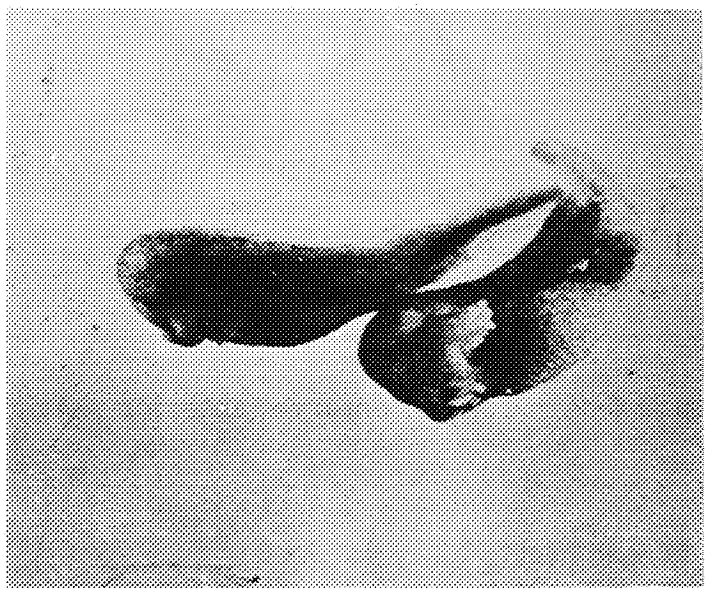

Figure 5-8. - Flight embryo returned alive after 4 days in flight. Shown fixed after recovery.

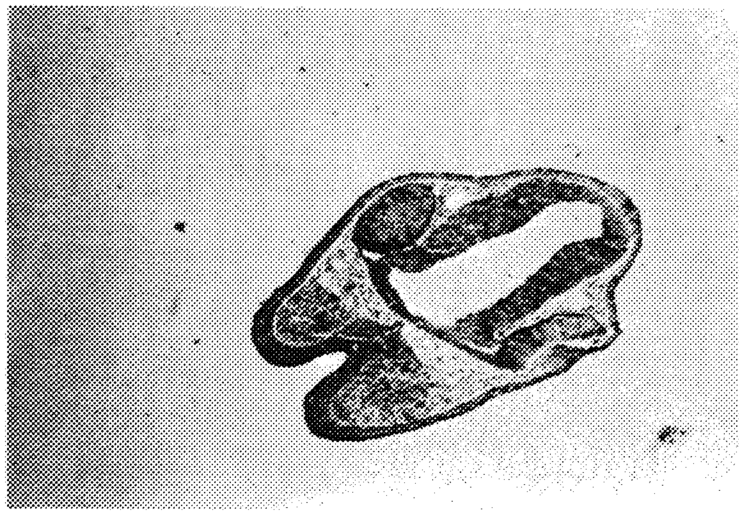

Figure 5-9. - Control embryo (anterior section).

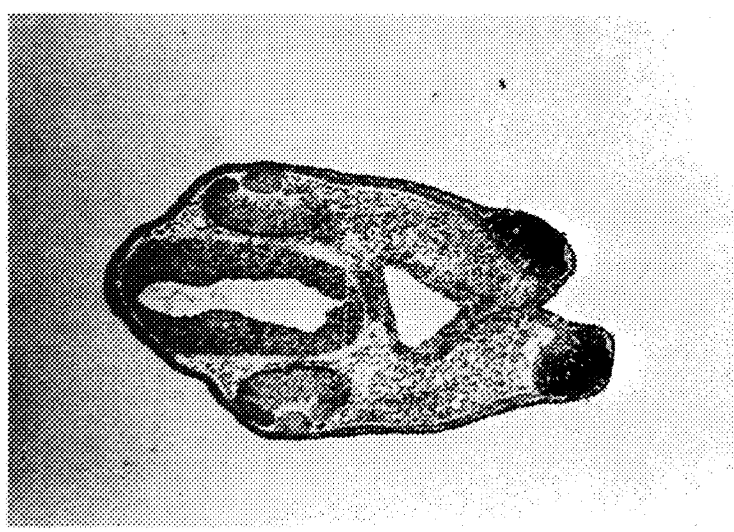

Figure 5-10. - Flight embryo (anterior section).

6. EXPERIMENT S005, SYNOPTIC TERRAIN PHOTOGRAPHY

By Paul D. Lowman, Jr. and
Herbert A. Tiedemann
Goddard Space Flight Center

SUMMARY

The S005 Synoptic Terrain Photography experiment was successfully carried on the Gemini XII mission. The objectives of the experiment were the procurement of high-quality color photographs of selected areas for geologic, geographic, and oceanographic study. About 130 usable pictures were obtained, covering northern Africa, the Middle East, Mexico, the Texas coastal plain, and other areas. Study of pictures of the Makran Range, Iran and Pakistan, suggests the possibility that major thrust faulting has displaced the entire mountain range to the south, possibly by gravitational gliding. A picture of the Sierra Madre Oriental, showing geologic structure, does not support the theory that the deflection of fold axes south and west of Monterrey was the result of a major wrench fault resulting from regional compression and shearing. Tentative conclusions are (1) the scientific value of orbital photography is confirmed, (2) oblique photographs are useful for certain specific geologic applications, (3) focal lengths as short as 38 mm are useful for orbital photography, and (4) interpretation of orbital photographs of heavily vegetated areas requires knowledge of terrain, soil, and vegetation factors.

OBJECTIVES

The Synoptic Terrain Photography experiment, first flown formally during the Gemini IV flight and later on flights V, VI-A, VII, VIII, X, and XI (ref. 1), was again carried on Gemini XII. Experience gained from the earlier missions permitted better experiment planning, but the basic objectives and procedures remained the same.

The purpose of the S005 experiment was to obtain high-quality, small-scale (large-area) color photographs of selected land and ocean areas for geologic, geographic, and oceanographic research.

Continuous strip photography was to include the following areas:

a. Southern India: for geologic study of the Precambrian area and Indian Upper Mantle Project

b. Lower Baja California: for geologic study of the structure of the Gulf of California and for improving geologic maps of the peninsula

c. West Pakistan: requested by U.S. Geological Survey for geologic mapping photography of Gulf of Cambay to the south; also desired for oceanographic research by Bureau of Commerical Fisheries

d. African Rift Valley: for geologic study of the structure of the Rift Valley, which is a prime area of the Upper Mantle Project interest

e. Northwest South America: for geologic study of the structure of the Andes Mountains

f. Southern Mexico, Yucatan Peninsula, Yucatan Straits: for geologic study of the Neovolcanic Plateau, believed to be the continental expression of the Clarion fracture zone, and for oceanographic research

Individual photographs or small groups of photographs of the following areas were desired for oceanographic research by the Navy Oceanographic Office and Bureau of Commercial Fisheries:

a. Mississippi Delta and adjacent waters

b. Ganges Delta and adjacent waters

c. Amazon Delta and adjacent waters

d. Bay of Bengal

e. Arabian Sea

The objectives of the photographs for oceanographic research included photography of the muddy water flowing into the ocean from major rivers and of slicks (relatively smooth patches of water visible as dark areas in glitter patterns).

EQUIPMENT

Two cameras, the Hasselblad SWA Superwide Angle 70-mm camera and the Maurer 70-mm space camera, were used for the S005 experiment. The Hasselblad camera was equipped with a Zeiss Biogon lens of 38-mm focal length and a Hasselblad Haze 63 filter (essentially a UV filter with cutoff at 3400 Å). The film used was Ektachrome MS, S.O. 368. Recommended settings for this film over general terrain were 1/250 second at f 11 and 1/250 second at f 16 for desert areas.

PROCEDURES

As on previous missions, the procedure for the S005 experiment was to take pictures through the spacecraft window when over the selected area or any other cloud-free land area. Specific points emphasized were:

a. Vertical photographs are strongly desired; camera should be pointed straight down or as nearly vertical as possible.

b. Strip photographs (mode 1) should be taken at 5-second intervals; individual or small numbers of photographs (mode 2) should be taken as necessary to cover the area.

c. The spacecraft window should be in the shade to prevent light scattering.

d. Pictures should be taken within about 3 hours of local noon, except for sun glitter pictures, which may require low sun angles.

e. The crew should record time, area, mode, magazine, and frame numbers on the onboard voice recorder and/or the log book.

The crew followed this procedure as closely as possible. In addition, the pilot took a number of photographs during standup EVA which were of excellent quality.

RESULTS

Approximately 130 photographs usable for the purposes of this experiment were obtained during the flight of Gemini XII. Almost all of the photographs were made with the Superwide Angle-equipped Hasselblad camera. The photographs are listed with the reference to the preflight objectives in table 6-I.

The photographs of greatest potential value for photogeological interpretation appear to be those of the areas of southwestern Asia, the northern Red Sea, the Gulf of Mexico, and the Gulf Coastal Plain. In many of the photographs of other areas, enhancement and rectification will be necessary to overcome the effects of poor lighting, tilt, and haze. Cloud cover was, as on previous flights, intense even over normally clear areas such as the Sahara. Representative photographs are discussed in detail and all conclusions are tentative and subject to possible revision.

Figures 6-1 and 6-2 show part of the Zagros-Makran Mountains of southern Iran and western Pakistan. A geologic sketch map has been drawn on the photograph in figure 6-2 to show geologic features of considerable interest. The large anticlines in the foreground, west of the Strait of Hormuz, are most prominent. This area is the source of a substantial part of the world's oil production.

A feature of considerable geologic importance, shown clearly in both figures 6-1 and 6-2, is the abrupt change in structural trends and lithology on the north side of the Strait of Hormuz. This discontinuity is generally shown on small-scale geologic maps as simply a bend in the regional structure. Study of these photographs, in conjunction with the available geologic maps of the area (refs. 2 and 3), suggests that there has been a general southward movement of the Makran Range between the Strait of Hormuz and the Kirthar Range north of Karachi. The apparent displacement of the Pliocene and Miocene rocks, with the continuity of structure along the north side of the Gulf of Oman, is strikingly similar to the outcrop pattern shown by major overthrust faults such as the Pine Mountain overthrust of the southern Appalachian Mountains. It is also similar to the pattern of the Salt Range in northern Pakistan (ref. 4) for which an overthrust origin is suspected.

The Makran Range may represent a remarkable example of overthrust faulting by gravitational gliding, that is, the movement of sheets of rock down slight slopes under their own weight after initiation by uplift and lateral compression. Conditions favorable for gravitational gliding, as summarized by Hubbert and Rubey (ref. 6), include thick sedimentary sections and the existence of a stratum which can serve as a lubricating layer. The stratigraphic section (ref. 2) at Bandar 'Abbas, just north of the Strait of Hormuz, consists of over 24 000 feet of post-Cambrian rocks, and overlies the Cambrian Hormuz salt layer. The Hormuz salt layer could serve as a lubricating stratum because of the plasticity of salt.

Figure 6-3, an oblique view to the north over northeast Mexico, and taken by canting the camera, is another exception to the general rule that vertical photographs are more valuable than oblique ones. In normal practice the camera is aimed directly at the horizon and the principal line is normal to the horizon. The area shown here includes the major deflection of the Sierra Madre Oriental Range south of Monterrey, Mexico, as well as the sharp front of the range to the southeast. The origin of this deflection is not known, but it has been suggested that the folds of the Sierra Madre Oriental Range have been shifted around to the west by a major left-lateral wrench fault, for which the name Saltillo-Torreon fracture zone has been proposed (ref. 6). In a study of the Sierra de la Gavia, northwest of Monterrey, Krutak (ref. 7) applied the strain ellipsoid theory of deformation to the structure and concluded that the Saltillo-Torreon fracture zone is a shear resulting from southwesterly-directed compression.

The Saltillo-Torreon fracture zone is not evident east of the mountain front in figure 6-3. However, because of the foreshortening caused by the camera angle, subtle stream alinements might easily be missed. The foreshortening can be interpreted by applying strain ellipsoid mechanics to the structure. If the Saltillo-Torreon fracture exists and is a shear caused by southwesterly compression, a complementary shear direction at a high angle to the fracture should be evident. As shown on the sketch map, this direction should pass directly under the spacecraft from the vicinity of the bend in the Sierra Madre, and might take the form of stream alinements, rows of igneous intrusives, or alined breaks in ridge lines in the Sierra Madre itself. Furthermore, the foreshortening in the northwesterly direction should accentuate any such trends. Examination of the photograph reveals no definite evidence of the predicted complementary shear direction. Although more orbital photographs of this area should be studied before reaching a conclusion, it appears that the structure south of Monterrey is not a complementary shear structure of the Saltillo-Torreon fracture.

Figure 6-4 shows almost the entire Gulf Coastal Plain of Texas from San Antonio northeast into Louisiana. Interpretation of this photograph is much more difficult than that of photographs of desert regions, chiefly because of the dense vegetation and intensive cultivation. The prominent curved boundary just west of San Antonio is probably the contact between the Cretaceous Comanche and the Navarro series (ref. 8). A dark band just east and southeast of San Antonio appears to correspond to the Tertiary Midway group. Further distinction among Tertiary units to the east cannot reliably be made. It is somewhat surprising to find that the central mineral district, or Llano Uplift, cannot be delineated on this photograph, although the Paleozoic-Cretaceous contact northwest of it can be delineated. To the north, the general outcrop pattern of Gulfward-dipping sediments, which is paralleled by many normal faults, is clearly visible. In this area the effects of bedrock geology are obscured by the combined effects of natural vegetation, farming, topography, and soil types. To the east, in the Gulf of Mexico, sedimentation patterns are visible, which can be used in studying recent sedimentation in this area.

The branching of the Rift Valley into the Gulf of Suez and Gulf of Aqaba is shown in figure 6-5. The fracture pattern expressed in the topography of the opposing shores and the Sinai Peninsula should indicate whether the nature of the faulting which produced the rift is predominatly transverse or normal.

The photograph in figure 6-6, showing the northern Bahama Islands, was taken during the standup EVA. Since the view was not obscured by the spacecraft window, the photograph has excellent color rendition and clarity, and the high degree of visible submarine topographic detail is of particular interest. Such photographs have potential value for revising hydrographic charts after new channels have been cut by major storms.

Comparison of this photograph and similar photographs taken in the same sequence with maps of about the same scale (ref. 9) suggests that the bottom is observable to depths well over 20 meters. In the photograph the boundaries of the Northwest Providence Channel appear to follow closely the 100-fathom contour. In view of the fact that the bottom drops off rapidly, precise position measurements must be made before the actual depths which are visible can be determined.

The mouths of the Irrawaddy River, Burma, and the Gulf of Martaban are shown in figure 6-7. The striking color boundary between the Gulf of Martaban and the Andaman Sea appears to correspond to the 50-meter contour. The color of the Gulf of Martaban is probably affected by muddy water coming from the various major rivers. The nature of the two dark patches in the center of the photograph is unknown and may represent deep water. The dark land areas at the mouths of the Irrawddy River correspond to mangrove swamps typical of deltas in this region (ref. 10).

Figure 6-8 will probably be of little specific geologic value because of the camera angle. However, the photograph shows approximately 250 000 square miles of the western United States, as well as part of northern Chihuahua, Mexico. Topographic features are indentifiable for a remarkable distance. All the major ranges in the photograph are easily indentifiable. In particular, the Wind River Mountains and the Bighorn Mountains in northwest Wyoming are visible in the center far horizon.

CONCLUSIONS

Several tentative conclusions can be derived from the results of the Synoptic Terrain Photography experiment on Gemini XII.

a. The photographs provide further confirmation of the feasibility and value of orbital photographs for geology, geography, and oceanography. The photographs have proved to be of value in the study of the tectonic problems of the Makran Range and the Sierra Madre Oriental province.

b. Although vertical or near-vertical photography is superior to oblique photography, Gemini XII photographs have shown that low oblique photographs, and even high oblique photographs, may be of value for certain situations. The oblique views of the Makran Range served as useful substitutes for vertical photographs. Equivalent areal coverage by vertical photographs would have necessitated a camera altitude of several hundred miles. The oblique views of the Sierra Madre Oriental have been used in the search for structures approximately normal to the horizon and enhanced by the foreshortening due to the photograph.

c. The value of short focal length wide-angle lenses (38 mm) for orbital photography of the earth's surface from altitudes of about 100 nautical miles has been demonstrated. Although the normal focal length lens (80 mm) still appears to provide the best combination of field of view and resolution, the short focal length wide-angle lens (38 mm) can be used successfully under favorable conditions of attitude and visibility.

d. Interpretation of orbital photographs of heavily vegetated regions, such as the Texas Coastal Plain, requires a comprehensive knowledge of a wide range of factors because of the combined effects of bedrock geology, soil, natural vegetation, cultivated areas, and topography. Interpretation of orbital photographs is similar to interpretation of conventional aerial photographs.

REFERENCES

1. Lowman, P. D., Jr.: Geologic Applications of Orbital Photography. Goddard Space Flight Center, X-641-67-68, 1967.

2. Geological Maps and Sections of South-West Persia. Prepared by the geological staff of the British Petroleum Company Limited for the Proceedings of the 20th International Geological Congress, Mexico City, Mexico, 1956.

3. Iran 1:250,000 Series (geological maps). Compiled by Survey Branch, British Petroleum Company, Limited: Bandar 'Abbas (sheets G-40 C and D), Strait of Hormuz (Sheets G-40 I and J and part of G-40 P), 1963.

4. Geological Map of Pakistan, 1:2,000,000. Geological Survey of Pakistan and U.S. Geological Survey, 1964.

5. Hubbert, M. K.; and Rubey, W. W.: Role of Fluid Pressure in Mechanics of Overthrust Faulting. Bull. Geol. Soc. America, vol. 70, 1959, pp. 115-166.

6. Murray, G. E.: Geology of the Atlantic and Gulf Coastal Province of North America. Harper & Bros., New York, 1961.

7. Krutak, P. R.: Structural Geology of the Sierra de la Gavia, Coahuila, Mexico. Bull. Geol. Soc. America, vol. 78, 1967, pp. 59-76.

8. Geological Highway Map of Texas. Compiled by P. F. Oetking, Dallas Geological Society, Dallas, Texas, 1959.

9. National Geographic Atlas of the World. National Geographic Society, Washington, D.C., 1963.

10. The Time Atlas of the World, Mid-Century Edition. Vol. I, Houghton Mifflin Company, Boston, Mass., 1958.

TABLE 6-I.- S005 PHOTOGRAPHY COVERAGE

Area	Number usable photos	Comments
Mode 1 (strip photography), southern		
India	0	One good picture of Great Indian Desert, northwest India
Lower Baja California	16	Several good pictures of Vizcaino Desert
West Pakistan	6	Frames 50 to 54, mag. 11, give continuous coverage of Makran Ranges, with good quality though slightly out of focus
African Rift Valley	13	Excellent coverage of northern Red Sea, Gulf of Suez, Gulf of Aqaba, and Sinai Peninsula
Northwest South America	0	--
Southern Mexico, Yucatan Peninsula, Yucatan Straits	10	Several taken during stand-up EVA, chiefly high-obliques but some good for structure
Mode 2 (individual or pairs)		
Mississippi delta	0	Over a dozen excellent photos of the western Gulf of Mexico taken showing effluent patterns from Rio Grande to Sabine River
Ganges delta	0	--
Amazon delta	0	--
Bay of Gengal	6	Good coverage of Irrawaddy River effluent
Arabian Sea	3	Slicks visible in glitter pattern

TABLE 6-I.- S005 PHOTOGRAPHY COVERAGE - Concluded

Area	Number usable photos	Comments
Unscheduled areas		
Bahama Islands	Several	Excellent pictures, some taken during standup EVA
Southeast Texas	12	Excellent photos of coastal plain
Southern Florida	Several	Fair pictures
Southwest United States	Several	Good high-oblique views to north
Iran	6	Excellent pictures of southern Zagros Mountains
Northern Mexico	Several	Oblique pictures of geologic value
Northern Africa	6	Strip of overlapping obliques of Richat structures; several other excellent pictures of northwest Africa

Strait of Hormuz and Persian Gulf is shown at bottom center; Arabian Peninsula at right.

Figure 6-1. - View to east over Southeast Iran and western Pakistan.

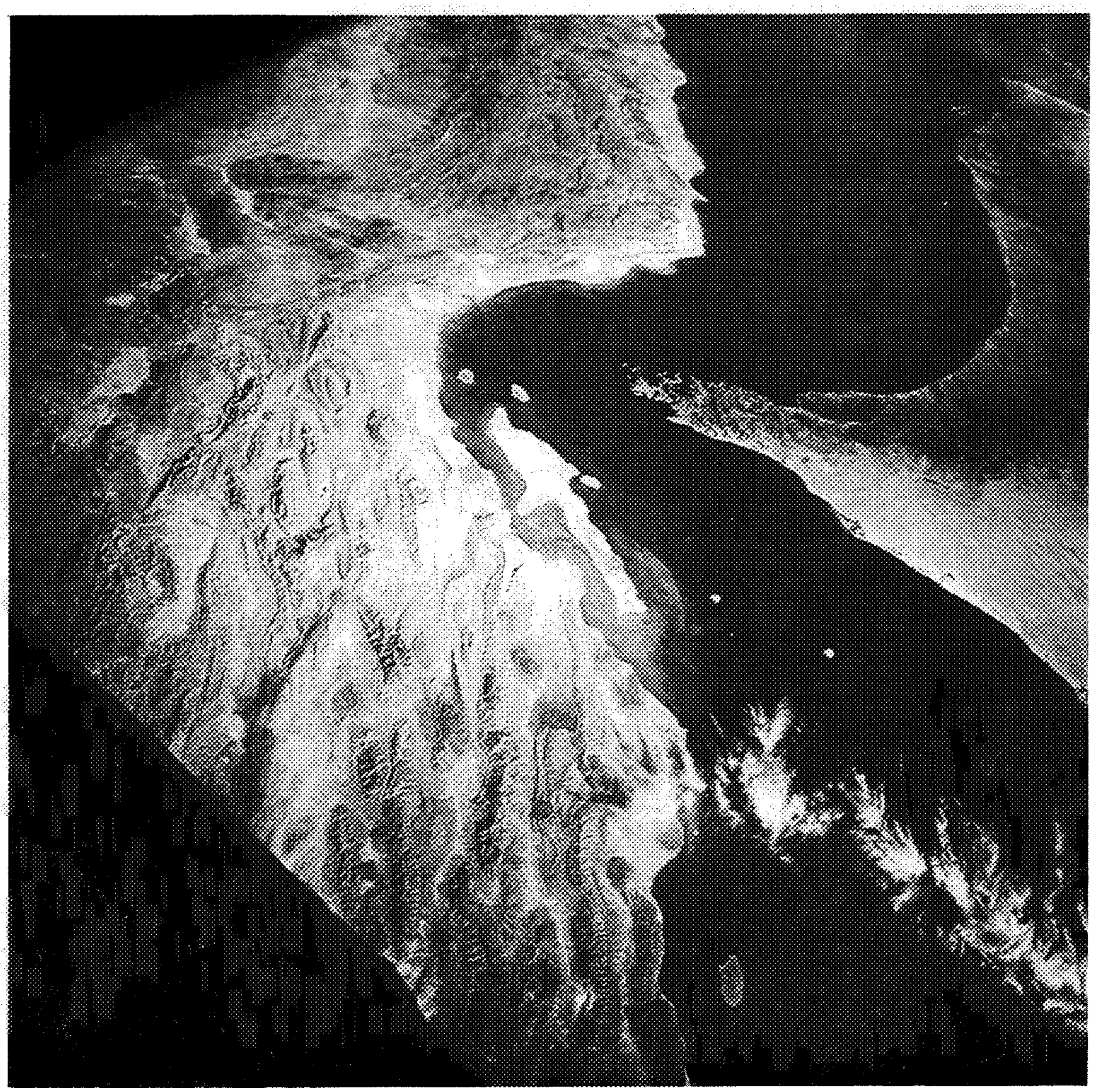

(a) View to east over southeast Iran and western Pakistan (taken on different revolution than figure 6-1).

Figure 6-2. - Photograph of southeastern Iran and and corresponding geologic sketch map.

GEOLOGIC SKETCH MAP
From Gemini XII Photograph S-66-63486
(Magazine 8, Frame 101)

anticlinal axis

generalized fold axes

s salt plug (Hormuz salt)

Lithology from geologic maps of British Petroleum Company, Ltd., U.S. Geological Survey of Pakistan

(b) Geologic sketch map.

Figure 6-2. - Concluded.

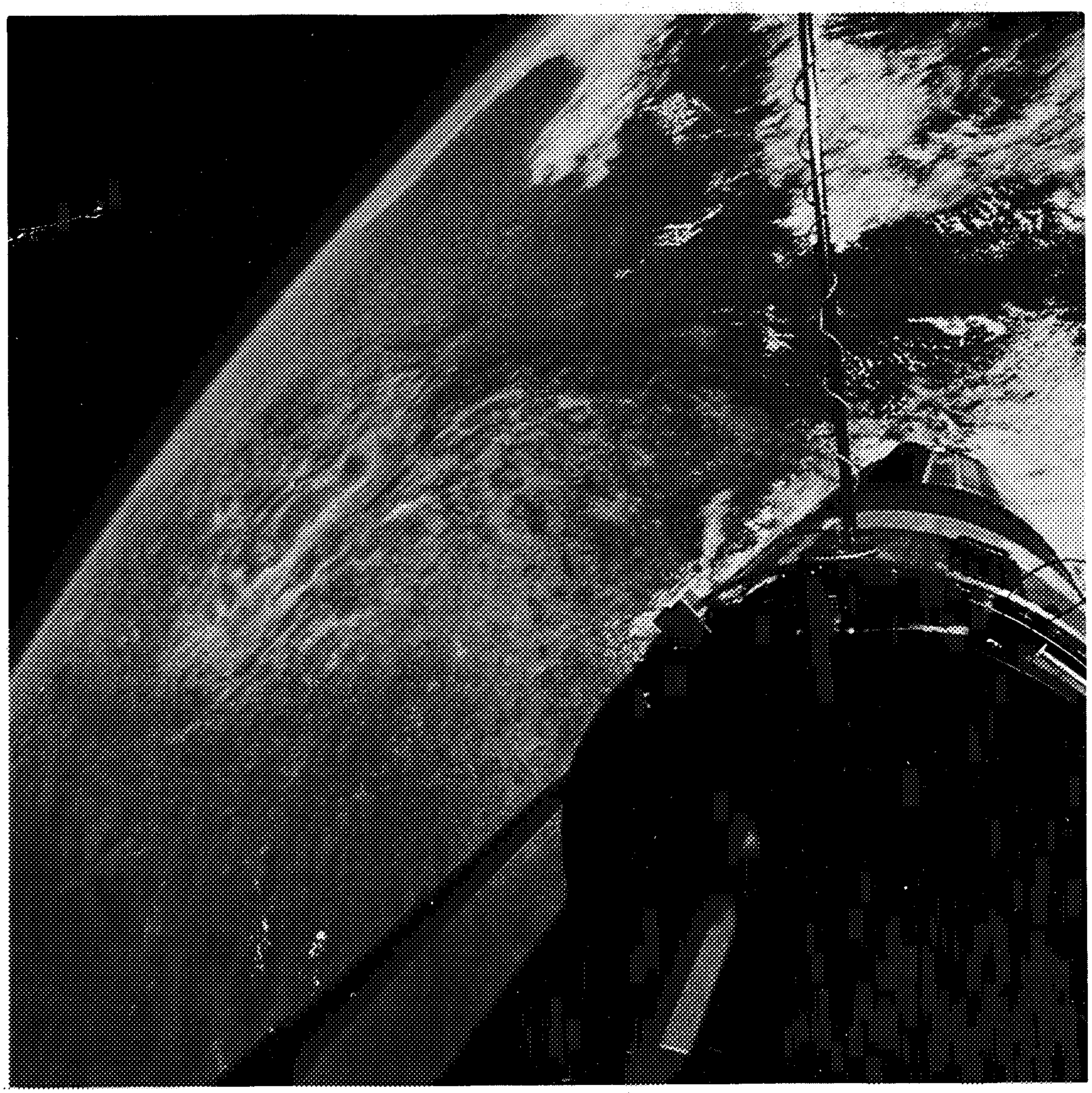

(a) View looking north, taken during standup extravehicular activity.

Figure 6-3. - Photograph of northeastern Mexico and southern Texas and corresponding geologic sketch map.

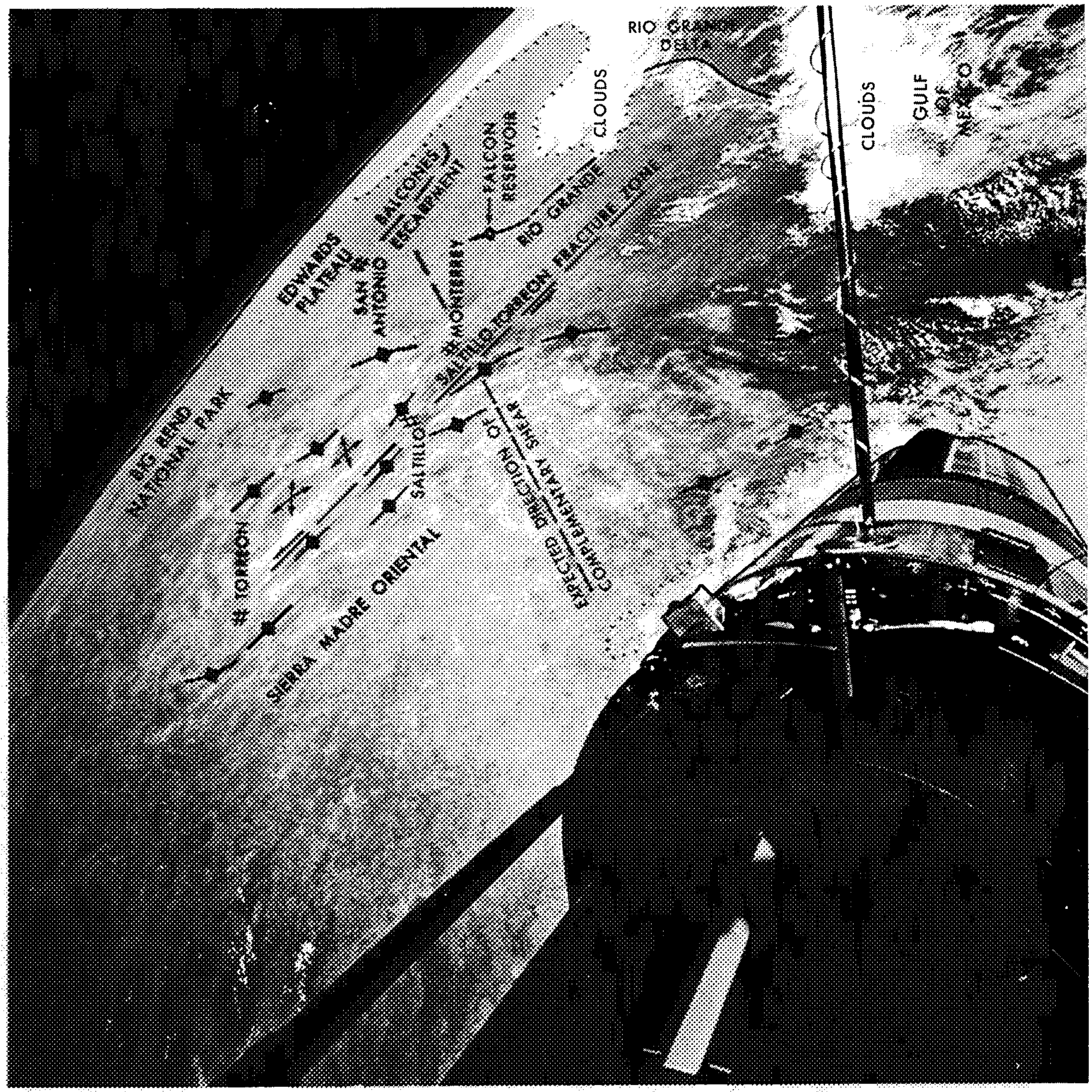

(b) GEOLOGIC SKETCH MAP

From Gemini XII photograph S-66-62889
(Magazine 17, frame 23)

generalized fold axes

city location

uplift

Sources: Krutak (1967), de Cserna (1961)

Figure 6-3. - Concluded.

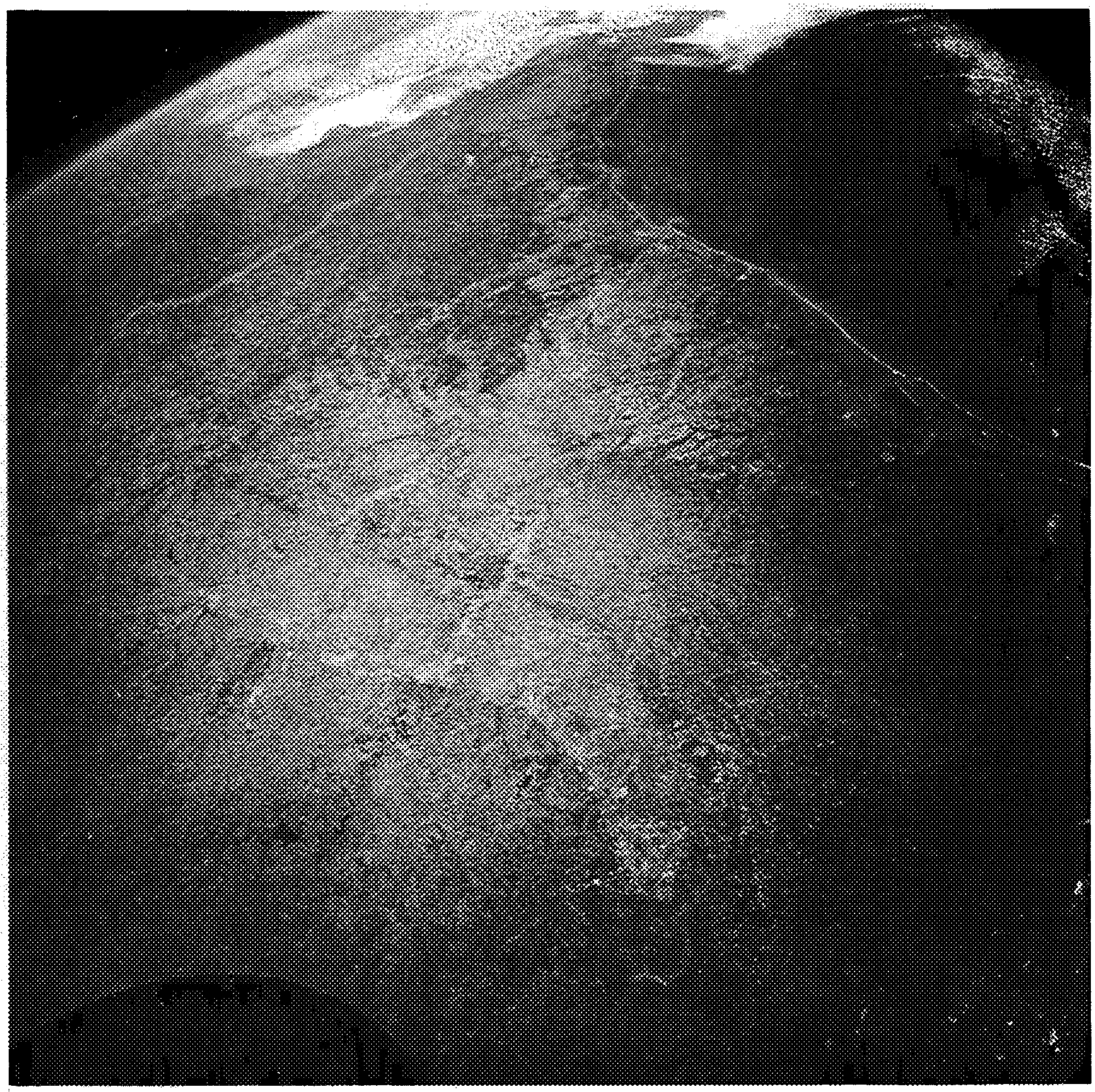

The Gulf of Mexico is visible at upper right; the city of San Antonio is at bottom center, located east of the Balcones Escapement. The boundry of the darker region is the Edwards Plateau.

Figure 6-4. - View to north over Gulf Coast of Texas.

A pipeline fire is visible at extreme upper right; the fire had started a few minutes before photograph was taken.

Figure 6-5. - View to northeast over southern Eygpt, Sinai Peninsula, and Red Sea (lower right).

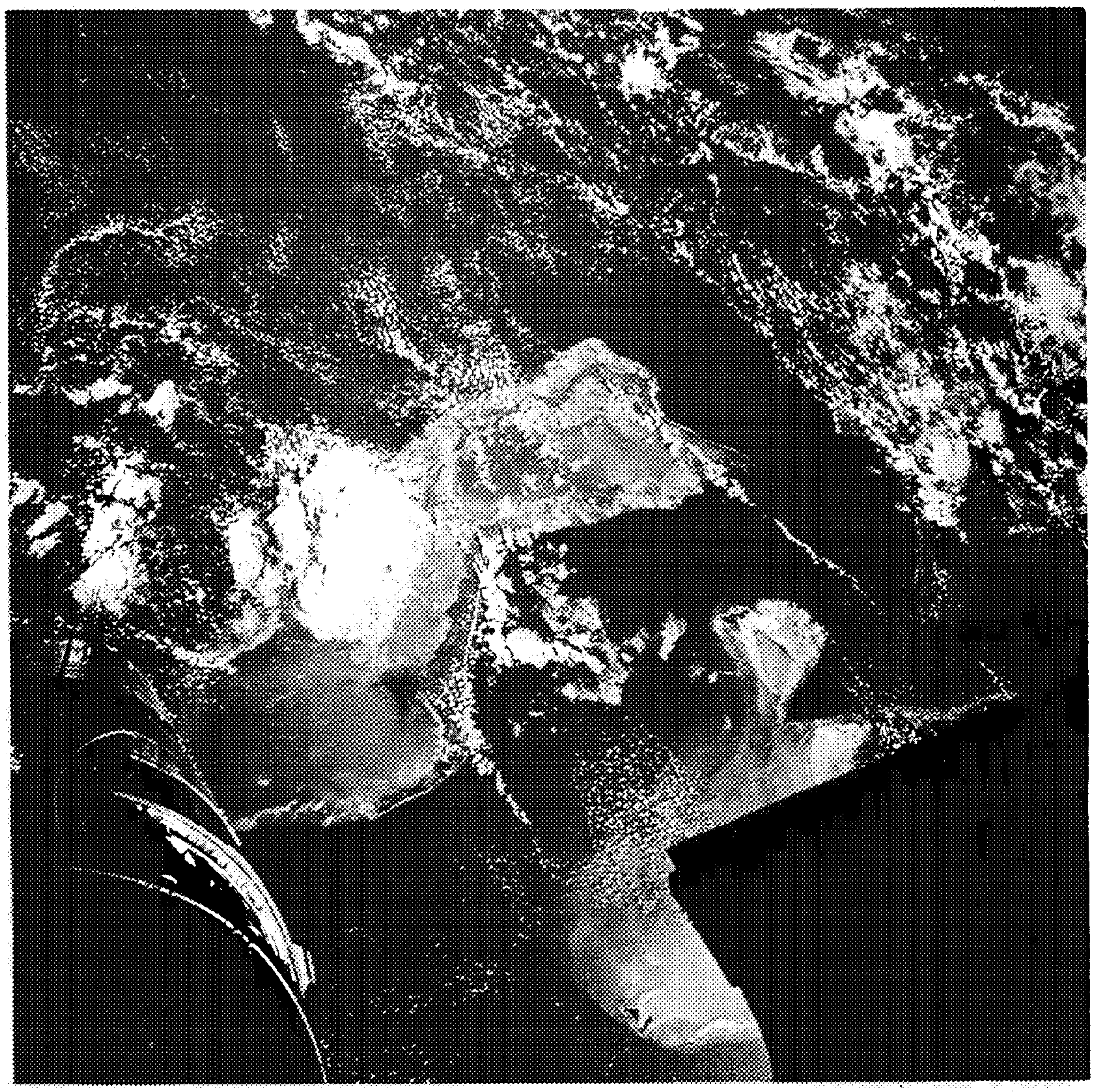

Little Bahama Bank is at left, Great Bahama Bank is below open hatch. Nassau and Eleuthera at upper right, partly cloud-covered. The water depth in light areas generally 10 to 20 feet; depth in dark areas up to several thousand feet.

Figure 6-6. - Photograph of Bahama Islands taken during standup extravehicular activity.

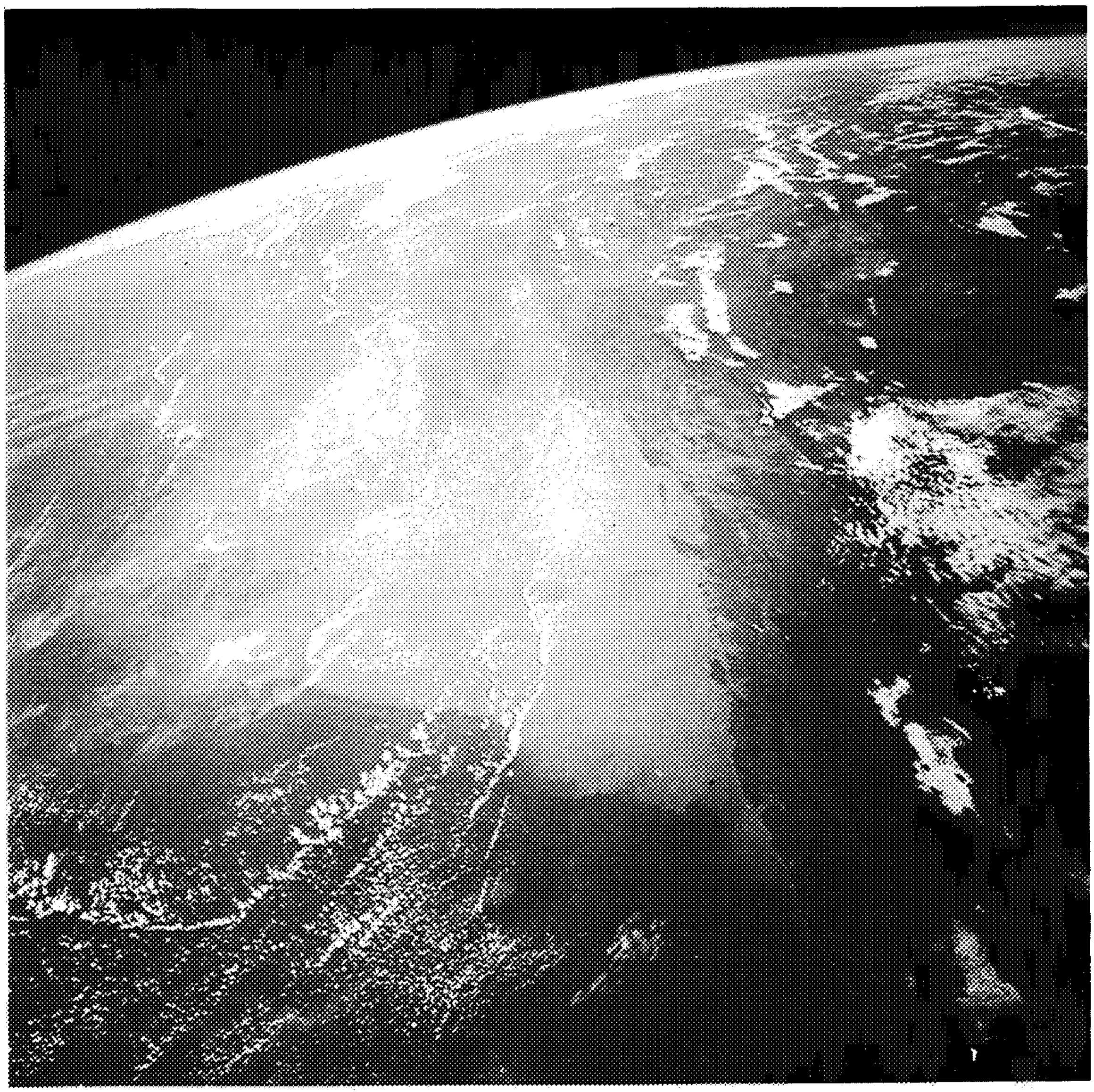

Figure 6-7. - View to north over Gulf of Martaban (light-colored water) and mouths of the Irrawaddy River (left), Burma.

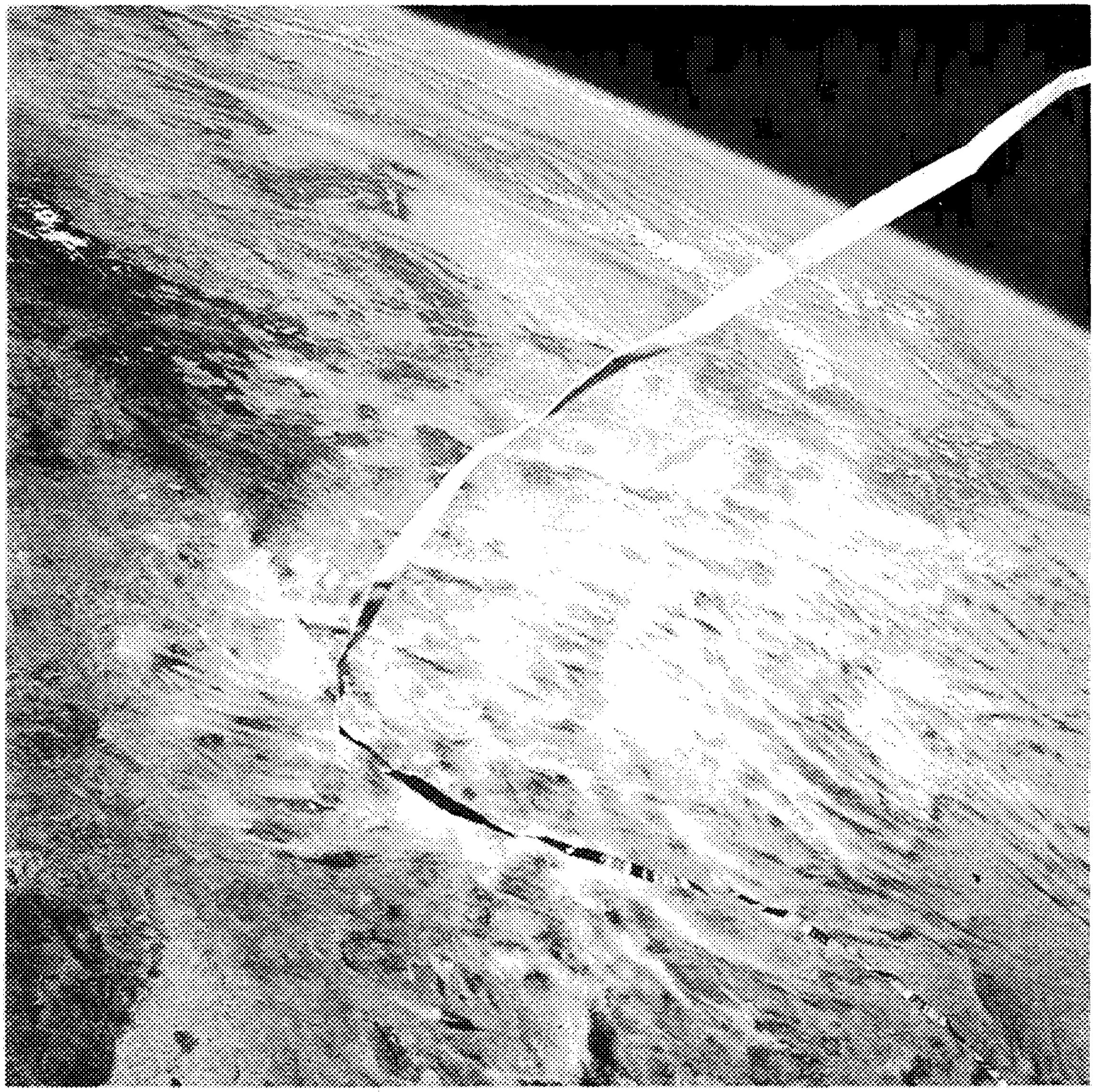

Northern Chihuahua, Mexico, is directly below at bottom; White Sands, New Mexico, is right of bend in spacecraft tether cord. Dark boundry at far right is the eastern boundry of the Rocky Mountains, Colorado. Colorado Plateau is at far left.

Figure 6-8. - View to north of western United States.

7. EXPERIMENT S006, SYNOPTIC WEATHER PHOTOGRAPHY

By Kenneth M. Nagler
U.S. Weather Bureau

and

Stanley D. Soules
National Environmental Satellite Center

SUMMARY

A number of high quality color views of the earth's cloud systems were obtained which are useful in studying atmospheric behavior, in interpreting meteorological satellite pictures, and in teaching meteorological satellite technology.

OBJECTIVE

The objective of the S006 Synoptic Weather Photography experiment was to obtain photographs of clouds for use in studies of the earth's weather systems, and to aid in interpreting weather satellite photography. Another objective stressed in this mission was to obtain views of the same areas on at least two passes during the same day to provide data for the study of cloud change and movement.

EQUIPMENT

Photographs of meteorological interest were taken with the same camera as used for the S005 Synoptic Terrain Photography experiment. Most views were obtained with the superwide-angle 70-mm camera, using a 38-mm focal length and f/4.5 lens. Some pictures of interest were taken with the 70-mm general-purpose camera, using an 80-mm focal length and f/2.8 lens. A haze filter was attached to both cameras.

PROCEDURES

Based on ideas collected from the meteorological community, the crew was briefed well in advance of the mission as to which cloud types were of particular interest. During the mission, weather maps and, especially, weather satellite depictions were studied in order to select areas of potential interest. Constraints of time and fuel for orienting the spacecraft permitted only a limited opportunity during the flight for information on these areas to be passed to the crew and for them to look for the specific meteorological targets and to photograph them.

RESULTS

Approximately 200 photographs obtained during the mission show cloud patterns and are of excellent quality. Several categories of photographed cloud systems are of particular interest for study.

Cirrus Bands

Observations made on the ground and in aircraft have indicated that there often is a band of cirrus clouds on the equatorial side of the core of the upper westerly winds. These "jet stream" cirrus clouds also appear frequently on weather satellite pictures and are used to approximate the location and orientation of upper-wind maxima. These cloud bands have been observed recently to extend for thousands of miles, sometimes from near the equator to middle latitudes. The flight crew obtained several excellent views of this phenomenon in response to real-time requests. Figure 7-1 shows a narrow cirrus band of this type above the Red Sea. A photograph taken on the previous revolution showed the band location to be about the same, but with certain changes in the cirrus elements comprising the band.

Other views of "jet stream" cirrus were obtained over western North Africa, over western Mexico, and (above lower frontal cloudiness) across the southeastern United States as shown in figure 7-2. The wind maximum at the cirrus level in that area (approximately 30 000 feet) was about 100 knots.

Vortices in the Lee of Islands

Vortices occurring in stratocumulus clouds in the lee of mountainous islands have been the subject of several recent studies. Figure 7-3 shows several such vortices in the lee of Guadalupe Island, off the west coast of Mexico.

Cellular Patterns

Also shown in figure 7-3 are cellular patterns which are the result of organized convection in areas of little wind shear. In this photograph, both the "open" and "closed" types occur in proximity, the former with ascending motion around the edges of the cell and descending motion in the center, and the latter with a circulation in the opposite sense.

Sunglint

Sunglint patterns, often appearing on weather satellite pictures, are related to sea conditions and, hence, to wind speed. The flight crew obtained a number of sunglint photographs. Figure 7-4 shows a very large area of reflected sunlight. Winds in the area were less than 10 knots and in some parts of the area less than 5 knots. Ship observations in the same area reported sea waves of 3 feet or less in height.

Views of Areas on Several Passes

Of interest are views of the same cloud systems on successive revolutions, notably over the southern United States. These are being studied relative to change and cloud movement.

Atmospheric Pollutants

Several interesting pictures of atmospheric contaminants were obtained. For example, figure 7-5 shows that fires on the Louisiana coast (on Marsh and Pecan Islands) created smoke plumes which were visible some 100 miles out over the Gulf of Mexico. The western plume, from Pecan Island, provides an example of weak atmospheric diffusion. The line of brighter clouds where the plume enters the cumulus cloud area may be related to condensation nuclei in the smoke.

Figure 7-6 shows a striking view of a duststorm. Clouds of dust from southern Iran were carried by northerly winds for nearly 100 miles over the Gulf of Oman.

Other Features

Other features of interest photographed during this mission are the smoke spread from fires, clouds near island weather stations which can be related to a concurrent atmospheric sounding, cloud streets, and clouds associated with a typical frontal low pressure system in the North Pacific and another in the North Atlantic.

Comparison with Weather Satellite Photography

Daily coverage of most of the world by the ESSA III meteorological satellite provides photographic data for comparison with the photography from this experiment. The Gemini XII photographs and those taken on previous flights are being extensively used in studying and interpreting the meteorological satellite views.

CONCLUSIONS

The flight crew obtained a variety of interesting and significant views of cloud formations. Added to the collection of views from previous missions, these Gemini XII pictures will continue to be used in research and training for many years. The Synoptic Weather Photography experiment has made a definite contribution to the knowledge of the earth's cloud systems.

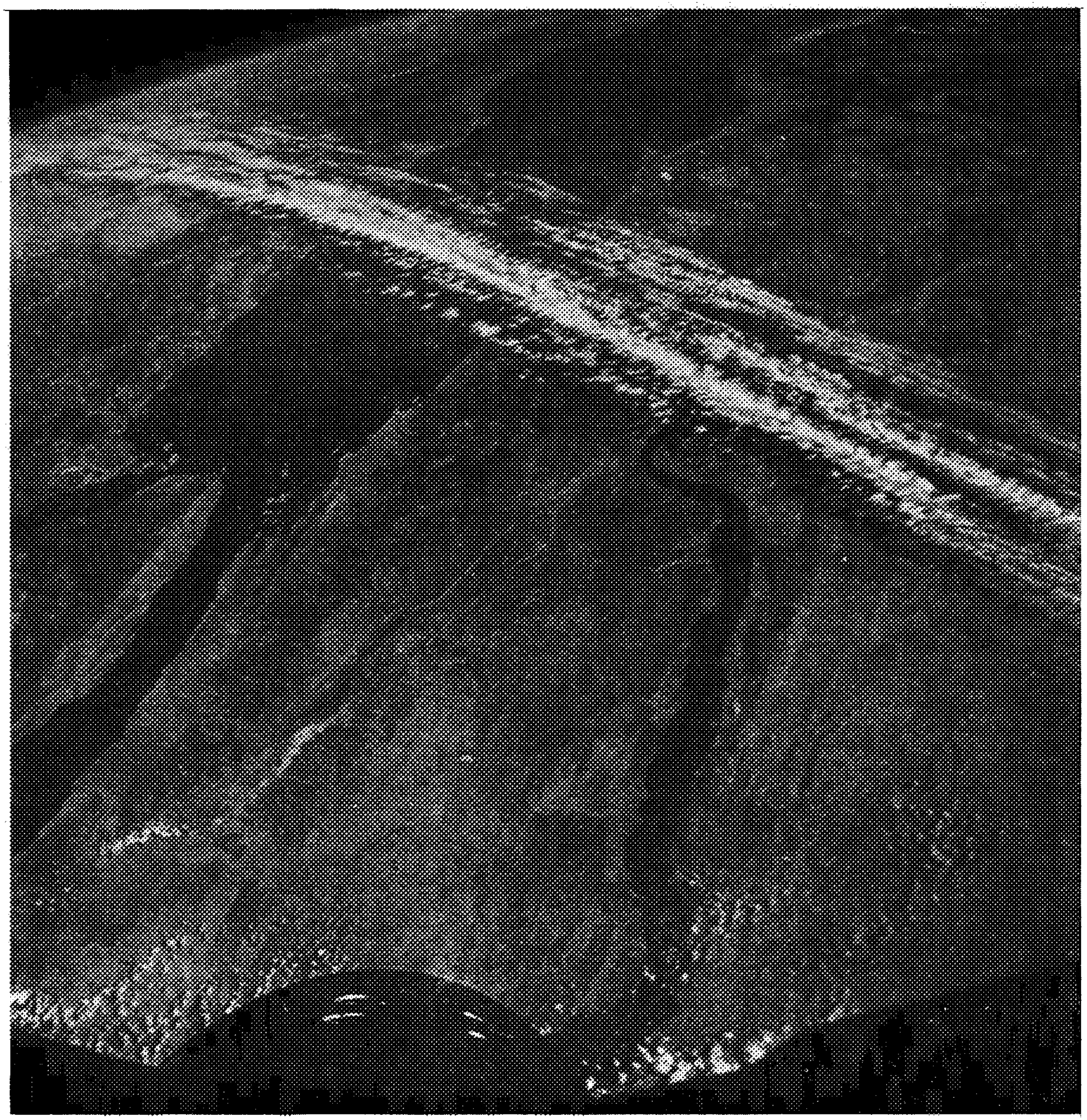

Spacecraft is looking down with southeast at top of page. Taken at 61 hours 18 minutes g. e. t. on November 14, 1967.

Figure 7-1. - A band of cirrus clouds showing strong upper winds above the Red Sea area.

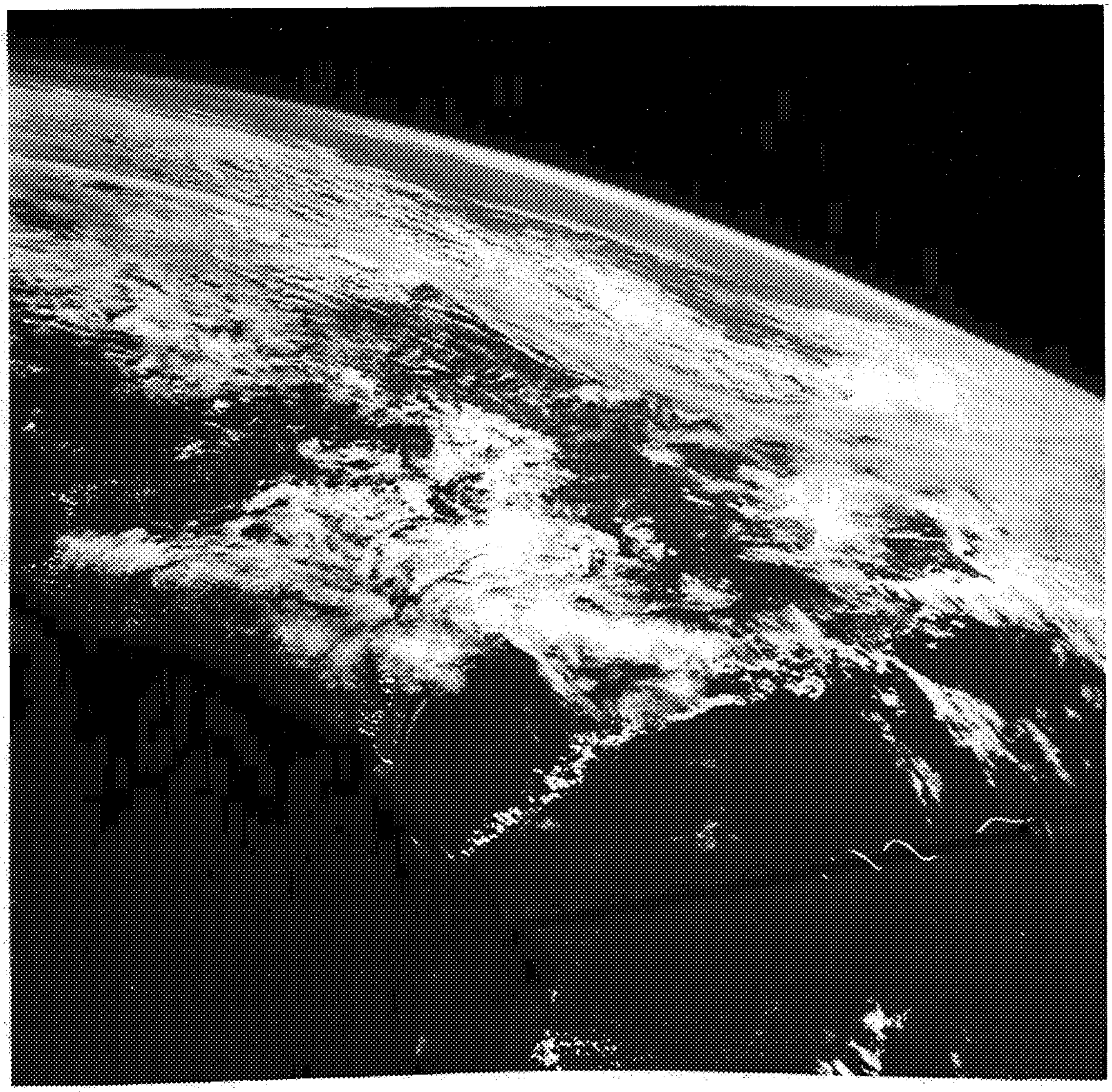

Spacecraft is pointing down looking northward with Florida in the foreground. Taken at 19 hours 15 minutes g. e. t on November 12, 1966.

Figure 7-2. - A narrow band of cirrus shown is above lower frontal clouds over the southeastern United States and adjacent portion of the Atlantic Ocean.

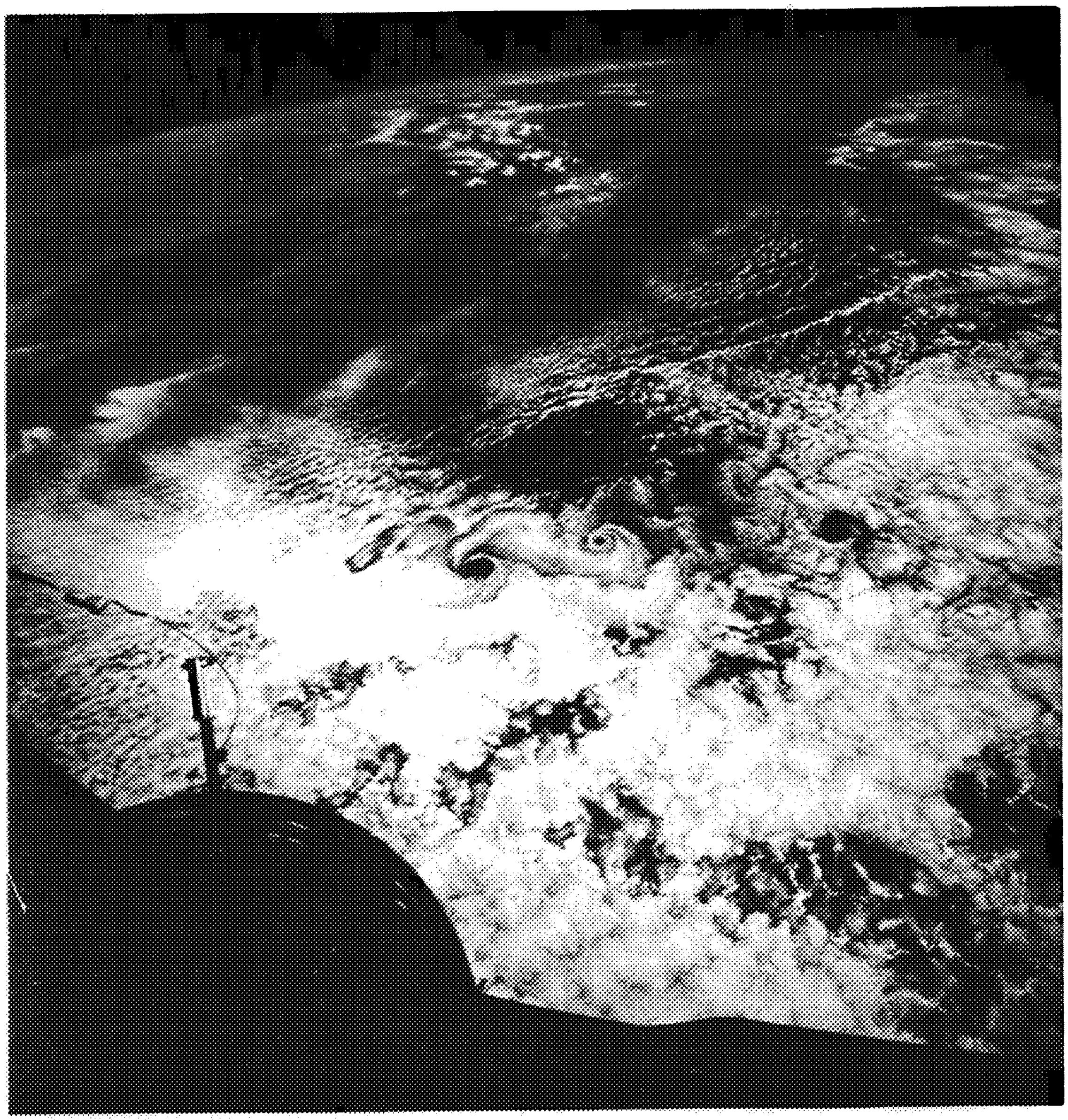

Spacecraft is pointing toward Baja, California, looking eastward. Taken at 46 hours 13 minutes g.e.t. on November 13, 1966.

Figure 7-3. - Vortices and cellular cloud patterns in stratocumulus clouds near the Guadalupe Islands.

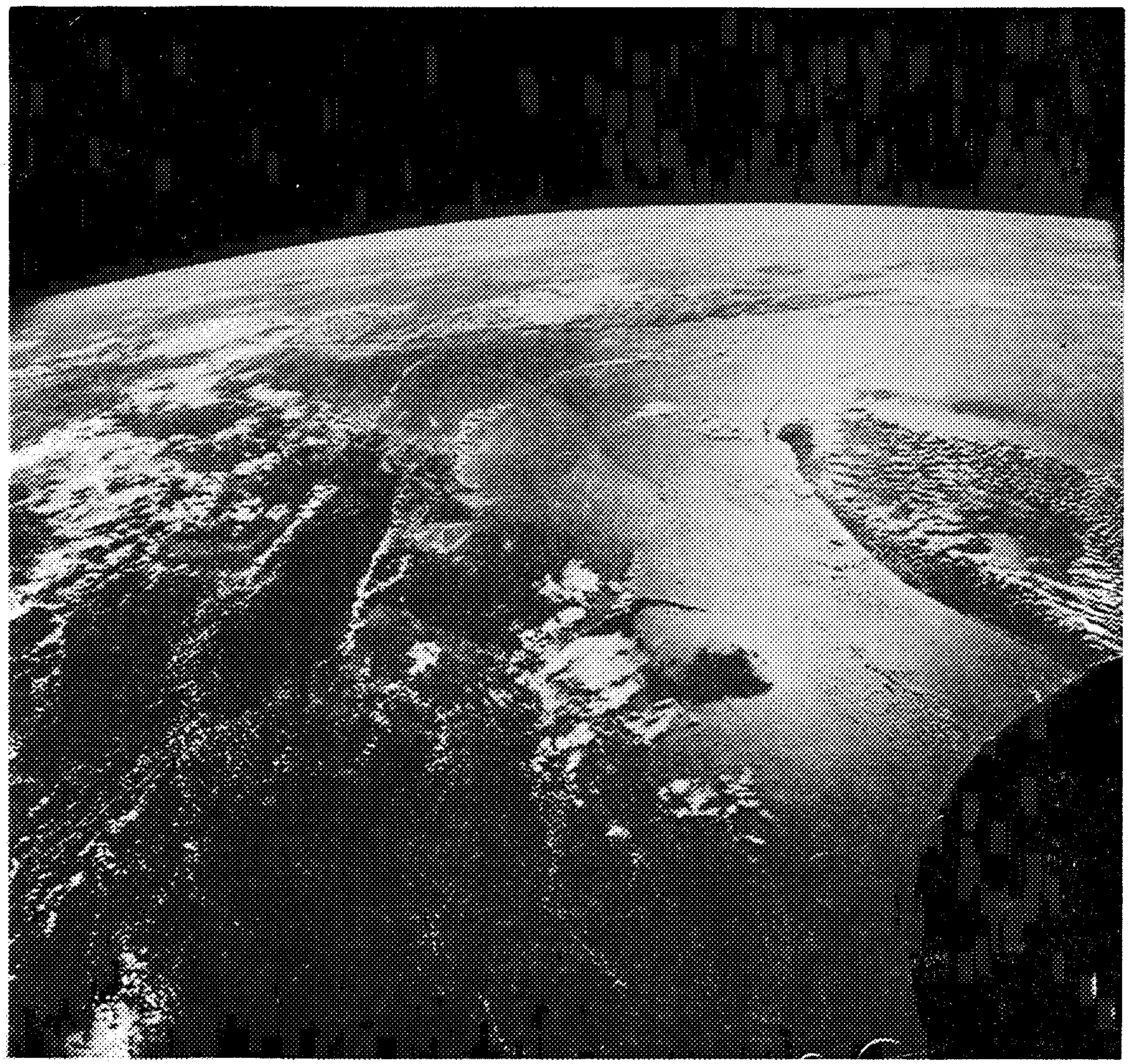

Spacecraft is pointing south with Cuba in the background. Taken at 22 hours 32 minutes g. e. t. on November 11, 1966.

Figure 7-4. - Sunglint from the ocean surrounding the southern part of Florida on the right and nearby Bahama Islands in the foreground.

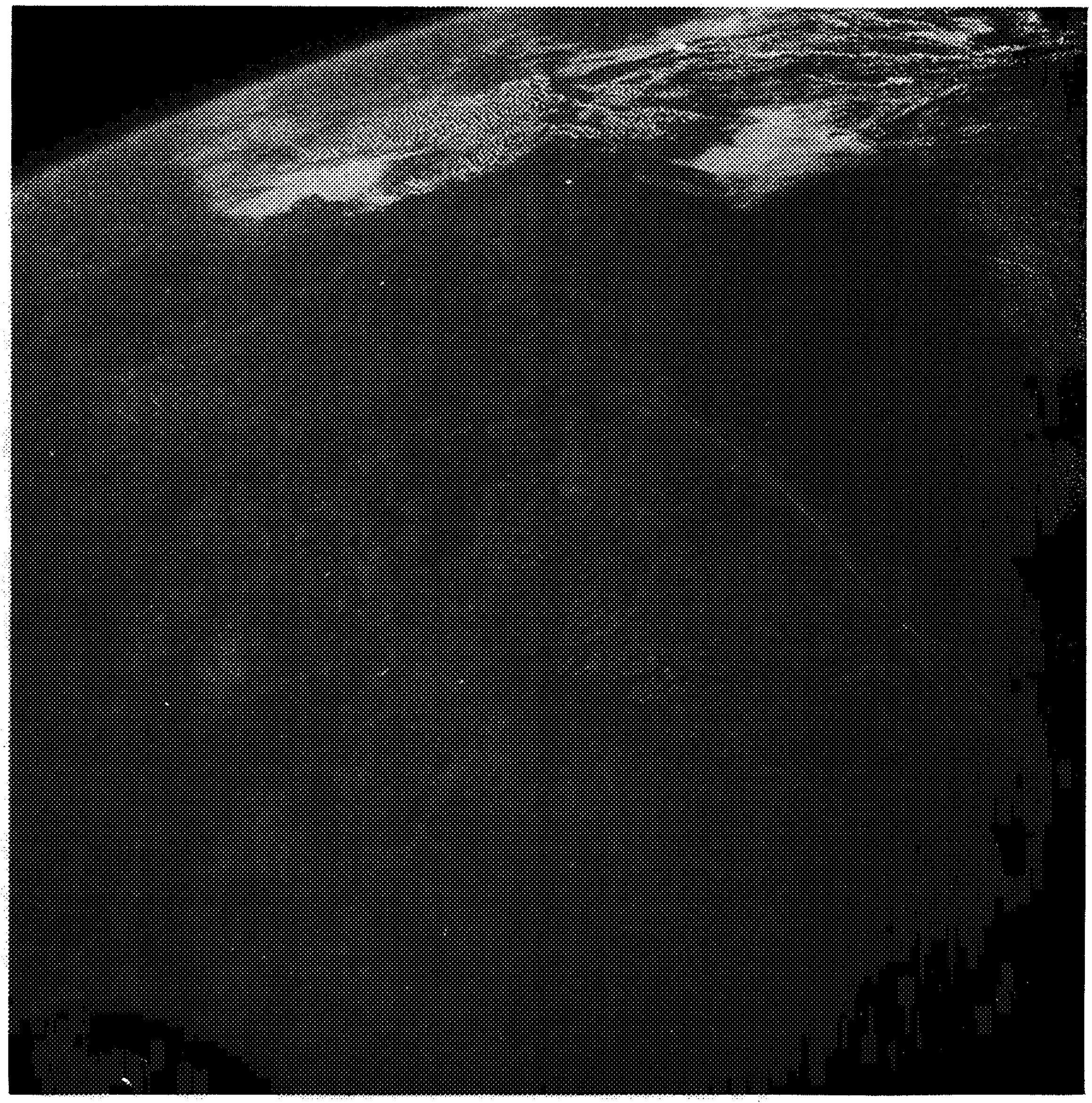

Plumes of smoke extend from the Louisiana coast well out over the Gulf of Mexico. The western-most plume is very narrow and seems to have caused increased cumulus cloud development where it intersects the cloud area.

Figure 7-5. - A view of Texas-Louisiana area looking eastward.

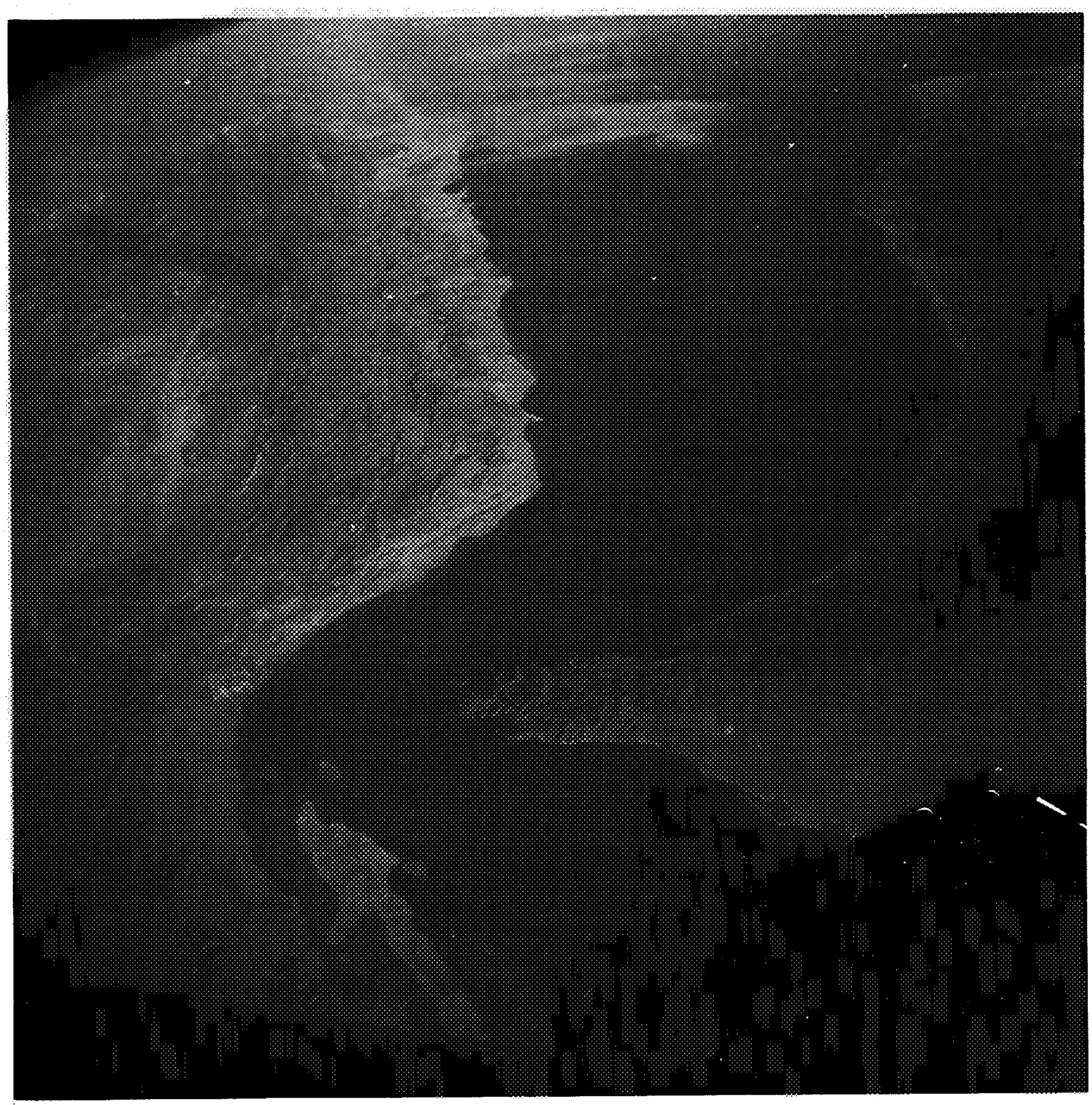

Windblown dust from Iran on the left extends about 100 miles offshore.

Figure 7-6.- A view looking eastward of the Gulf of Oman.

8. EXPERIMENT S010, AGENA MICROMETEORITE COLLECTION[a]

SUMMARY

During extravehicular activity (EVA) when the Gemini spacecraft was docked to the Gemini Agena Target Vehicle (GATV), the S010 micrometeorite experiment hardware was activated by the extravehicular pilot. The S010 hardware was left on the GATV for possible recovery during a later mission. The calculated GATV lifetime was 84 days, which was insufficient for experiment retrieval during any later mission. Consequently, no data are available for evaluation and analysis.

OBJECTIVE

The scientific objective of the S010 Agena Micrometeorite Collection experiment was to study the micrometeorite content of the upper atmosphere and near-earth space environment. This was to be accomplished by (1) exposing polished metal and plastic surfaces to the particle flux for later study of the resulting impact craters, (2) exposing highly polished sections of meteorite material to the particle flux for obtaining direct measurement of meteor-erosion rates, (3) exposing optically polished glass surfaces to the particle flux for determining the deterioration of optical surface properties, (4) exposing thin films to the particle flux to observe thin-film penetration, and (5) exposing extremely clean surfaces to the particle environment in an attempt to collect ultrasmall particles.

EQUIPMENT

The hardware configuration consisted of an aluminum structure designed to provide a mounting platform for the polished plates and collection surfaces. The device was interfaced with the GATV by a mounting plate which allowed detachment of the experiment hardware from the vehicle. Cratering samples were installed on the outside surface of the aluminum structure. During powered flight and the insertion phase of the mission, these external surfaces were protected from direct impact of airborne particles by a fairing which directed airflow over the

---

[a]Principal Investigator is Dr. Curtis L. Hemenway, Dudley Observatory.

mounting. During EVA the pilot removed this fairing cover. Figures 8-1 and 8-2 show the S010 hardware in both the closed and open positions attached to the GATV. Figure 8-2 includes the actual placement of specimens within the hardware package.

PROCEDURES

During EVA and while the spacecraft was docked with the GATV, the extravehicular pilot activated the S010 micrometeorite experiment hardware, thereby exposing the inner collection surfaces to the outside environment. This occurred at 43 hours 11 minutes g.e.t.

RESULTS

The S010 hardware was left on the GATV for possible recovery during a later mission. After Gemini XII recovery operations were completed, an attempt was made to put the GATV into a higher, longer-life orbit. The attempt failed because of primary propulsion system malfunctions. The calculated GATV lifetime was 84 days, which is insufficient for experiment hardware retrieval during any later missions.

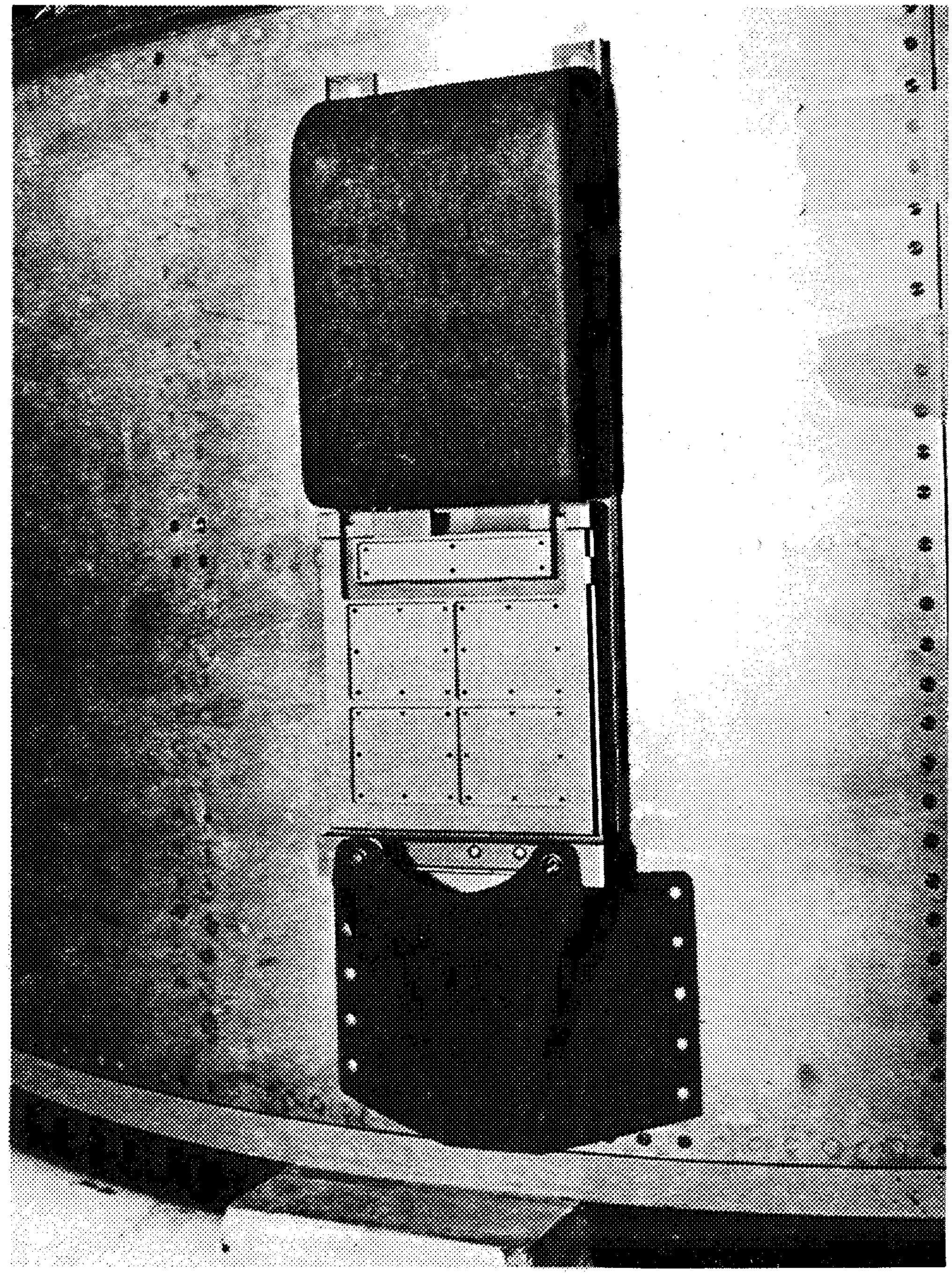

Figure 8-1. - Experiment S010, micrometeorite collection device installed in launch configuration.

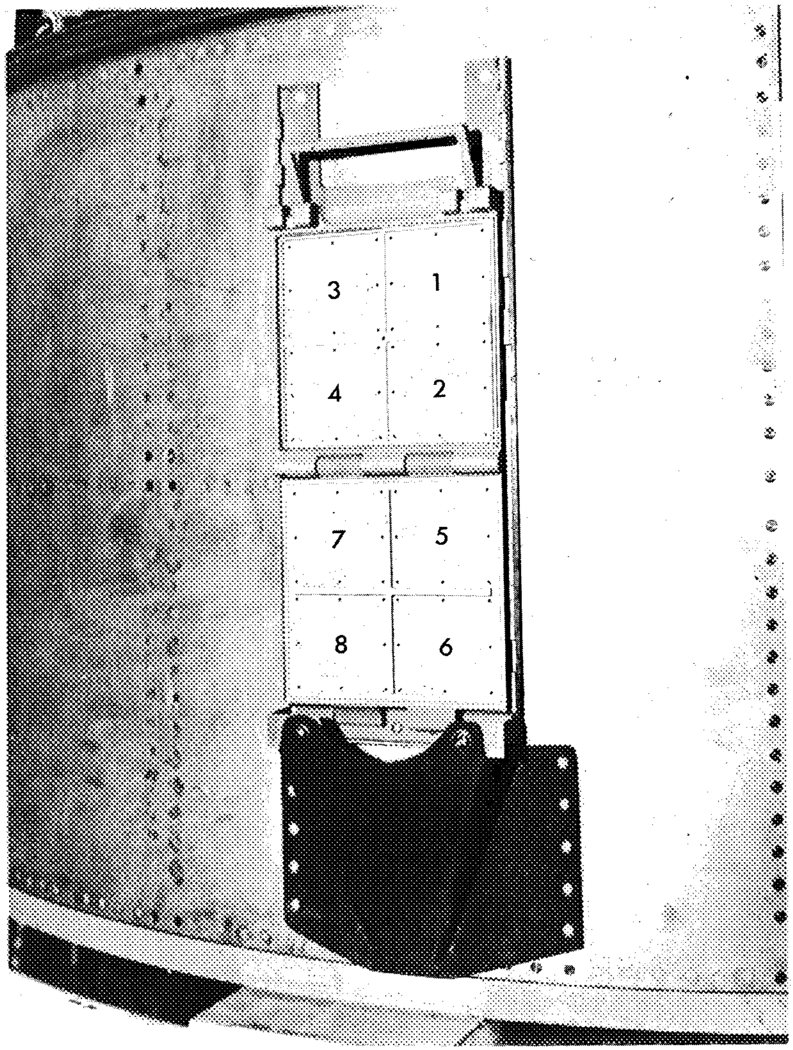

1. Shielded screening
2. Chronium-coated glass
3. Biological exposure with filters
4. Glass
5. Polished glass
6. Gold foil two μ thick; two layers plus thick plastic film below
7. Stereoscan samples, copper and stainless steel
8. Stainless steel

Figure 8-2. - Experiment S010, specimen loading.

9. EXPERIMENT S011, AIRGLOW HORIZON PHOTOGRAPHY

By M. J. Koomen and R. T. Seal, Jr.
E. O. Hulburt Center for Space Research
Naval Research Laboratory

and

J. Lintott
Manned Spacecraft Center

SUMMARY

Twenty-three useful photographs of the sunlight and night airglow were obtained with the 70-mm general-purpose still camera using narrow-band objective filters or without filters during the Gemini XII Missions The objective filters band half-widths were 55 Å, 44 Å, and 150 Å, centered respectively on three optical emission bands of 5577 Å, 5893 Å, and 6330 Å. A shutter malfunction in the red lens assembly occurred during the experiment and produced several overexposed frames.

OBJECTIVE

The primary objective of the S011 Airglow Horizon Photography experiment for the Gemini XII Mission was to obtain photographs of the twilight and nighttime airglow using narrow-band objective filters. Another objective was to take several photographs without the use of optical filters.

Three optical emissions bands were chosen for study — the green line at 5577 Å caused by atomic oxygen, the sodium D lines at 5893 Å, and the oxygen red line at 6330 Å. The first two emission band lie in layers centered at an altitude of approximately 100 kilometers and can be photographed edge-on from nominal orbital altitudes (fig. 9-1). The red line occurs at a higher altitude and must be photographed from an altitude 300 kilometers or greater.

EQUIPMENT

The basic components are shown in figure 9-2. These include the 70-mm general-purpose still camera with a f/0.95 lens and two film magazines loaded with black and white Eastman 103-D film. These magazines were shared with the S029 and S051 experiments. The split-field focal plane filter arrangement used on previous missions was not used on this mission. A circular mask at the focal plane gave a total field of 45°. Three narrow-band objective filters which allowed passage of more selected color radiation were used instead of the split-field arrangement. These filters have peak transmittances occurring at wavelengths of 5577 Å (green), 5893 Å (yellow), and 6330 Å (red). The green and yellow filters had half widths of 45 Å and 55 Å, respectively. The red filter had a half width of 150 Å in order to photograph the 6300 Å to 6364 Å doublet emission bands caused by atomic oxygen. An illuminated sight mounted on top of the camera was used with an adjustable window-mounted bracket so that camera motion in the pitch plane could be minimized. The camera could be aimed toward the horizon for exposure times up to 20 seconds.

PROCEDURE

To obtain as many twilight exposures as possible, the experiment activities were scheduled and accomplished during three revolutions. The first two sequences were scheduled for the two planned high-apogee orbits. During the first sequence, beginning at 24 hours 13 minutes ground elapsed time, five exposures using the red filter were made of the western sunlight airglow after sunset. Exposure times ranged from 4 to 40 seconds, increasing with time from sunset. Seven exposure were made during the night portion of this same revolution. These included three photographs without any filter and two each with the red and green filters.

For the second sequence, beginning at 25 hours 43 minutes ground elapsed time, the procedures were the same except that the yellow filter replaced the red filter. The third and last sequence commenced at 70 hours 45 minutes ground elapsed time, and consisted of three twilight exposures with the yellow filter, followed by eight 3-second exposures of the night airglow without any filter. For these latter pictures, the spacecraft was yawed 50° between exposures.

RESULTS

The flight crew obtained 23 good pictures of the sunlight and night airglow in the wavelength bands described. Since data reduction is continuing, only 12 photographs have been closely examined. The average of all photographs including several at twilight yielded an airglow altitude of 88 ± 5 km with no geographical dependence. The two emissions, 5577 Å and 5893 Å, were within the same altitude range. The greater variation in measure altitude from the ± 3 km limits of the airglow measurements from the Gemini IX Mission, may reflect an increased experimental error. This could be present because the Gemini XII Mission occurred during the period of new moon.

The airglow photographs from the Gemini XII Mission are typically like that of figure 9-3 which shows a 3-second exposure taken to the west over South Africa. The earth is now completely dark except for the light from the cities or lightning flashes, and the top of the atmosphere is now defined not by the moonlight horizon line but by the attenuation of stars and airglow background. This photograph also shows that the atmospheric attenuation has an extremely steep gradient. The top of the atmosphere for attenuation is effectively at 25 kilometers. This value has been included in the computed airglow heights.

In the oxygen-green and solium yellow photographs, there is clear evidence that the primary emission line is recorded on the film, with negligible contaminating radiation. A minimum thickness of 18 kilometers was recorded for the yellow band, and 20 kilometers for the green. The maximum thickness recorded with some reliability was 30 kilometers for both yellow and green. A typical 20-second exposure using the green filter in showing in figure 9-4.

No high-apogee orbits were attained during the mission; however, the twilight photographs with the 6300 Å filter do show a low-layer emission band, presumably caused by the OH radical which emits in the red wavelengths (fig. 9-5). This is the first photograph of an OH from a spacecraft and represents an interesting and useful addition to airglow observations.

The shutter in the f/0.95 lens assembly stuck in the open position many times during the experiment and caused several overexposed frames in addition to the 23 good photographs that were obtained. The flight crew repeated several frames when they were aware of the malfunction. Much of the experimental success can be attributed to the crew's inflight efforts. Since the shutter malfuction did cause deviations from the timing of the scheduled experiment sequences, the geographical location of the spacecraft during some of the exposures will have to be redetermined.

Camera Failure Analysis

The primary camera failure was an open shutter in the red lens assembly, thereby overexposing the photographic film. The probable cause for the open-shutter condition was the use of forces exceeding design limits when mounting the red lens assembly to the camera body and misalinement of the shutter actuating coupling due to partial camera shutter cock. The coupling misalinement can cause dowel pin deformation, resulting in a chain of misalinement and possible shutter override, thereby preventing the return movement of the shutter mechanism.

Rocket Experiments

Though it appears that the important yellow and green emissions arise at almost the same altitude, it may still be of interest to measure small differences in altitude by the split field method of figure 3-5 using narrow band filters. This was attempted from an altitude-controlled Aerobee rocket launched from White Sands, New Mexico on June 9, 1967. An objective filter having two 120 Å bands centered at 5577 Å and 5893 Å was used with an f/2.8, 50-mm camera. An image intensifier was interposed between the image and film (Eastman No. 2475).

The radiations entering the filter bands differ in altitude by no more than 5 km. The equipment was recovered in operating condition, and the experiment will be repeated with filter bands of 15 to 20 Å half-width.

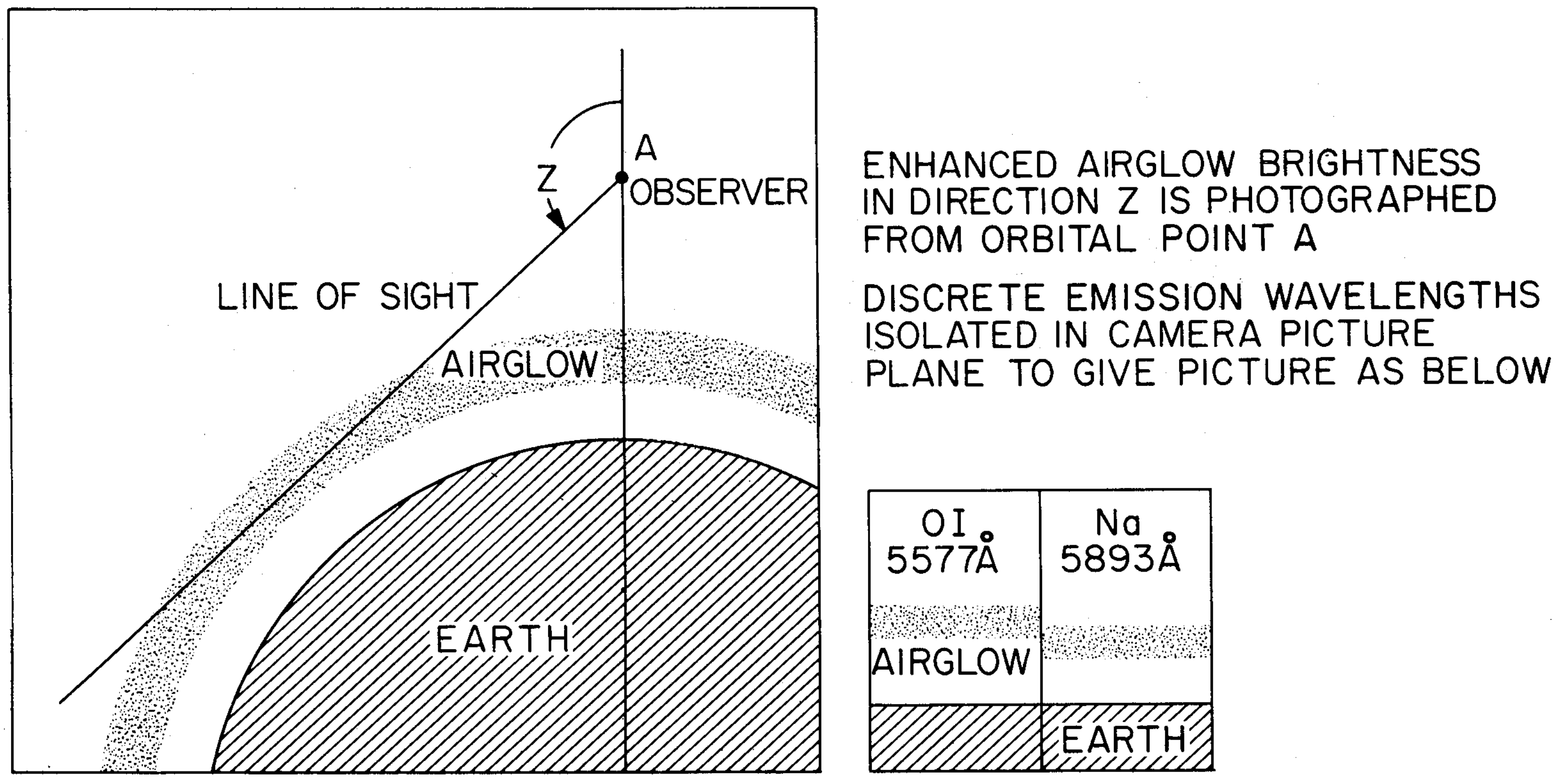

Figure 9-1. - Airglow horizon photography from nominal orbital altitudes.

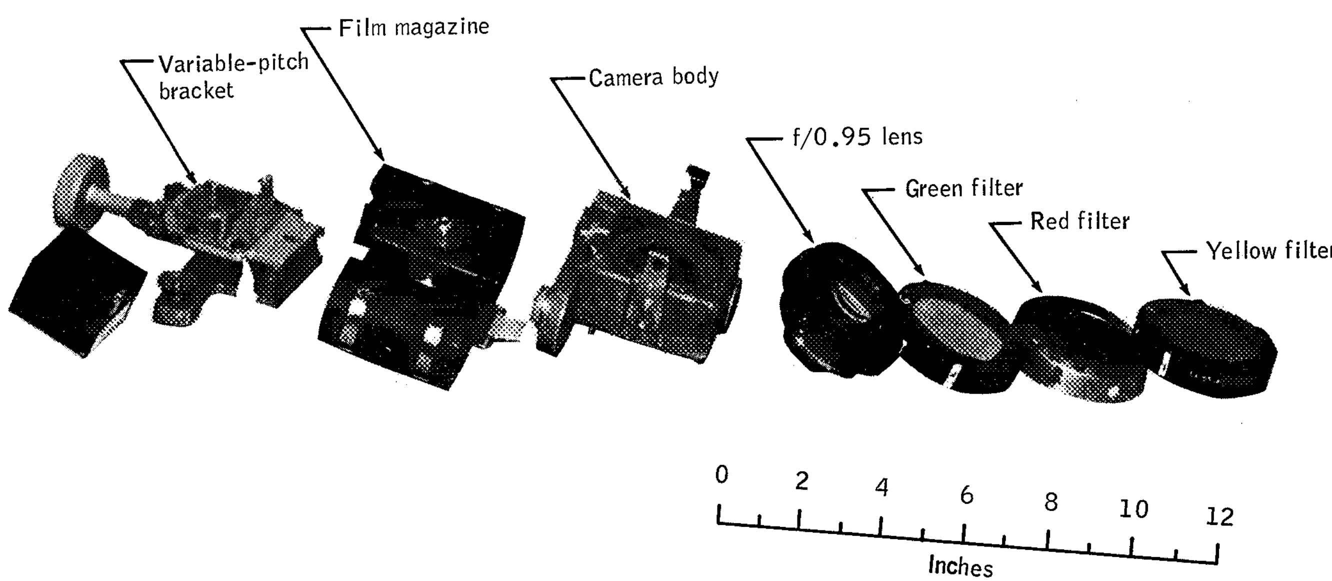

Figure 9-2. - Experiment S011, camera system.

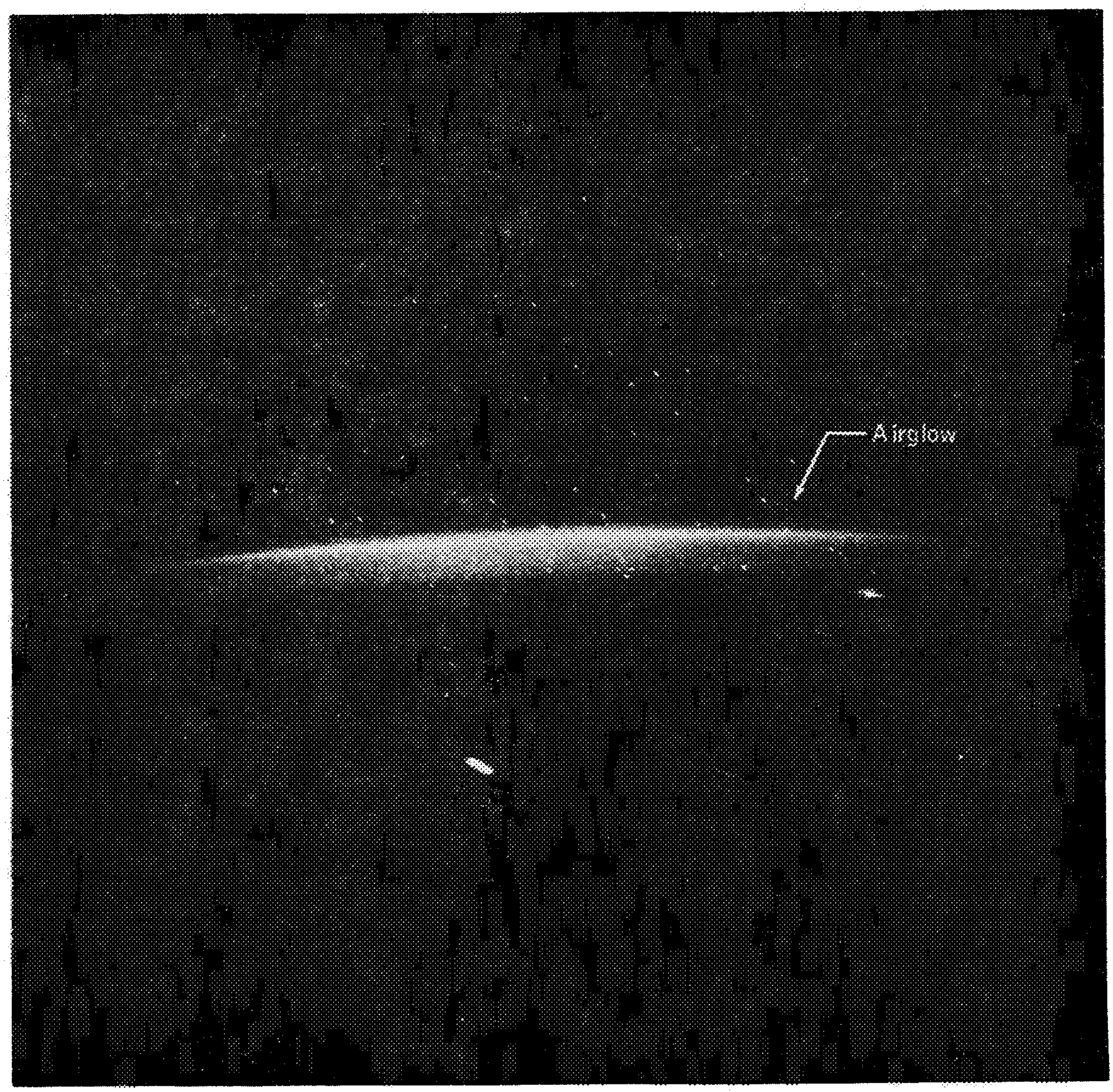

Figure 9-3. - A 3-second exposure of the night airglow without optical filters. Stars and lights from cities are easily observable in the upper and lower areas, respectively.

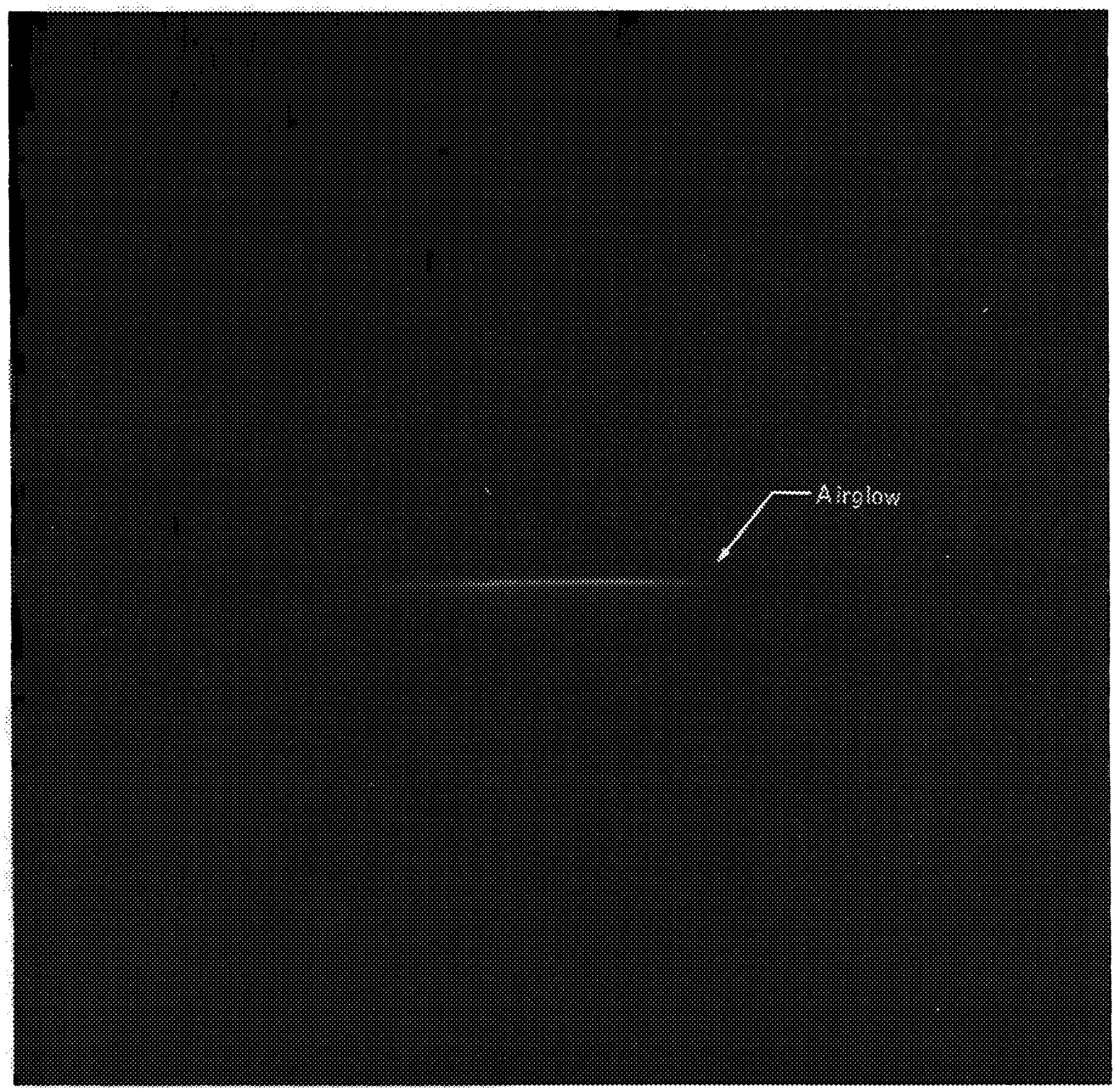

Figure 9-4. - A 20-second exposure using a green interference filter. The airglow does not extend the entire width of the picture as was anticipated.

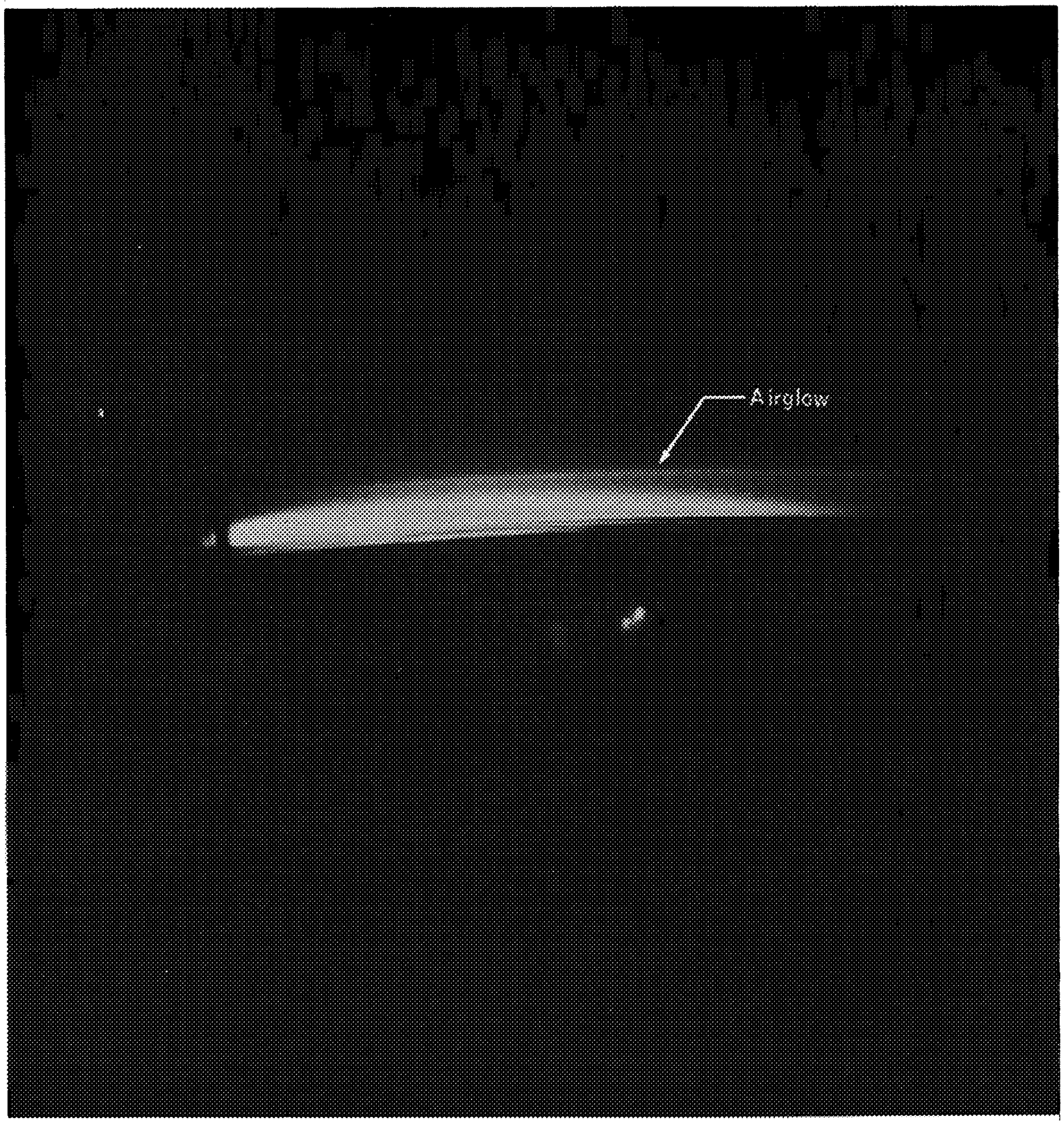

Figure 9-5. - A 20-second exposure using a red filter — taken 4 minutes after sunset. The emission layers observed are probably due to the OH radical.

10. EXPERIMENT S012, MICROMETEORITE COLLECTION

By C. L. Hemenway, D. S. Hallgren, R. E. Coon, and L. A. Bourdillon
Dudley Observatory and The State Univeristy of
New York at Albany

and

J. Hotchin and P. Lorenz
New York State Dept. of Health

SUMMARY

Micrometeorite activity in a near-earth environment and the effect of this environment on biological micro-organisms were studied by exposing polished metal and plastic surfaces to the environment outside the Gemini spacecraft. The cumulative influx rate of the micrometeorites in the size range of 10^{-15} to 10^{-14} gram was about 2 particles/meter^2/sec during the Gemini XII Mission and for the Gemini IX Mission was approximately 200 particles/meter^2/sec having a mass of 10^{-7} gram.

No living organisms either aerobic or anerobic were found on the Gemini XII sterile collection surfaces. The results of the Gemini XII exposure of ubiquitous agents, *Penicillium roqueforti* spores and *Escherichia coli* bacteriophage T_1, indicate that there was no survival of the *Pencillium* mold while a small fraction of the T_1 phage survived. The space exposure caused about a 50 percent reduction in titer compared to laboratory control samples when solar radiation was shielded by approximately 0.4 mm of aluminum metal.

OBJECTIVES

The objectives of the S012 Micrometeorite Collection experiment were to determine the micrometeorite activity in a near-earth environment and to study the effect of this environment on biological micro-organisms.

EQUIPMENT

The basic objectives were to be accomplished by exposing polished metal and plastic surfaces to the environment outside the Gemini spacecraft. Environmental data to be acquired included the particulate material collected, holes and craters in the specially prepared surfaces, and numbers of viable micro-organisms remaining on the biological exposure plates. The micro-organisms used were ubiquitous agents which were absolutely harmless to man. Laboratory tests have shown these organisms to be resistant to adverse conditions, hence their selection for space studies. All material specimens were to be returned to earth by stowage in the Gemini spacecraft for postflight examination and analysis.

The micrometeorite collection hardware consisted of an aluminum structure mounted on the spacecraft adapter retrograde section. The S012 experiment hardware was approximately 28-cm long, 14-cm wide, and 3.5-cm thick and weighed about 2690 grams. Mounting spaces contained 24 slides. Figure 10-1 shows the hardware configuration on the spacecraft. The location and the type of specimens used within the experiment are listed in table 10-I. The sponsoring agency for each test object is also shown. Photographs of these specimens and their placements are shown in figure 10-2. The collector cover door was remotely controlled by ground command, thereby allowing the cover to be opened or closed, as required, to expose the experiment samples.

PROCEDURES

The loading of the S012 equipment slides was carried out at the Dudley Observatory in a small clean room under a dust hood equipped with filters. The air to which the samples were exposed during loading was doubly filtered. Two collector units were loaded for each flight, one for flight and the other as backup unit.

The sterile compartment was loaded first and all slides within that compartment were loaded prior to sterilization. The collector was inserted in a stainless steel box with a small Millipore filter covered port (10 mμ porosity) with an electrical connection. The collector was sterilized for 4 hours with ethylene oxide at 54° C at a pressure of about 1000 torr and 40 percent relative humidity. After sterilization the compartment was closed electrically and sealed with a temporary door clamp. The collector was then removed from the steel box and returned for loading of the nonsterile compartment.

The two units were taken to Cape Kennedy 3 days prior to launch and stored in a sealed clean air-conditioned locker compartment. The flight unit was mounted on the spacecraft behind the copilot's hatch approximately 16 hours prior to launch. The outside of the collector was then given a final cleaning by swabbing with a nylon cleaning cloth dampened with ethyl alcohol.

The cover door of the micrometeorite collection unit remained in the closed position during flight until the first crew sleep period. This closed period was required to prevent exposing sample surfaces to particles caused by thruster firings, fuel-cell purging, or the dumping of liquids overboard. The collector door was opened for one period of 6 hours 24 minutes.

The exposure was made while the spacecraft was coupled to the Agena and oriented such that the collector surfaces faced outward away from the earth and tilted forward about 15° in the direction of vehicle travel. Orientation was maintained during the exposure time by the use of cold-gas vernier thrusters on the Agena.

The opening and closing of the collector was verified by including in the unit photographic film. The film was so blackened by exposure to sunlight that development was not necessary. The biological exposure experiments also verified that the opening and closing functions had been successful. Both compartments of the collector were under vacuum when returned after flight exposure.

After recovery of the spacecraft, the S012 flight unit was immediately flown to Dudley Observatory. The contents of the nonsterile compartments were unloaded first in a clean room. The collectors were sent to the Virus Research Laboratory of the New York State Department of Health and placed in a sealed box. Sterilization of the collector unit and tools was accomplished by using an ultraviolet germicidal lamp for 15 minutes. The collector was then left overnight in the box with air recirculating through a Cambridge Absolute filter. The following day, the sterile samples were removed. The collector box was shut and returned to Dudley Observatory clean room where micrometeorite samples in the sterile compartment were removed.

RESULTS

The experiment equipment was opened by ground command at 8 hours 5 minutes ground elapsed time (g.e.t.), during the crew sleep period. The collector was closed and locked by ground command at 14 hours 29 minutes g.e.t. The equipment package was retrieved by the pilot during the standup extravehicular activity at 20 hours 26 minutes g.e.t. and stowed in spacecraft. Recovery for the postflight analysis was satisfactory.

The sample preparation of the thin nitrocellulose films for the experiment was carried out in a similar manner employed in previous rocket sampling experiments (refs. 1 and 2). Preflight and postflight metal shadowing was employed to reduce contamination noise level.

Inflight controls were included by using slides of half-thickness and letting the controls slide face-down in the individual slide compartments. The flight control and flight exposed films were made at the same time for each sample location.

When the S012 experiment was exposed during the Gemini IX Mission relatively large numbers of holes were found; however, this experiment flown on the Gemini XII Mission has produced very few holes. Only one has been observed in the first 23 mm^2 of the Gemini XII thin film data scanned and reduced to date. It appears that the flux inferred from the two flights are in disagreement by about a factor of 100 in the size range from 0.1 to 1 micron. A discussion of various types of holes found in the S012 experiment on Gemini IX Mission and expected but not found on Gemini XII Mission follows.

Figure 10-3(a) is an electron micrograph of a typical isolated flapped hole found in palladium-shadowed nitrocellulose film. The nitrocellulose film also has been deformed in the vicinity of the hole. Figure 10-3(b) shows another individual flapped hold without any film de-deformation in the nitrocellulose film adjacent to the holes.

A group of flapped holes clustered together is shown in figure 10-4. In this figure, the nitrocellulose films show significant film deformation adjacent to many of the individual holes. Similar film deformations have been observed in surfaces exposed during rocket sampling experiments. The cluster is believed to be result of an impact of a slightly brokenup, fragile, extremely irregular particle. It is possible that the particle consisted of several relatively large solid particles lightly held together by a material which appear to easily evaporate and react with the nitrocellulose film. The slight separation of the individual holes may be due to an interaction with a weak atmosphere in the vicinity of the spacecraft prior to particle impact.

Figure 10-5 shows a different multiple hole structure with a somewhat different film deformation in the vicinity of the individual holes. Here the deformations of the film contain large numbers of low-density particles in the size range of 100 to 500 Å in diameter and are consequently close to the resolution limit of the photo-analysis processes. In the center of the film a rounded particle is also observed which could be a portion of the impacting particle structure.

In addition to the flapped hole structures, significant numbers of structures not previously observed in rocket collection experiments have been found. Figure 10-6 shows two separate examples of these large structures. The structures appear to consist of an elongated hole, surrounded by an elliptical, deformed area which in turn is surrounded by an area of film deformation of circular symmetry. These structures are believed to be the result of an ultrahigh velocity impact on the film, the size of the impacting particle being of the order of the width of the elongated hole. The area of near-circular symmetry surrounding the hole may represent energy dissipation in the impact. The second shadows observed around these structures indicate that the surface of the film has been elevated somewhat above the normal plane of the film.

Table 10-II shows typical data from Gemini IX and all of the data from Gemini XII. The masses of the impacting particles have been estimated from the width of the individual holes. Multiple hole structures have been counted as single impact sites. It should be noted that data given are conservative in that only hole structures clearly distinguishable from those in the inflight controls were counted. Ten-to-twenty times as many holes were discarded as were assumed to be real penetration holes. Most of the discarded holes could be clearly identified as holes commonly found in thin nitrocellulose films.

Flux values from the preliminary results from the S012 and S010 Gemini micrometeorite experiments are shown in figure 10-7. A rough correction for earth shielding has been made by multiplying the raw fluxes by two. These values are compared with several other flux measurements: the satellite and rocket microphone data as published by McCracken and Dubin for curve A, (ref. 3); the Pegasus data (ref. 4); the non-shower balloon-top collections (ref. 5); Venus Fly Trap and the Noctilucent Cloud control collection of 1962 (ref. 6); Zodiacal Light estimates of Ingham (ref. 7); and Elsasser (ref. 8); and the flux implied by a large crater observed in Project Mercury periscope lens during the flight of Enos (ref. 9). In addition, some previously unpublished data from the Dudley Observatory is included from a rocket sampling with the Pandora collector in four discrete altitude ranges 2 days after the peak of the Leonid shower of 1965.

Preliminary S010 and S012 Gemini results may be summarized as follows:

a. The cumulative influx rate in size ranges from 10^{-15} to 10^{-14} gram is about 2 particles/meter^2/sec as determined from the S010 experiment and S012 experiment on Gemini XII.

b. The cumulative influx rate in the same mass range as determined by the data from the S012 experiment on Gemini IX is near 200 particles/meter^2/sec.

c. The large particle cumulative influx rate is approximately 3×10^{-5} particles/meter^2/sec with a mass of the order of 10^{-7} gram.

Sterile Collection Attempts

No living organisms could be found on the Gemini XII sterile collection surfaces after recovery and handling using extreme precautions against contamination within a sterile chamber. The experiments flown on both the Gemini IX and Gemini XII Missions failed to show any evidence of living entities having been collected in space during the exposure periods. Tests for the presence of live organisms in an aqueous solution of the sterile surfaces included several different broth media for aerobic and anaerobic bacteria, fertile chicken egg inoculation, and monkey kidney and Hela cell tissue culture inoculation. All of these tests were negative.

Survival of Terrestrial Micro-organisms in Space

The results of the Gemini XII exposure of *Penicillium roqueforti* spores and *Escherichia coli* bacteriophage T_1 are shown in table 10-III. In this experiment there was no survival of the *Pencillium* mold but a small fraction of the T_1 coliphage survived. The space exposure caused only about 50 percent reduction in titer compared to laboratory controls when solar radiation was shielded by approximately 0.4 mm of aluminum metal.

The biological samples on board the spacecraft were exposed to cosmic radiation plus the solar electromagnetic radiation. The fact that a shield of 0.4 mm thickness of aluminum in the Gemini experiments could nearly completely protect the *Penicillium* and protect to the extent of at least 3000-fold higher survival of the T_1 coliphage indicates the nonpenetrating radiation, probably solar ultraviolet and soft X-rays, was responsible for the killing of micro-organisms directly exposed to space. Previous sounding rocket experiments using very thin film metal filters (ref. 10) showed the same conclusion that solar ultraviolet radiation and soft X-rays were probably responsible for the inactivation.

A measure of the lethal effect of the solar radiation from the results of two Gemini flights are shown in table 10-IV expressed as surviving fractions relative to the shielded flight controls. Variations in stability of the sample batches, prepared some months apart, are controlled as are differences due to inactivation during transportation and storage of the flight units. The coliphage samples indicate a remarkable similarity of survival. Since radiation flux is essentially constant during exposure periods, the extreme resistance of a fraction of the population of organisms is likely due to differences in the susceptibility individuals in the population. This was presumably due to shielding of a small proportion at the base of the air-dried layer of organisms by the aggregated individuals.

The Gemini XII results plus those of previous Gemini missions and other spaceflight experiments were presented at the COSPAR Symposium, in London, England, during July 1967.

REFERENCES

1. Hemenway, C. L.; and Soberman, R. K.: Studies of Micrometeorites Obtained from a Recoverable Sounding Rocket. Astron. J., vol.67, June 1962, pp. 256-266.

2. Hemenway, C. L.; Soberman, R. K.; and Witt, G.: Sampling of Noctilucent Cloud Particles. Tellus, vol. 16, June 1964, pp. 84-117.

3. McCracken, C.; and Dubin, M.: Dust Bombardment on the Lunar Surface. NASA-TN-D-2100, 1963.

4. Stuhlinger, E.: Meteoroid Measurements with Project Pegasus. N. E. Electronics Research and Engineering Meeting, Boston, Mass., 1965.

5. Hemenway, C. L.; Hallgren, D.; and Coon, R.: High Altitude Balloon-Top Collections of Cosmic Dust. COSPAR, Vienna, 1966.

6. Soberman, R. K.; and Hemenway, C. L.: Meteoric Dust in the Upper Atmosphere. J. Geophys. Res., vol. 70, Oct. 1965, pp. 4943-4949.

7. Ingham, M.: Observations of the Zodiacal Light from a High Station IV. The Nature and Distribution of Interplanetary Dust. M. N. Royal Astron. Soc., vol. 122, no. 2, 1961, pp. 157-175.

8. Elsasser, H.: Die Raumliche Verteilung der Zodiakalichtmaterie Z. f. Astroph., vol. 32, 1964, p. 274.

9. Hemenway, C. L.; Linscott, I.; Secretan, L.; and Dubin, M.: Preliminary Studies of Possible Cosmic Dust Impacts on Project Mercury Vehicle Periscope Lenses. Annals of the N. Y. Academy of Sciences, vol. 119, Nov. 1964, pp. 106-115.

10. Hotchin, J.; Lorenz, P.; Markusen, A.; and Hemenway, C. L.: The Survival of Microorganisms in Space. Further Rocket and Balloon-Borne Exposure Experiments. COSPAR, Vienna, May 1966.

TABLE 10-I.- S012 LOADING FOR GEMINI XII

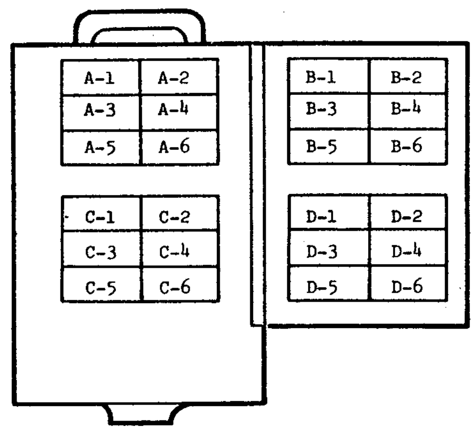

Location	Sponsor	Specimen type
A-1	Dudley Observatory	Nitrocellulose film over glass
A-2	Air Force Cambridge Research Laboratory	Nitrocellulose film
A-3	Dudley Observatory	Biological exposure
A-4	Dudley Observatory	Biological exposure
A-5	Dudley Observatory	Stereoscan sample, gold and indium-coated glass
A-6	Dudley Observatory	Nitrocellulose film over glass
B-1	Air Force Cambridge Research Laboratory	Layers of nitrocellulose film
B-2	Dudley Observatory	Stereoscan sample - copper
B-3	U. S. Geological Survey	Nitrocellulose on gold mesh
B-4	Tel Aviv University	Penetration through film
B-5	Dudley Observatory	Layers of silicon oxide film
B-6	Max Planck Institute	Layers of nitrocellulose film
C-1	Dudley Observatory	Nitrocellulose film over glass
C-2	Max Planck Institute	Stereoscan plates
C-3	Dudley Observatory	Sterile collection plates
C-4	Dudley Observatory	Sterile collection plates
C-5	Ames Research Laboratory	Gold-coated plastic
C-6	University of Washington	Polished copper
D-1	Dudley Observatory	Stereoscan samples - stainless steel
D-2	Manned Spacecraft Center	Aluminum on stainless steel
D-3	Birkbeck College	Aluminum on stainless steel
D-4	Smithsonian Observatory	Gold on plastic
D-5	Goddard Space Flight Center	Chromium on glass
D-6	Ames Research Laboratory	Metal-coated plastic

TABLE 10-II.- DATA SUMMARY OF S012 EXPERIMENT

Exposed	Control
Gemini IX Aluminum shadowed nitrocellulose (location B-2)	
2735 frames[a] 28 holes	825 frames 0 holes
Gemini IX Aluminum shadowed nitrocellulose (location A-1)	
528 frames 13 holes	95 frames 0 holes
Gemini XII Aluminum shadowed nitrocellulose (location A-1)	
2858 frames 1 hole	1394 frames 0 holes

[a]A frame has an area of approximately 8100 square microns.

TABLE 10-III.- SURVIVAL OF *PENICILLIUM* MOLD AND T_1 PHAGE AFTER 6-HOURS EXPOSURE TO SPACE AND SOLAR RADIATION DURING THE GEMINI XII MISSION

Micro-organism	Lab control	Flight shielded	Flight exposed
Penicillium roqueforti	5.5×10^5	2.0×10^5 (0.4)	0 (<0.000002)
T_1 phage	7.7×10^4	3.1×10^4 (0.5)	9.1 (0.0001)

TABLE 10-IV.- SURVIVAL OF *PENICILLIUM*, SPORES AND T_1 PHAGE ON THE GEMINI SPACECRAFT IN ORBIT

Micro-organism	Survival fraction[a] (relative to shielded flight control)	
	Gemini VIII (17 hr)	Gemini XII (6 hr)
Penicillium roqueforti	0.00004	<0.000005
T_1 phage	0.0003	0.0005

[a]Surviving fraction = $\dfrac{n_{exposed}}{n_{shielded}}$

NASA-66-11353 DEC 16

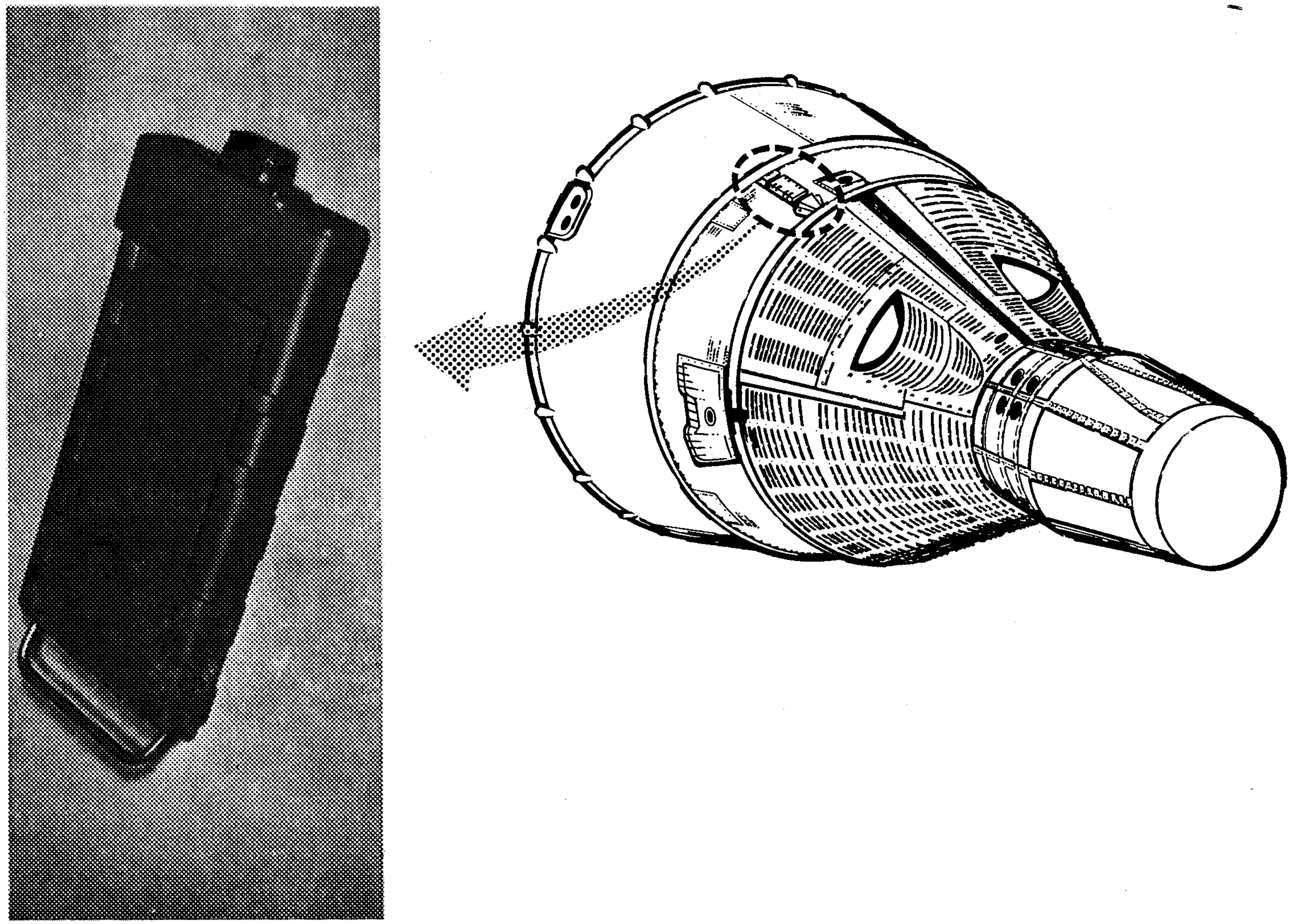

Figure 10-1. - Experiment S012, hardware location.

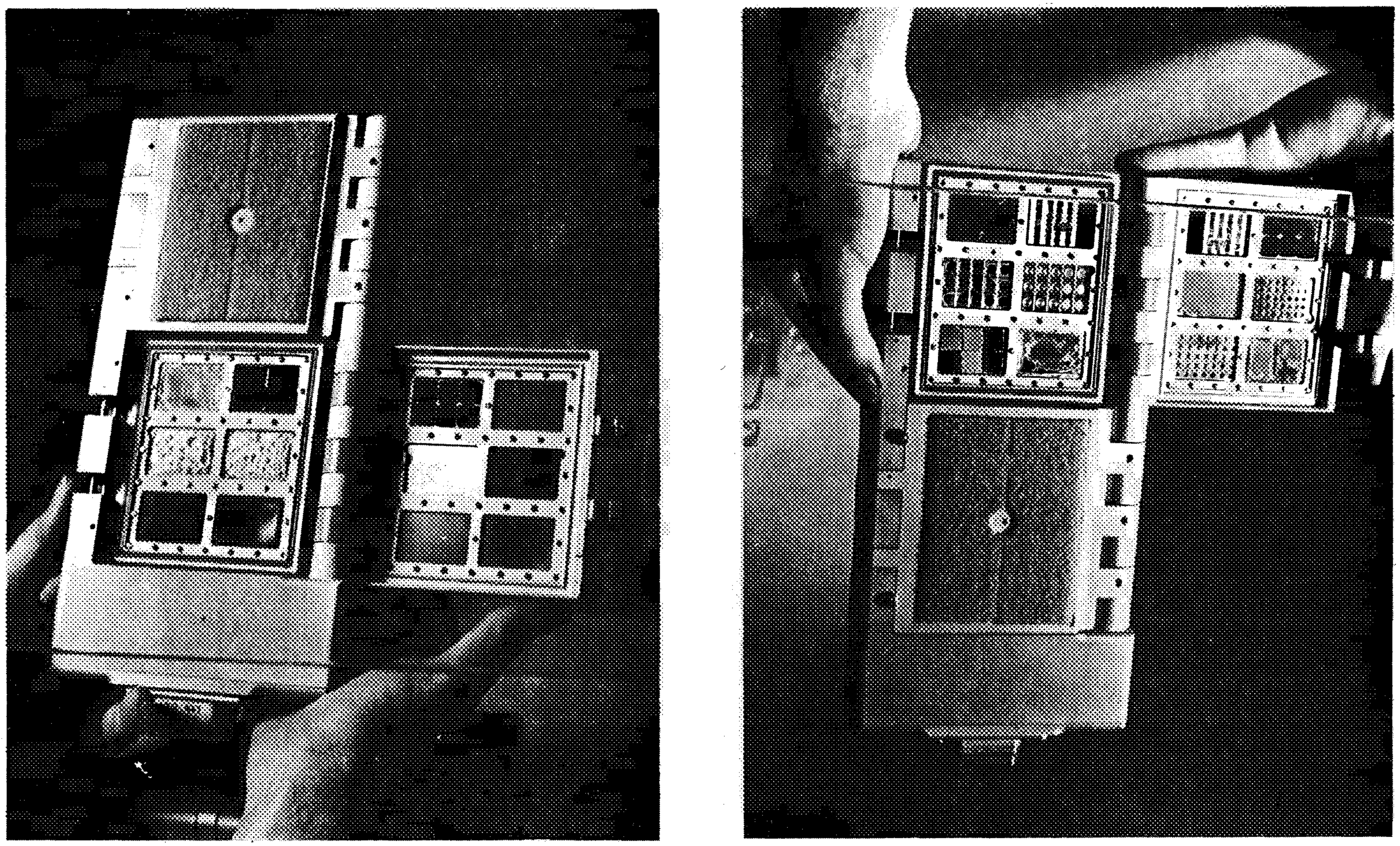

Figure 10-2. - Experiment S012, specimens (see table 10-I for identification).

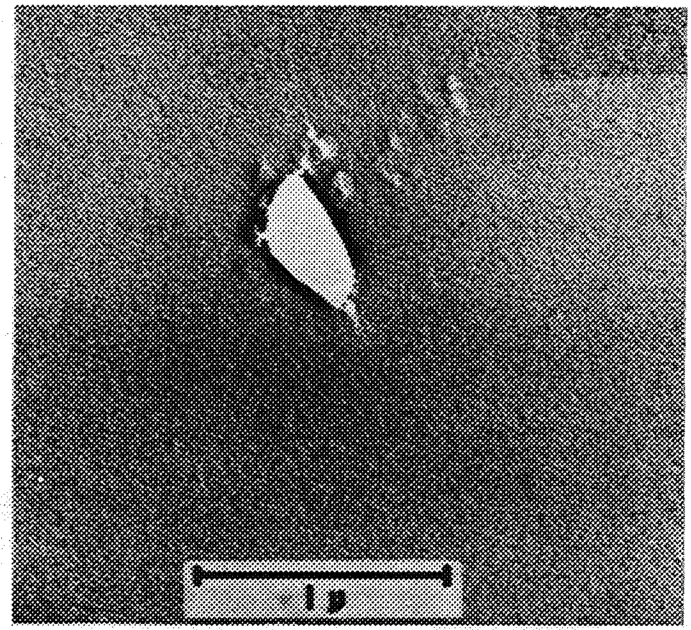

(a) Deformation is visible in area of hole.

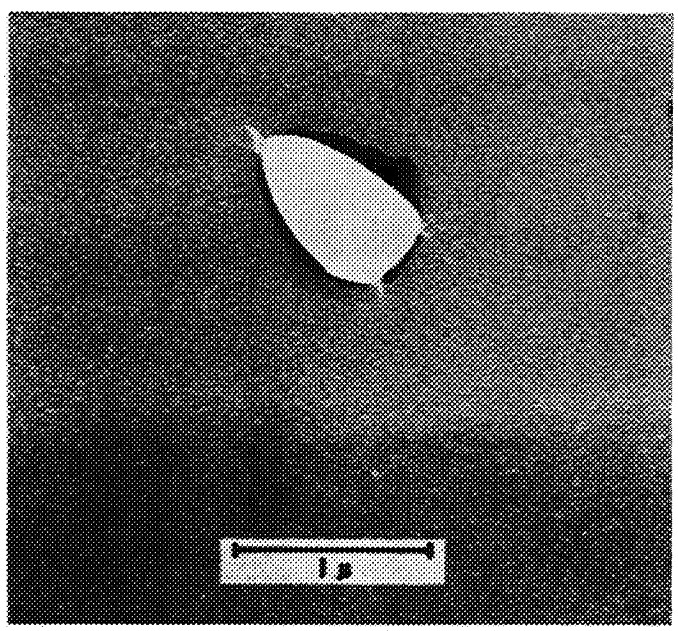

(b) No deformation is visible.

Figure 10-3. - Thin film penetration holes.

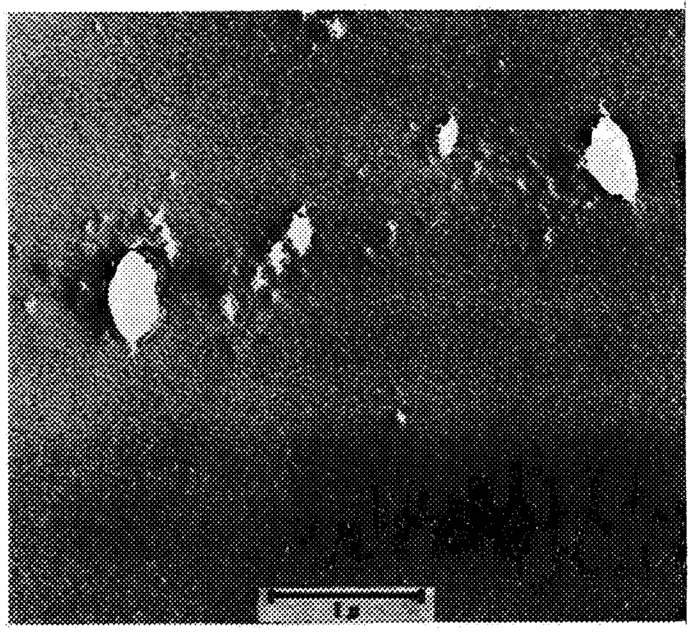

Figure 10-4. - Group of thin film penetration holes with adjacent deformation.

Figure 10-5. - Multiple hole structure with deformations from low-density 100 to 500 Å.

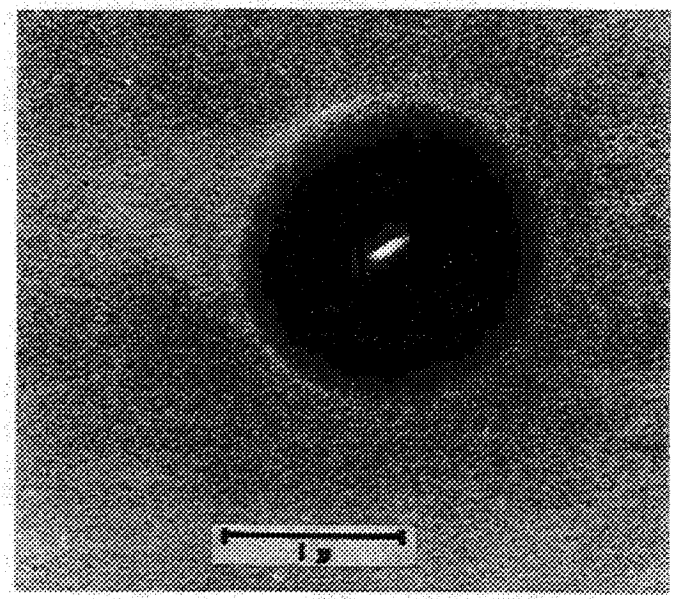

(a)

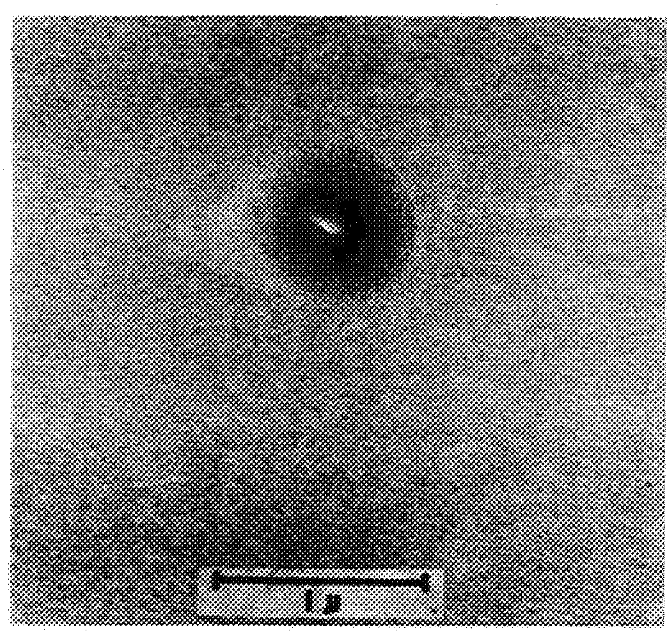

(b)

Figure 10-6. - Enlongated hole surrounded by elliptical, deformed area.

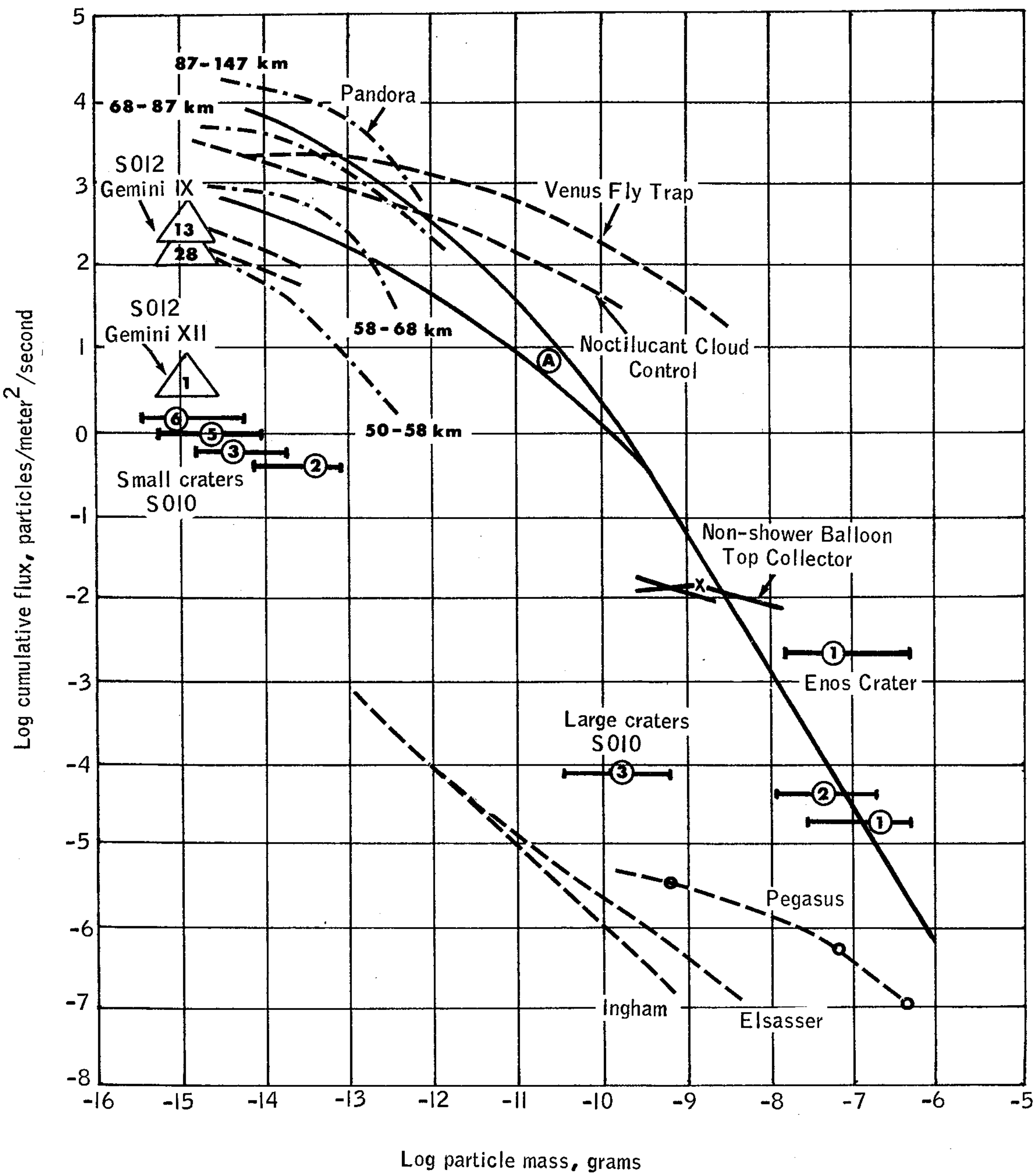

Figure 10-7.- Flux values from the preliminary results from the S010 and S012 Gemini micrometeorite experiments.

11. EXPERIMENT S013, ULTRAVIOLET ASTRONOMICAL CAMERA

By Karl G. Henize and Lloyd R. Wackerling
Dearborn Observatory
Northwestern University

SUMMARY

Line spectra and the energy distribution of the ultraviolet radiation (2200 to 3000 Å) of early-type (O, B, and A) stars were obtained in four star fields. The spectra were recorded with the 70-mm general-purpose camera and objective prism or objective grating. Moderate dispersion objective-grating spectra were obtained in regions centered on γ Cassiopeiae and Sirius and low dispersion objective-prism spectra were obtained in regions centered on Deneb and γ Velorum.

OBJECTIVE

The fundamental objective of the S013 Ultraviolet Astronomical Camera experiment was to record the ultraviolet radiation of stars in the wavelength regions from 2000 to 4000 Å. An analysis of the surface temperatures of these stars, of the absorption effects taking place in their atmospheres, and of the absorption effects of the interstellar dust will be made of the photographic data obtained.

In addition to the acquisition of basic astronomical data, techniques by which objective-prism spectra may be best obtained were determined. The practical experience gained through this experiment will be useful in planning similar astronomical observations with larger telescopes on future missions.

EQUIPMENT

The experiment equipment consisted of the Maurer 70-mm general-purpose camera with an ultraviolet lens that had a 22-mm aperture, 73-mm focal length, and a field 30° in diameter. The film magazine carried 50 frames of Kodak spectroscopic I-O emulsion on an Estar base. Grating spectra with a dispersion of 180 Å/mm were produced by a 600-line/mm objective grating blazed at 2000 Å. Prism spectra with a dispersion of 1400 Å/mm at 2500 Å were produced by a quartz objective prism with a 10° prism angle.

PROCEDURE

Prior to the standup EVA, the pilot unstowed the camera and the prism or grating, then locked them to the lens. The camera was then attached to the bracket located near the pilot's seat.

After hatch opening, the spacecraft was pointed toward the first star target, using a reticle located on the command pilot's window. Because the camera axis was parallel to the roll axis of the spacecraft, the roll rate was the least critical of the three spacecraft motions. Roll rates up to 0.5 deg/sec could have been tolerated with little loss of image definition. Both pitch and yaw rates were to be decreased to 0.1 deg/sec or less. Pitch motion was the most critical because the pitch axis was parallel to the direction of dispersion and motion would degrade the wavelength resolution of the spectra.

Six time exposures were made on each star field and the film advanced between each exposure. Two exposures of 1 minute and two of 2 minutes were made during periods when the stabilizing thrusters were operated to hold the spacecraft attitude constant. The additional two exposures were of less than 30 seconds duration.

The experiment was performed while the spacecraft was docked with the Gemini-Agena Target Vehicle (GATV) in order to use the GATV control system for stabilization. During each set of exposures, the GATV was stabilized using flight control mode 2, with the geo-rate and horizon stabilization switched OFF.

RESULTS

Four star fields were photographed: two with the grating and two with the prism. The grating fields were centered on γ Cassiopeiae and Sirius. The prism fields were centered on Deneb and γ Velorum. Grating spectra in the γ Velorum field and prism spectra in the Algol field were not obtained because of crew workloads. The decision not to use platform orientation required the crew to use planned observing time at the beginning of each night in order to acquire the first star field.

There were apparently no major problems in the assembly and operation of the camera. Problems do remain, however, concerning focus, static marks, and light leaks.

The image quality produced by the camera (as judged by zero-order grating images) was considerably better than that obtained during the previous Gemini flights. In particular, the central area of very poor

This experiment is expected to yield data pertaining to the following questions:

(a) What is the number of dust layers in the upper atmosphere, and is there a dust layer in the 140-kilometer region?

(b) Do noctilucent clouds exist only at high latitudes in the summer months and during twilight conditions?

(c) Do noctilucent clouds appear as often in the Southern as in the Northern Hemisphere?

(d) Are the high-altitude dust particles concentrated in patches or are they continuously distributed?

EQUIPMENT

Photographs of the atmosphere were taken with a 70-mm general-purpose camera, equipped with an ultraviolet quartz lens and a filter allowing only the 2000- to 2500-Å scattered radiation to actuate the film.

The equipment used was the same as that used for Experiment S013, with the exception of the film and a simple ultraviolet filter in place of a prism or grating.

PROCEDURES

During the second standup EVA at approximately 67 hours g.e.t., the pilot took 42 ultraviolet photographs of star fields and sunrise. The crew indicated that all sequences were performed as planned.

RESULTS

Evaluation of the photographic data shows that the carbon-dioxide cartridge within the ultraviolet film magazine did not eliminate the static electricity caused by film movement. All exposures show intense fogging by this internal radiation and it is extremely doubtful that useful information can be extracted from these photographs.

15. OBJECTS OF OPPORTUNITY — ULTRAVIOLET PHOTOGRAPHY OF UPPER ATMOSPHERIC DUST CLOUDS[a]

SUMMARY

Approximately 42 ultraviolet photographs were taken of the earth's upper atmosphere in the ultraviolet wavelength regions from 2000 to 2500 A. All exposures show intense fogging by static electricity caused by film movement. It is extremely doubtful that useful information can be obtained from the photographs.

OBJECTIVE

The objective of this experiment was to photograph the earth's upper atmosphere in the ultraviolet wavelength regions of 2000 to 2500 Å, as a means to detect cosmic dust particles and to measure their relative regional concentration.

Recent theoretical and experimental programs have yielded information indicating the high possibility for the existence of dust clouds in the upper atmosphere. Rocket experiments show concentrations on the order of 5×10^{10} particles per square meter for particles 0.05 of a micron and larger in size. Computations of the dynamic response of small particles entering the earth's upper atmosphere with cosmic velocities show that the "effective braking layer" for these particles extends from 70 to about 110 kilometers. It would be expected that a sharp increase in the concentration of cosmic dust at these altitudes would be observed when viewed from above.

The absorption characteristics of the upper atmosphere change radically with altitude in the 1000- to 3000-Å range. A dust-free atmosphere should look black in this range of wavelengths when viewed from above. Because dust particles approximately 0.1 of a micron in size scatter strongly in the ultraviolet range, regions of high concentrations should register bright patches of light on an ultraviolet photograph superposed on a dark background.

---

[a]Principal Investigator is Dr. Curtis L. Hemenway, Dudley Observatory.

NASA-S-66-11329 DEC 14

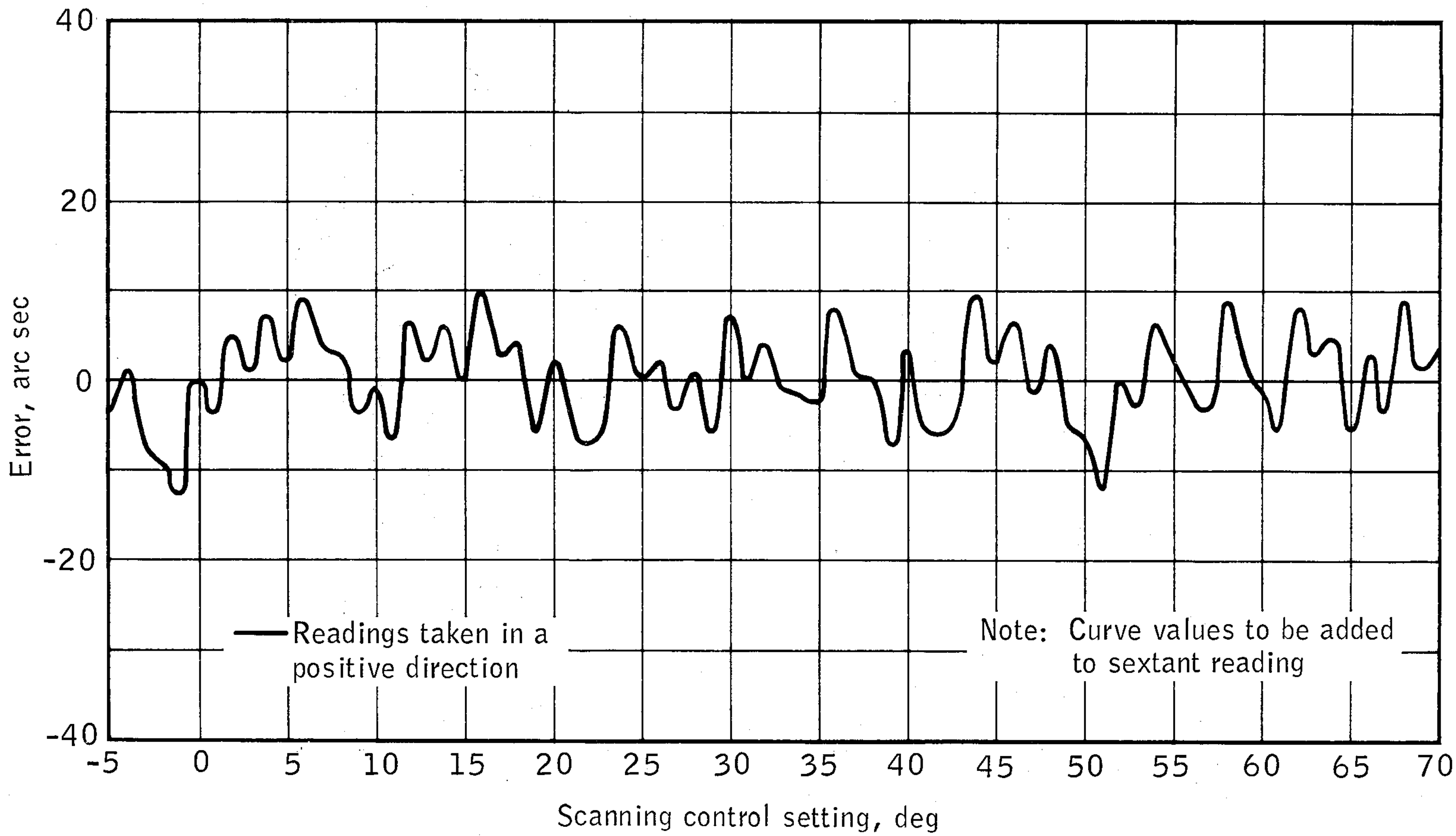

Figure 14-3. - Preflight T002 sextant calibration.

NASA-S-66-11317 DEC 13

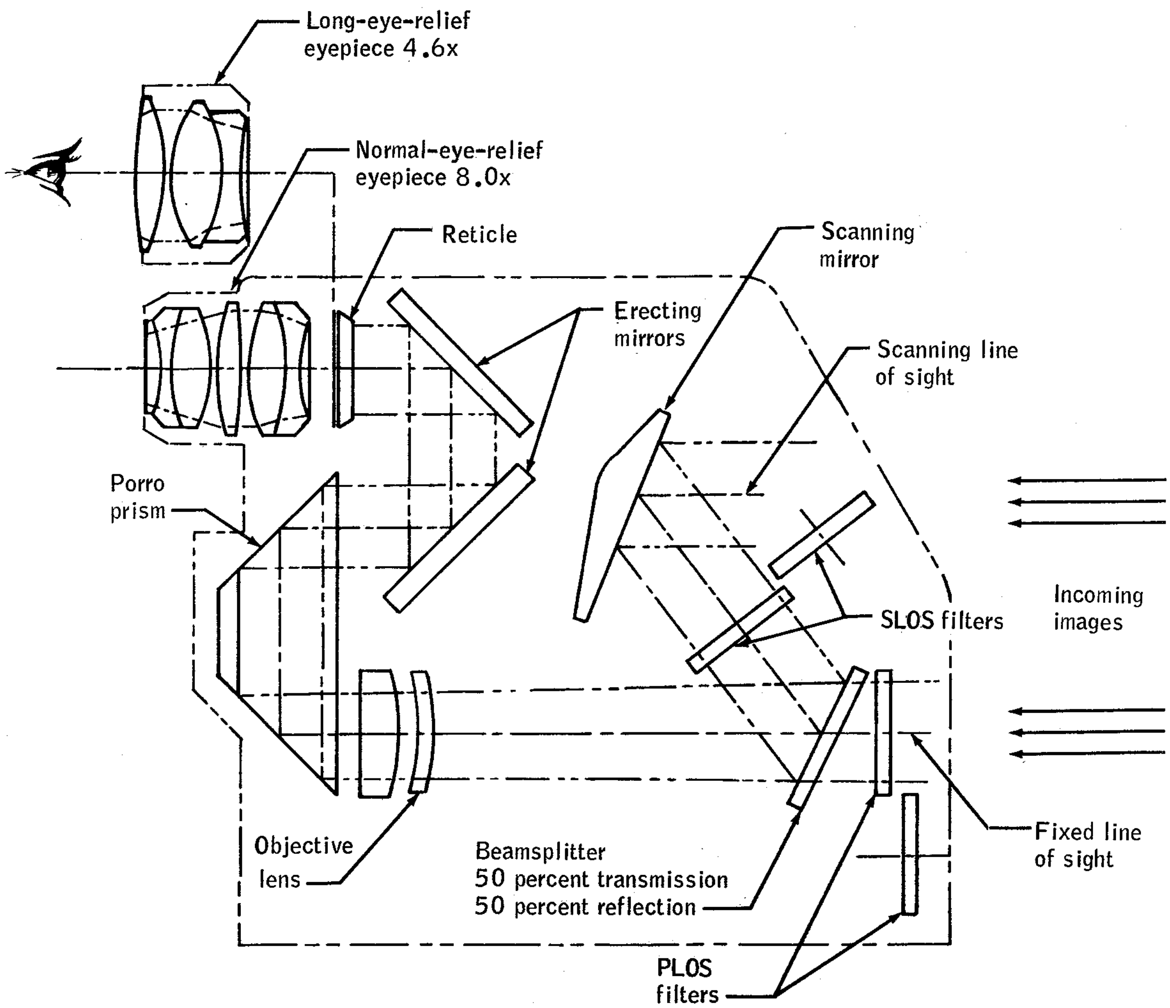

Figure 14-2. - Optical schematic of T002 space sextant.

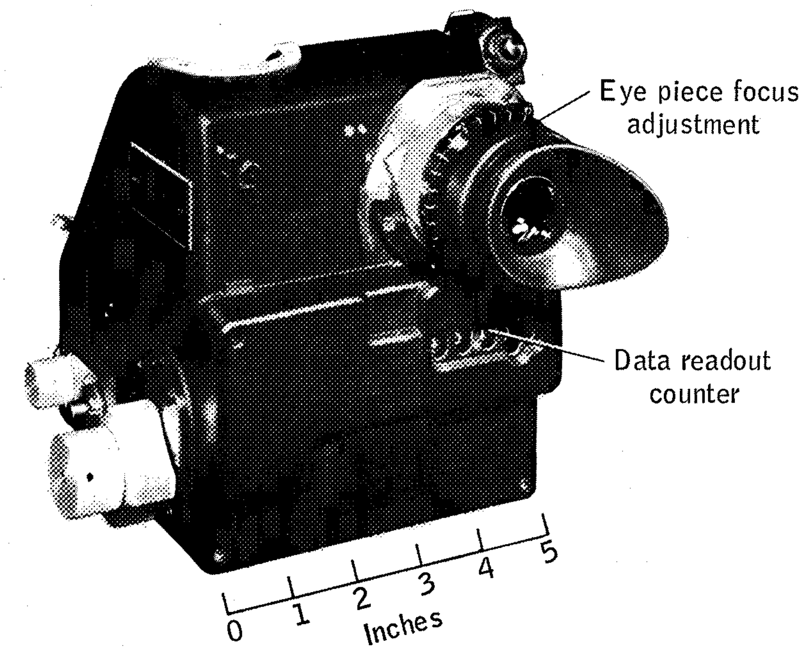

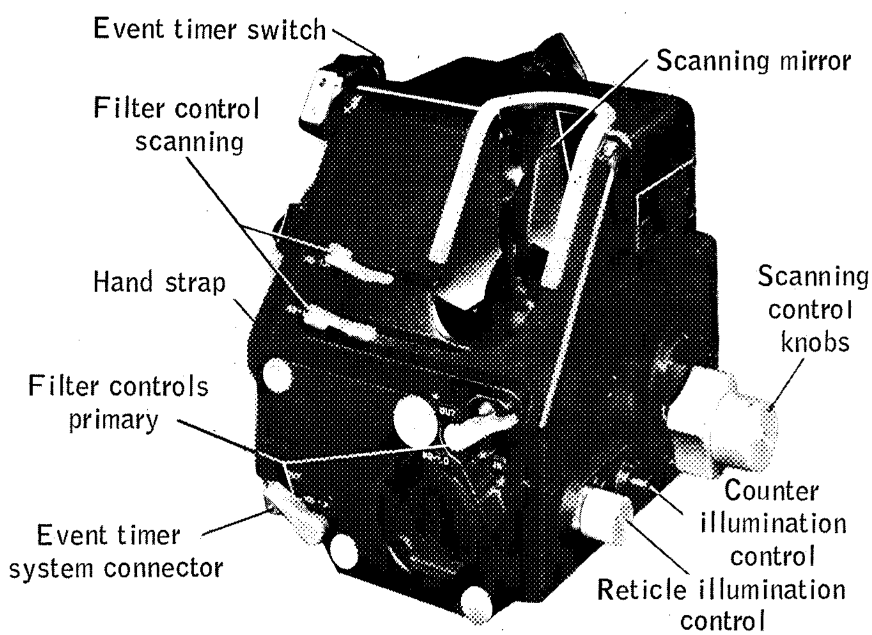

Figure 14-1. - Experiment T002, sextant configuration and operating controls.

TABLE 14-III.- PILOT INFLIGHT DATA

Sighting target	Pressure suit configuration	Revolution	Ground elapsed time, approx, hr:min	Time, sec	No. of measurements	Standard deviation of measurements, arc sec	Measurement bias error, arc sec[a]
Betelgeuse/Rigel	Helmet off, gloves off	40	63:15 to 63:47	32	13	±9.0	+5.8
Betelgeuse/Rigel	Helmet off, gloves off	48	75:17 to 75:50	33	14	±5.4	+1.4
Betelgeuse/ Bellatrix	Helmet off, gloves off	54	85:45 to 86:20	35	15	±7.6	-1.1
Betelgeuse/ Bellatrix	Helmet off, gloves off	55	87:15 to 87:48	33	15	±4.5	-1.8
Betelgeuse/Rigel	Helmet on, visor down gloves off	56	88:45 to 89:20	35	15	±7.5	+9.7

[a]Measurement bias error is the mean-measured target angle minus computed target angle.[b]

[b]Computed target angle is the angle between the targets corrected for annual aberration.

TABLE 14-II.- PILOT BASELINE DATA - REAL TARGET

Sighting target	Helmet configuration	No. of sighting sessions	No. of measurements per session	Standard deviation of measurements, arc sec	Mean measurement bias error, arc sec[a]
Altair/Vega	Helmet off	1	10	±4.7	0.0
Altair/δ Cyg.	Helmet off	1	10	±3.4	+1.2
Altair/δ Cyg.	Helmet on, visor down	1	10	±8.2	-9.8

[a]Mean-measurement bias error is the mean-measured target angle[b] minus computed target angle.[c]

[b]Mean-measured target angle is the mean-measured angle corrected for instrument calibration and measured zero bias.

[c]Computed target angle is the angle between the targets corrected for annual aberration and atmospheric refraction.

TABLE 14-I.- PILOT BASELINE DATA FROM AMES SIMULATOR

Sighting target	Helmet configuration	No. of sighting sessions	No. of measurements per session	Standard deviation of measurements, arc sec	Mean measurement bias error, arc sec[a]
Star/Star	Helmet off	7	10	±5.2	+1.8
Star/Star	Helmet on, visor down	3	10	±7.4	-1.6

[a]Measurement bias error is the mean-measured target angle[b] minus calibrated target angle.

[b]Mean-measured target angle is the mean-measured angle corrected for instrument calibration and measured zero bias.

The pilot's performance as indicated by the baseline data obtained both in a simulator and using real stars from earth-based observatories was virtually the same as that obtained in the space-flight environment, thus validating the usefulness of simulators and earth-based observatories in evaluating space-navigation measurement techniques.

No operational difficulties were encountered which were associated with the space environment.

sextant lines-of-sight to establish an instrument-operator-measured zero bias. Subsequently, 10 consecutive measurements of the angle between the selected sighting targets were made. Measurements were made with the helmet off (normal-eye-relief eyepiece) and helmet on, visor down (long-eye-relief eyepiece). The standard deviation of the measurements about their mean value and the mean-measurement bias error for all sessions are summarized in table 14-I. Additional baseline data obtained using real targets are summarized in table 14-II.

The standard deviation of the measurements obtained in both the simulator and using actual stars are substantially below the ±10-arc second level and agree well for both helmet configurations. The mean-measurement bias errors are also small except for the helmet-on, visor-down configuration.

Inflight Data

The Gemini XII pilot's inflight sextant-measurement data were obtained on November 14 and 15, 1966. The measurements were made from the stabilized spacecraft, with the pilot looking through the right-hand window. A summary of the standard deviation of the measurements and the measurement bias error is presented in table 14-III.

The standard deviation of the measurements for all sighting conditions is below ±9 arc seconds, agreeing well with the baseline data. The measurement bias errors of the inflight data are generally small except for the helmet-on, visor-down configuration. This is in agreement with baseline data. It should be noted that the measurement bias error is uncorrected for window-induced measurement errors, for errors caused by the difference in index-of-refraction of the light-transmitting media within and outside the spacecraft, and for measured zero bias. A more detailed analysis of the data, including these factors, will be published at a later date.

CONCLUSIONS

The standard deviation of the inflight measurements was ±9.0 arc seconds or below, indicating that the handheld sextant may be suitable for making navigational measurements during the midcourse phase of lunar- or interplanetary-space flight.

The handheld sextant with a long-eye-relief eyepiece can be used to make accurate navigational measurements (1σ < 10 arc seconds) with the pressure suit helmet on and visor down.

pair. A selected number of the sextant measurements were transmitted to the ground for real-time evaluation of the pilot's performance in making the prescribed measurements.

RESULTS

The results of the T002 experiment consist of learning-curve data obtained during the initial period of familiarization and training with the sextant, baseline data for comparison with flight results, and in-flight data obtained during the Gemini XII flight.

Initial Training and Familiarization

The initial training of the pilot was performed in the Docking Simulator at the Manned Spacecraft Center during the period of August 5 to 10, 1966. Two simulated star targets were installed in the simulator room. These targets consisted of 12-inch parabolic mirrors which projected toward the sighting station the collimated light of a small source placed at the focal point of the mirror. A second magnitude star was simulated. Using the handheld sextant in the darkened Docking Simulator, the pilot performed 15 consecutive measurements of the angle between the simulated stars and 10 consecutive measurements of the sextant angle when sighting on one star with both sextant lines-of-sight. These measurements were repeated in 15 sighting sessions over a period of 4 days. The standard deviation of the 15 measurements of the angles between the two stars from their mean value was used as a measure of the pilot's proficiency. The standard deviation varied throughout the training period from a maximum value of about 13 arc seconds near the beginning of the training period to a minimum of about 4 arc seconds near the end. These data indicate that the pilot had achieved a high degree of proficiency during the 4 days of training.

Baseline Data

All baseline data were obtained at Ames Research Center, Moffett Field, California, during the period from September 7 to 9, 1966. The majority of these data were obtained in the Ames Midcourse Navigation and Guidance Simulator. The basic components of the simulator are a visual scene that simulates a moon-star field and a movable cab which simulates a manned space vehicle. The two simulated stars used in the initial training were employed in obtaining the baseline data. Using the handheld sextant the pilot made five consecutive measurements of the angle obtained when viewing the same simulated star through both

Field of view, degrees 7

Exit pupil

Normal-eye-relief eyepiece, millimeters 4
Long-eye-relief eyepiece, millimeters 60

Diopter adjustment . . . . -3 to +3

Resolution, arc seconds 7

Image . . . . Erect

Range, degrees 76

The preflight calibration of the instrument is presented in figure 14-3.

PROCEDURES

The T002 experiment was performed during the dark periods of revolutions 40, 48, 54, 55, and 56.

The sextant was taken from its stowed location and the pilot hooked up the timing-event system connector to the spacecraft utility cord. The command pilot installed his reticle on the left-hand window and started his elapsed timeclock on an even minute, noting the time; then the spacecraft lights were extinguished. The command pilot established spacecraft orientation with respect to the selected stars using his reticle and stabilized the spacecraft about all three axes within ±2° in pitch and yaw and ±10° in roll, with very low-limit cycle rates of less than 0.25 deg/sec.

After the spacecraft was stabilized, the pilot focused the sextant, set the reticle illumination to a comfortable level, and acquired the star Aldebaran in both lines-of-sight. The pilot then superimposed the two images and marked the time of superposition by depressing the event timer button. An oral time "Mark" was called out by the pilot and the command pilot read his elapsed time, noting the time in the experiment log, along with the measured angle read off the sextant by the pilot. This procedure was repeated five times for the same star to provide an indication of the zero bias of the sextant-operator combination.

The spacecraft was then reoriented and stabilized by the command pilot, and the pilot acquired the prescribed target pair for the sighting period. A procedure similar to that described above was then followed for at least 10 consecutive measurements of the angle between the target

The view through the fixed line-of-sight of the sextant was imaged in the focal plane through a plate beamsplitter and an objective lens and prism-mirror erecting system, shown in figure 14-2. The view through the scanning field was reflected from an articulated scanning mirror; it was then combined with the fixed field in the beamsplitter and imaged in the focal plane by the same objective lens and erecting system. The operator, by observing the focal plane through the eyepiece and adjusting the scanning fields-of-view, could superimpose the selected targets in the fixed and scanning fields-of-view and thus establish the angular separation of the targets. The angular rotation of the scanning mirror was controlled by the two-speed scanning control knobs which provided target optical motions of 1° and 5° per revolution of the knobs.

The sextant was equipped with two removable eyepieces, one providing normal-eye relief, and the other providing long-eye relief. The normal-eye-relief eyepeice was used when the sextant could be brought directly to the eye for viewing, while the long-eye-relief eyepiece allowed the sextant to be used with the pressure suit helmet on and the helmet visor down.

Data readout was accomplished by direct reading of a mechanical counter located below the instrument eyepiece. The measured angle between the fixed and scanning lines-of-sight was indicated on the counter in degrees and thousandths of a degree, the smallest count being 0.001° or 3.6 arc seconds. A dual-cell rechargeable nickel-cadmium 2.5-volt battery was contained within the sextant and was used for illuminating both the data readout and the reticle.

An event timer button and switch were located on the right side of the instrument. The event timer switch was connected to the spacecraft telemetry recorder through the utility cord. Depression of the event timer button placed a time-correlated signal on the onboard Pulse Code Modulation recorder tape for use in the data analysis.

Two filters of different density were provided in each line-of-sight to reduce the amount of light transmitted through them. The purpose of filters was to permit viewing images of widely varying intensities such as a star and a lunar landmark.

The general characteristics of the sextant are as follows:

Size, inches . . . . 7 by 7-1/4 by 6-1/16

Weight, pounds 6.25

Magnification

Normal-eye-relief eyepiece . . . . 8×
Long-eye-relief eyepiece . . . . 4.6×

14. EXPERIMENT T002, MANUAL NAVIGATION SIGHTINGS[a]

SUMMARY

The ability of a flight crew to make accurate navigational measurements in a space-flight environment using a handheld sextant was evaluated. The standard deviation of the inflight measurements was below ±9 arc seconds, indicating that the handheld sextant may be suitable for making navigational sightings in space flight. The pilot's performance as indicated by the baseline data obtained both in a simulator and using stars from earth-based observatories was virtually the same as that obtained in the space-flight environment.

OBJECTIVES

The general objective of the T002 Manual Navigation Sightings experiment was to make navigation-type measurements through the window of the stabilized Gemini spacecraft using a handheld sextant. The major objectives were to:

(a) Evaluate the flight crew's ability to make accurate navigational measurements using simple instruments in an authentic space-flight environment

(b) Examine the operational feasibility of the measurement techniques using the pressure suit helmet off and also with the helmet on and the visor closed

(c) Evaluate operational problems associated with the spacecraft environment

(d) Validate ground simulation techniques by comparison of the inflight results with baseline data obtained by the pilot using simulators and actual celestial targets from ground observatories.

EQUIPMENT

The equipment used in this experiment was a two-line-of-sight optical sextant, shown in figure 14-1. It was designed to measure (within 10 arc seconds) the angle between various types of celestial targets.

---

[a]Principal Investigator is Donald Smith, NASA Ames Research Center.

NASA-S-66-11347 DEC 16

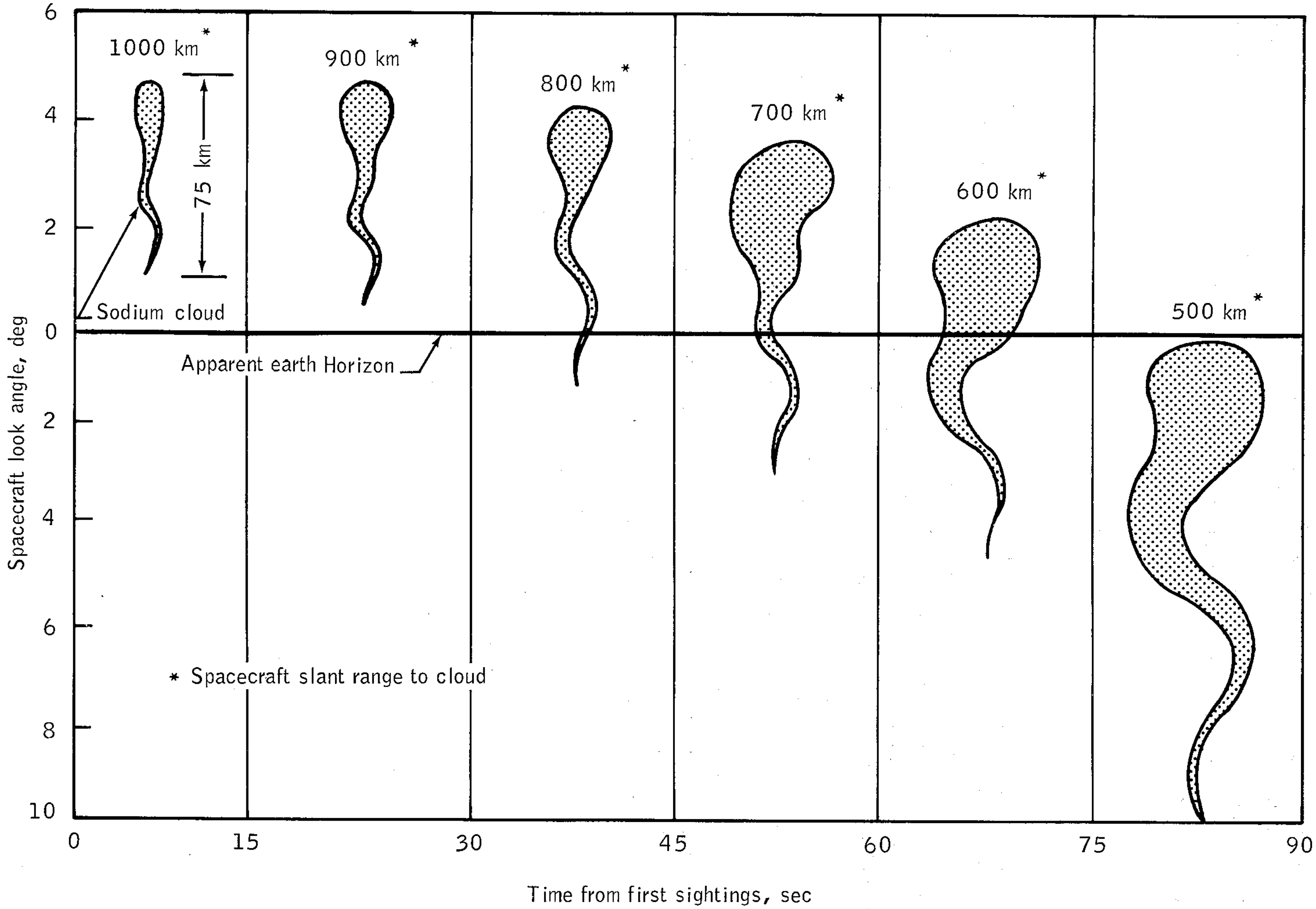

Figure 13-1. - Experiment S051, predicted sodium-cloud visual characteristics.

second identical pair of pictures taken some time later, the tridimensional configuration of the cloud could again be obtained. A comparison of the state of the cloud at different times would give the wind velocity in the atmosphere at all relevant altitudes, assuming that only horizontal winds exist. It has been found that a series of successive photographic pairs are necessary to reduce wind velocity errors to an acceptable level.

RESULTS

This experiment was performed following launch of the sodium rocket from the French launch site at 62:41:48 g.e.t. Visual acquisition was not established by the crew; however, the spacecraft was pointed in the direction of the anticipated sodium cloud location and 13 exposures were taken. Another sodium rocket was launched from the launch site near Hammaguir, Algeria, at 64:16:49 g.e.t. The crew again did not visually observe the sodium cloud. Thirteen additional photographs were taken of the geographical areas specified in premission planning. The launch crew at Algeria confirmed the successful firing, activation, and observation of sodium clouds from the ground during both of the spacecraft passes. Evaluation of the film indicated that all 26 photographs were overexposed during the photographic sequences. The overexposures were caused by a camera shutter locked in the open position. Useful photographic data were therefore not obtained for analysis.

The locked open-shutter was in the red lens assembly. The probable cause for this open-shutter condition was the use of forces exceeding design limits when mounting the red lens assembly to the camera body and the misalinement of the shutter-actuating coupling due to partial camera-shutter cock. The coupling misalinement can cause dowel pin deformation, resulting in a chain of misalinements and possible shutter override, thereby preventing the return movement of the shutter-closure mechanism.

PROCEDURES

The sodium release was made by a Centaur rocket from the Hammaguir, Algeria, launch site, which is under the responsibility of the CNES-French Space Agency. This was a two-stage solid-propellant rocket which ejected sodium continuously from 70 kilometers to an apogee of 180 kilometers and down to the ground.

Two rockets were launched from Hammaguir in the southeast direction, with approximately 1-1/2 hours between the two launches. The firing conditions were such that the rockets descended from apogee when the Gemini spacecraft was at a distance of 1000 kilometers. Assuming a nominal spacecraft altitude of 161 nautical miles, the position of the cloud relative to the horizon could be determined.

From pictures obtained of airglow (Experiment S011), it is apparent that the horizon line does not correspond to the real geometrical limit of the solid earth but to the sunlit atmosphere up to an altitude of 30 kilometers. This has been taken as the horizon line and the horizon angle had been taken as 16.50° below the spacecraft horizontal plane. Figure 13-1 shows the evolution of the sodium cloud sightings as predicted by observation by the flight crew. When the cloud is below the horizon, it is not visible because of poor contrast with sunlit background. The background may be 250 times more intense than the cloud. Therefore, this experiment can succeed only when the cloud is above the horizon.

From a study of this figure it is apparent that wind measurement can be obtained from slant distances between 1000 and 800 kilometers in the altitudes of interest. This was the basic objective of the experiment.

When the distance between the spacecraft and the cloud is less than 800 kilometers, the lowest part of the cloud begins to sink below the horizon. The possibility of obtaining useful pictures of the cloud on the top of the earth's background was another objective to be obtained. It necessitated obtaining a series of exposures during the time the spacecraft went from a distance of 800 to a distance of 500 kilometers.

The average wind velocity measured is of the order of magnitude of 50 to 100 meters per second. To measure this velocity, the motion of the cloud has to be a few times larger than the film resolution. This corresponds to a difference in time between successive exposures of approximately 30 seconds at a distance of 1000 kilometers.

Two cloud pictures taken about 60 kilometers apart would provide tridimensional cloud shapes by stereogrammetric recombination. From a

13. EXPERIMENT S051, DAYTIME SODIUM CLOUD[a]

SUMMARY

Measurements of the daytime wind velocity of the earth's high atmosphere as a function of altitude were to be obtained from the deformations of a rocket-made vertical sodium cloud. The clouds were to be sequentially photographed using the 70-mm general-purpose camera. The flight crew was not able to visually observe the sodium clouds; however, photographs were taken of the anticipated sodium cloud locations. Evaluation of the film indicated that all photographs were overexposed because of a camera shutter locked in the open position during the exposure periods.

OBJECTIVE

The objective of the S051 Daytime Sodium Cloud experiment was to measure the daytime wind velocity of the earth's high atmosphere as a function of altitude between 30 and 80 nautical miles.

The measurements were to be obtained from the deformations of a rocket-made vertical sodium cloud. Rockets launched in front of the spacecraft continuously ejected sodium vapor from approximately 35 to 100 nautical miles in altitude during ascent and descent. The vapor should have been visible from the spacecraft as a faint yellow-white cloud above the horizon.

EQUIPMENT

The clouds were to be sequentially photographed using the 70-mm general-purpose camera used on other experiments. At least 20 frames from the S011 experiment film pack were required for adequate photographic coverage.

An interference filter with wavelength response dependent on incidence angle was mounted on the camera. This filter allowed sodium yellow light to enter a camera cone angle of 10°. For larger entrance angles, the wavelength response was displaced toward the green. It was essential that the camera be aimed precisely at the cloud direction within a tolerance of 1°.

---

[a]Principal Investigator is Dr. Jacques Blamont, CNES-FRANCE.

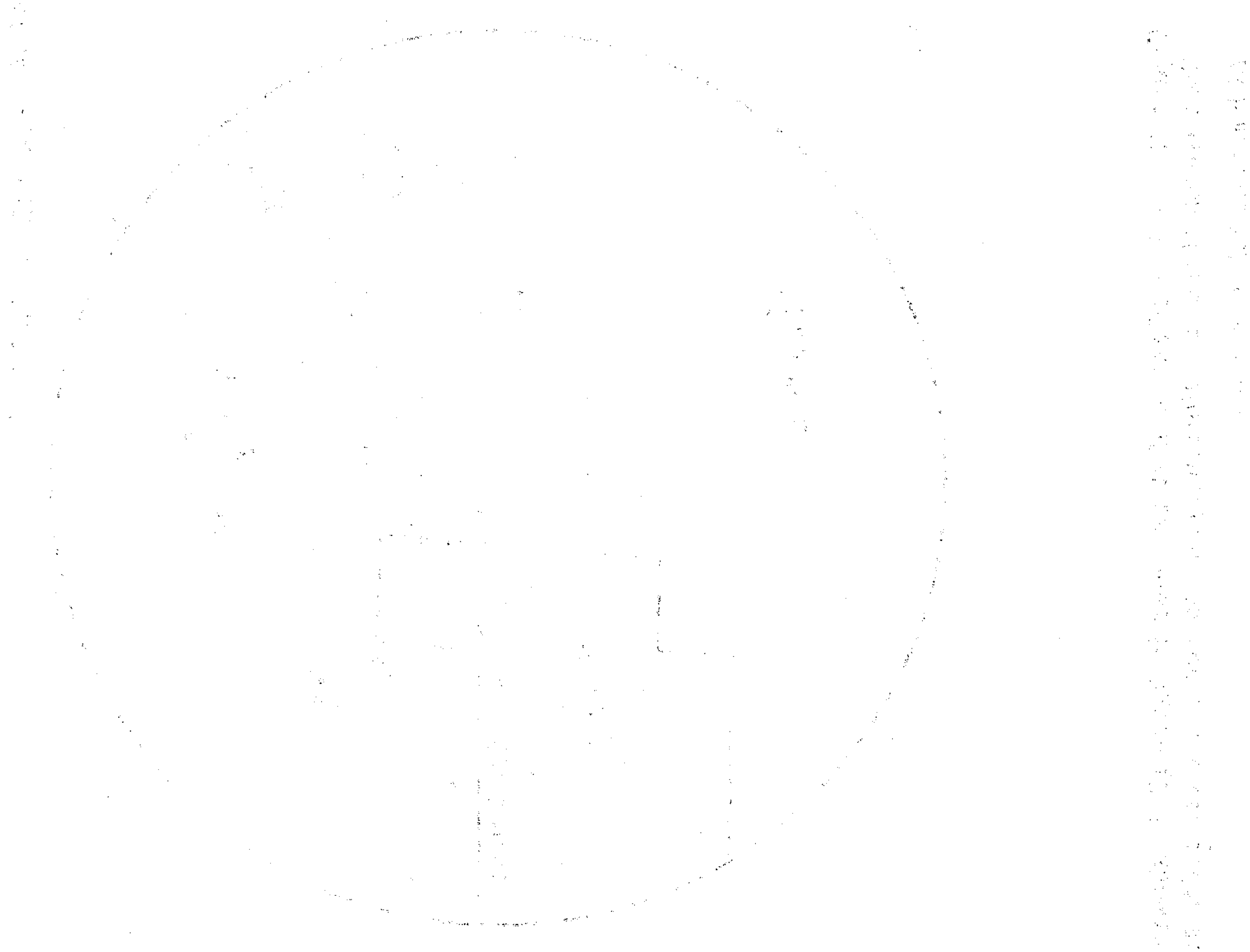

NASA-S-66-11315 DEC 13

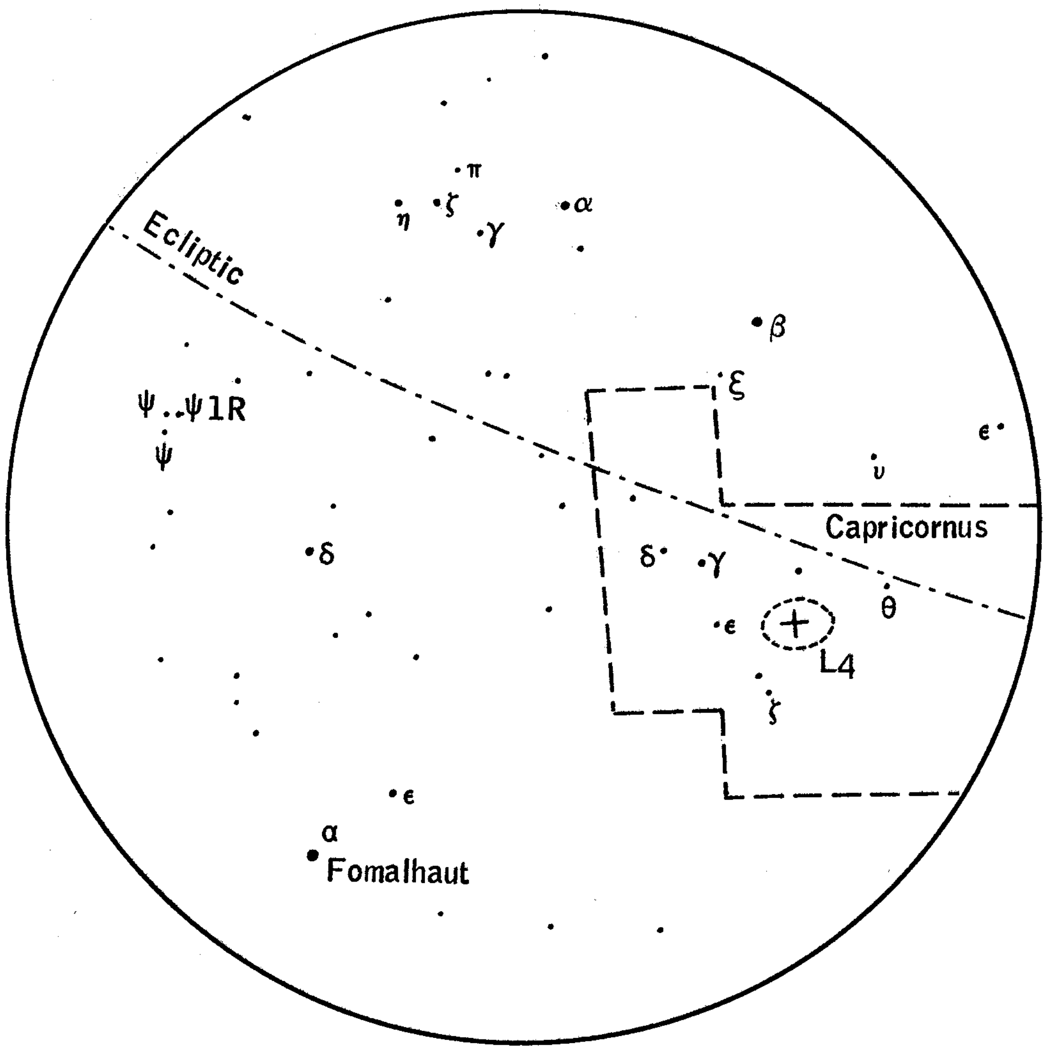

Figure 12-2. - Identification of stars shown in figure 12-1, showing the position of the L_4 libration point on November 14, 1966, at 73 hours 45 minutes g. e. t.

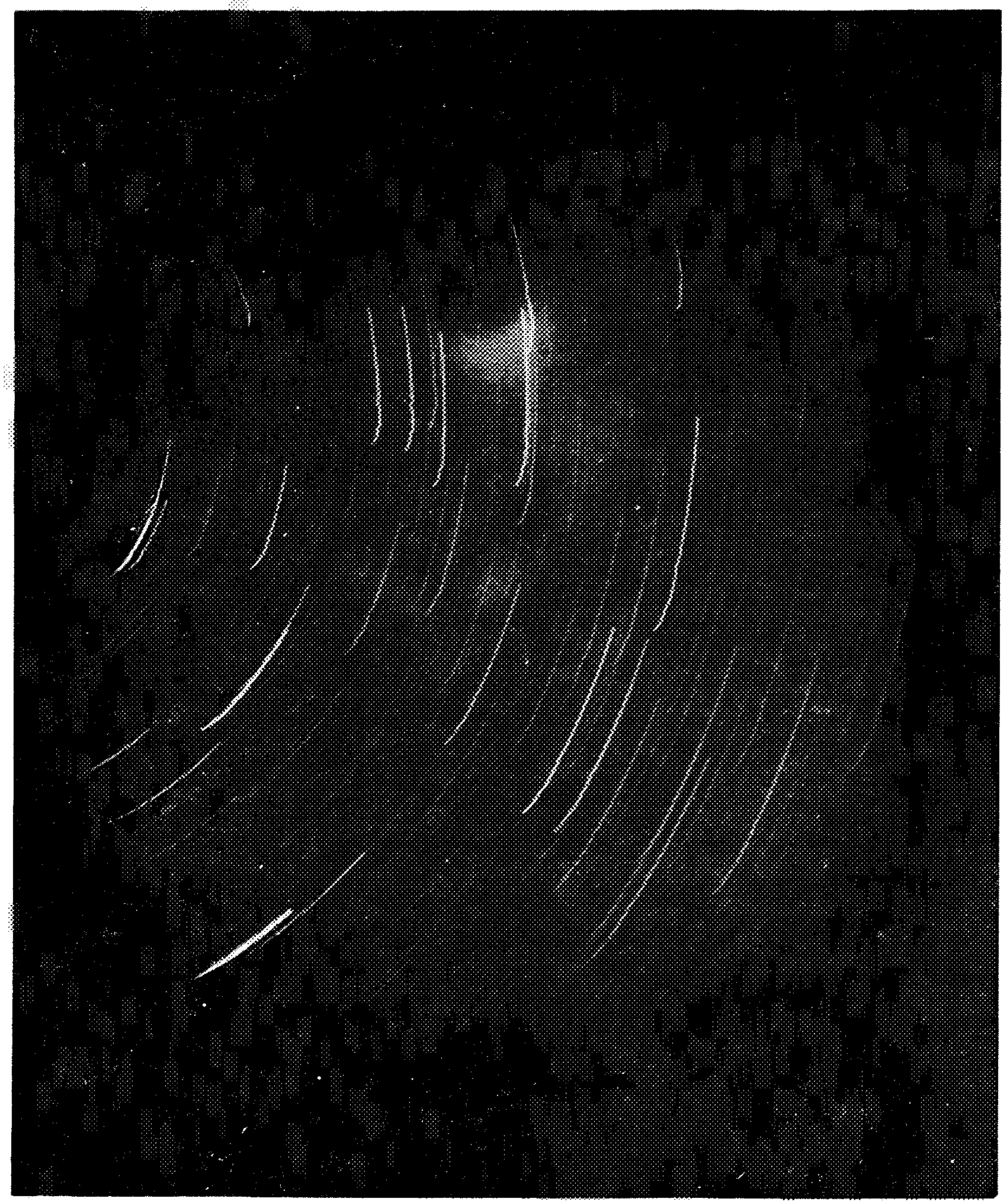

(b) Photograph of the L_4 libration region taken at approximately 73 hours 45 minutes g.e.t. with an exposure time of 60 seconds.

Figure 12-1.- Concluded.

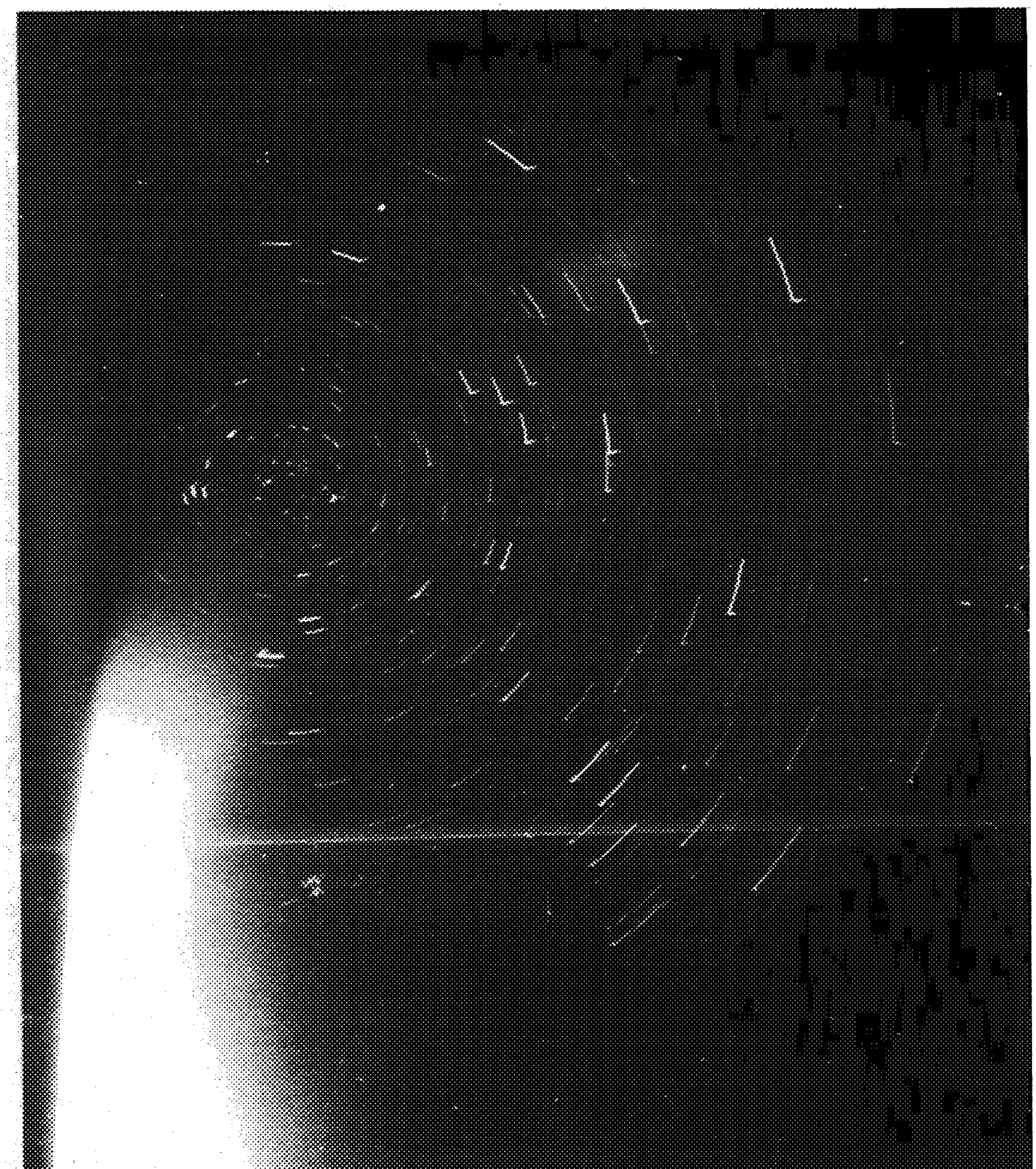

(a) Photograph of the L_4 libration region taken at approximately 73 hours 45 minutes g. e. t. with an exposure time of 30 seconds.

Figure 12-1. - Experiment S029, earth-moon libration region photography.

field area in which the L_4 libration region would be passing 45 hours later. Five photographs were taken of this area with a series of exposures approximately 30 seconds, 1 minute, and 2 minutes. They were taken with the spacecraft docked with the Gemini Agena Target Vehicle (GATV).

During the night pass of the 46th orbit, six exposures were taken of the L_4 libration point in the constellation Capricornus. The photographs were taken with the camera mounted on the Experiment S011 mounting bracket which alined the camera perpendicular to the pilot's window but not parallel to the spacecraft axis. The spacecraft was then oriented so that the camera would be pointed at the libration point. The spacecraft was not docked with the GATV during the second sequence of pictures. Exposure times for the second set of photographs were 30 seconds, 1 minute, and 2 minutes.

RESULTS

Eleven photographs were taken of the L_4 libration point, of which only three were exposed properly. A mechanical failure of the shutter mechanism in the red lens assembly (see Camera Failure Analysis in section 9) caused overexposure of many of the photographs. A failure of the film advance at the end of the first roll caused an unknown number of double exposures. None of the first sequence of five photographs could be identified, one of which was totally unrecognizable as to image content. Star fields could be recognized in the two remaining photographs as shown in figures 12-1(a) and (b); however, because of difficulties in stabilizing the spacecraft, the stars were badly smeared. A light flare, the source unknown but possibly caused by light reflecting off the window of the spacecraft, was present in both pictures. A reconstructed star field area as seen by the camera is shown in figure 12-2.

Isodensitraces of the two recognizable star fields were made. Because of image smear and the light flare, no conclusive results can be obtained.

12. EXPERIMENT S029, EARTH-MOON LIBRATION REGIONS PHOTOGRAPHY[a]

SUMMARY

Eleven photographs were taken of the L_4 earth-moon libration region, of which only three were exposed properly. A mechanical failure of the camera-shutter red lens assembly caused overexposure of many of the photographs. Isodensitraces of two recognizable star fields were made. Because of image smear caused by spacecraft movement and a light flare, no conclusive results can be obtained.

OBJECTIVE

The objective of the S029 Earth-Moon Libration Regions Photography experiment was to investigate by photographic techniques the possible existence of clouds of particles or dust orbiting the earth in these regions. The L_4 and L_5 libration points lie in the orbital path of the moon, 60° ahead of and 60° behind the moon. Dust clouds in these regions should be visible by reflected sunlight.

EQUIPMENT

The following equipment was used for this experiment:

(a) The 70-mm general-purpose camera with the f/0.95 lens.

(b) One film magazine with black-and-white, high-sensitivity film.

(c) Experiments T002 and S011 camera-mounting brackets.

PROCEDURE

During the night pass on the 17th orbit, the camera was mounted to the pilot's window with the experiment T002 bracket, which alined the camera to the spacecraft axis. In accordance with ground procedures, the spacecraft was oriented towards the constellation Capricornus, the star

---

[a]Principal Investigator is Elliot C. Morris; U.S. Geological Center, Flagstaff, Arizona.

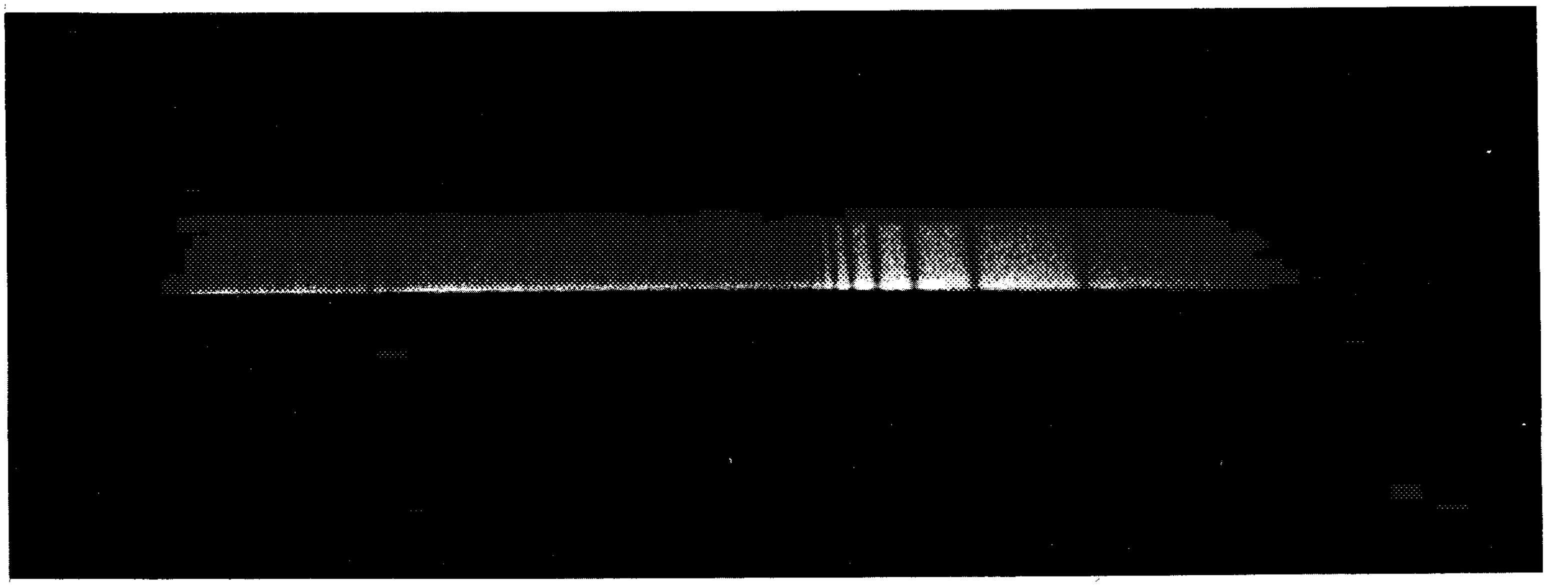

The Balmer series of hydrogen appears at right. The Mg II doublet at 2800 Å and several weak sharp lines of Fe II appear at left.

Figure 11-2. - Experiment S013, the ultraviolet spectrum of Sirius (exposure — 20 seconds).

Figure 11-1. - Experiment S013, grating spectra in the region of Cassiopeia (exposure — 2 minutes).

TABLE 11-II.- S013 INFLIGHT EXPOSURES WITH PRISM ATTACHED

Frame[a]	Field	Vehicle attitude hold	Remarks
S66-63571	Wasted frame	--	Grossly overexposed; positive image of GATV and sunlit earth
72	Cygnus	Fair	Spectra streaked; no detail
73	Cygnus	Poor	No detail
74	Cygnus	Poor	Some detail
75	Cygnus	Fair	Some detail
76	Cygnus	Poor	No detail in spectra
77	Puppis-Vela	Poor	Spectra very wide; possible detail
78	Puppis-Vela	Poor	No detail
79	Puppis-Vela	Poor	No detail
80	Puppis-Vela	Fair	Spectra streaked; apparent line in 3817
81	Puppis-Vela	Poor	No detail
82	Puppis-Vela	Good	Spectra smoothly widened; some detail
83	Puppis-Vela	Poor	Spectra streaked; no detail
84	Puppis-Vela	Fair	Spectra streaked; apparent detail in γ Vel, ζ Puppis
85	Puppis-Vela	Fair	Spectra streaked; no detail
S66-63586	Wasted frame	--	Lightstruck

[a]All frames are marred by static marks or light leaks.

TABLE 11-I.- S013 INFLIGHT EXPOSURES WITH GRATING ATTACHED - Concluded

Frame[a]	Field	Vehicle attitude hold	Remarks
69	Canis Major	Good	Spectra smoothly widened; lines around 2400 A; lines in α Lep, ν Ori
S66-63570	Canis Major	Good	Sirius ultraviolet superposed on sunlit GATV

[a]All frames are marred by static marks or light leaks.

TABLE 11-I.- S013 INFLIGHT EXPOSURES WITH GRATING ATTACHED

Frame[a]	Field	Vehicle attitude hold	Remarks
S66-63557	Wasted frame	--	Lightstruck
58	Cassiopeia	Fair	Images triple; spectra streaked; no lines
59	Cassiopeia	Excellent	Spectra smoothly widened; no lines
60	Cassiopeia	Good	Spectra unevenly widened; lines in β Cassiopeiae, δ Cassiopeiae
61	Cassiopeia	Fair	Spectra unwidened, slightly trailed in wavelength direction; lines β Cassiopeiae, δ Cassiopeiae ζ Cassiopeiae
62	Cassiopeia	Good	Spectra rather narrow; lines in β Cassiopeiae, ε Cassiopeiae, ζ Cassiopeiae, λ Cassiopeiae
63	Cassiopeia	Good	Spectra rather narrow; lines in β Cassiopeiae, ε Cassiopeiae, ζ Cassiopeiae, λ Cassiopeiae
64	Canis Major	Excellent	Spectrum rather wide; many fine lines below 3000 Å
65	Canis Major	Fair	Spectrum rather narrow; Balmer lines in Sirius
66	Canis Major	Fair	Spectra unevenly widened; lines of Mg II, Fe II
67	Canis Major	Good	Spectra smoothly widened; many lines below 3000 Å
68	Canis Major	Excellent	Spectra smoothly widened; lines below 3000 Å

[a]All frames are marred by static marks or light leaks.

The grating spectra from this mission were of high quality. The stronger grating spectra are listed in table 11-II. In both fields, the presence of very many weak spectra is suspected on the long exposures. The spectra listed in the table are for the most part well exposed to yield measures of energy curves.

The failure to obtain grating spectra of γ Velorum and ζ Puppis star fields is unfortunate, since they were well placed for observation during the mission.

focus has been eliminated, indicating that the increased tension of the film-retaining spring used in the Gemini XII camera prevented warping of the film. The worst image diameter on the Gemini XII photographs is about 100 microns whereas the worst image diameter on the Gemini XI photographs is about 200 microns. The superb resolution in the spectrum of Sirius (as shown in fig. 11-1) is a good illustration of the improved image quality with the grating.

The best prism spectra do not appear as sharp as those of the Gemini XI flight. The reason for this discrepancy between the performance with the grating and that with the prism is not immediately apparent.

All frames show effects of static electricity. The carbon dioxide cartridge was less effective in eliminating this effect than it had been during previous Gemini missions. Possibly the difference is due to gas loss by a greater-than-expected venting rate through the film back. The static marks do not interfere with the study of lines and bands in the spectra but they will reduce the accuracy of photometric measures on the film.

A frame-by-frame log of the flight film is given in table 11-I. The 2-minute exposures on Cassiopeia (fig. 11-2) gave essentially point images for the stars indicating that spacecraft stabilization remained accurate to $\pm 0.05^\circ$. The star γ Cassiopeiae is of particular interest for having ejected a shell which subsequently dissipated. The spectrum in recent years has been that of an ordinary, rapidly rotating B star, but within the past year indications of hydrogen emission lines have appeared. These observations provide negative evidence for the return of a shell spectrum at this time.

The spectra of δ Cassiopeiae and β Cassiopeiae show resolved absorption lines in the ultraviolet region while the middle-ultraviolet spectrum of ε Cassiopeiae is devoid of strong features.

The middle-ultraviolet spectrum of Sirius (fig. 11-1) has a resolution of about 5 Å and shows six or more fine absorption lines. The 2795.5- and 2802.7-Å lines are resolved for the first time in a photograph of a stellar spectrum. Preliminary measures of the wavelengths of the remaining lines indicate they are probably due to Fe II. Lines are also seen in the spectra of α Lepous and, possibly, ν Orionis.

Prism spectra of hundreds of stars were recorded in the region of Deneb and Velorum. On most frames, little detail is apparent in the spectra. The helium discontinuity is apparently present in the spectra of HR 7767 and 40 Cygni; metal multiplets are apparently present in the spectrum of γ Cygni; and some detail is suspected in the spectra of HR 3817, γ Velorum, and ζ Puppis.

DISTRIBUTION LIST

Number of copies	Addressees
2	Dr. Mac C. Adams, R Associate Administrator for Advanced Research and Technology National Aeronautics and Space Administration Washington, D.C. 20546
2	Dr. Luis W. Alvarez Lawrence Radiation Laboratory University of California Berkeley, California 94720
1	Dr. H. Anderson Rice University Houston, Texas 77001
30	William O. Armstrong, MB National Aeronautics and Space Administration Washington, D.C. 20546
2	Dr. Stanley Bennett Dean, Medical School University of Chicago Chicago, Illinois 60637
2	Dr. Lloyd Berkner President Graduate Research Center of the Southwest P. O. Box 30365 Dallas, Texas 75230
2	Mr. Edward Bialecki, HB34 North American Aviation, Inc. 12214 Lakewood Boulevard Downey, California 90241
2	Dr. Jacques Blamont Centre National D'Etudes Spatiales Paris 91 Verrieres le Buisson Paris, France

DISTRIBUTION LIST - Continued

Number of copies	Addressees
2	Brigadier General Jack Bollerud, MM Acting Director of Space Medicine Office of Manned Space Flight National Aeronautics and Space Administration Washington, D.C. 20546
2	Dr. Allan H. Brown Department of Biology University of Pennsylvania Philadelphia, Pennsylvania 19104
2	Dr. Loren D. Carlson Chairman, Department of Physiology and Biophysics University of Kentucky Medical Center Lexington, Kentucky 40506
2	Dr. Francis Clauser University of California Santa Cruz, California 95060
2	Mr. Charles T. D'Aiutolo, RV-1 Office of Advanced Research and Technology National Aeronautics and Space Administration Washington, D.C. 20546
2	Mr. G. A Derbyshire National Academy of Sciences 2101 Consitution Avenue Washington, D.C. 20418
2	Dr. Lee A DuBridge President, California Institute of Technology Pasadena, California 91109
2	Mr. Lawrence Dunkelman Goddard Space Flight Center National Aeronautics and Space Administration Greenbelt, Maryland 20771

DISTRIBUTION LIST - Continued

Number of copies	Addressees
2	Dr. Alfred J. Eggers, R Deputy Associate Administrator Office of Advanced Research and Technology National Aeronautics and Space Administration Washington, D.C. 20546
2	Major General Harry L. Evans USAF SAF-SL, MOL Program Office The Pentagon, Room 5D227 Washington, D.C. 20330
2	General James Ferguson SCG, Hq AFSC Andrews Air Force Base, Maryland 20331
2	Dr. John W. Findlay National Radio Astronomy Observatory P. O. Box 2 Green Bank, West Virginia 24944
2	Mr. Daniel J. Fink OSD DDR&E The Pentagon Washington, D.C. 20301
10	Mr. Willis B. Foster, SM Director of Manned Flight Experiments Office of Space Science and Applications National Aeronautics and Space Administration Washington, D. C. 20546
2	Dr. John French Brain Research Institute University of California Medical School Los Angelles, California 90024
2	Dr. Herbert Friedman Atmosphere and Astrophysics Division Code 7100 U.S. Naval Research Laboratory Washington, D.C. 20390

DISTRIBUTION LIST - Continued

Number of copies	Addressees
10	Dr. Jocelyn R. Gill, SM National Aeronautics and Space Administration Washington, D.C. 20546
1	Dr. T. Gualtierotti Ames Research Center National Aeronautics and Space Administration Moffett Field, California 94035
2	Dr. Leo Goldberg Harvard College Observatory Department of Astronomy Cambridge, Massachusetts 02138
2	Mr. George Trimble, MT Advanced Manned Missions Program Office of Manned Space Flight National Aeronautics and Space Administration Washington, D.C. 20546
10	Dr. Curtis L. Hemenway Dudley Observatory 140 South Lake Avenue Albany, New York 12200
2	Dr. Karl G. Henize Dearborn Observatory Northwestern University Evanston, Illinois 60201
1	Robert G. Hertz Department 650 Building 523 Lockheed Missiles and Space Company P. O. Box 504 Sunnyvale, California 94088

DISTRIBUTION LIST - Continued

Number of copies	Addressees
2	Dr. Harry H. Hess Department of Geology Princeton University Princeton, New Jersey 08540
1	Dr. Francis Johnson Graduate Research Center of the Southwest P. O. Box 30365 Dallas, Texas 75221
2	Dr. William W. Kellogg Associate Director National Center for Atmospheric Research Boulder, Colorado 80301
2	Mr. John E. Kirk OSD DDR&E Room 3E153, The Pentagon Washington, D.C. 20301
10	Mr. Martin J. Koomen U.S. Naval Research Laboratory Code 7141-K Washington, D.C. 20390
2	Dr. T. William Lambe Massachusetts Institute of Technology Cambridge, Massachusetts 02139
2	Dr. John H. Lawrence Donner Laboratory University of California Berkeley, California 94720
10	Mr. Douglas R. Lord, MTS National Aeronautics and Space Administration Washington, D.C. 20546

DISTRIBUTION LIST - Continued

Number of copies	Addressees
2	Dr. Paul Lowman Theoretical Division, Code MSSD Goddard Space Flight Center National Aeronautics and Space Administration Greenbelt, Maryland 20771
2	Dr. Gordon J. F. MacDonald University of California Los Angeles, California 90024
5	Mr. Charles L. Mathews, ML Saturn/Apollo Applications Directorate National Aeronautics and Space Administration Washington, D.C. 20546
2	Dr. Nicholas U. Mayall Director, Kitt Peak National Observatory 950 North Cherry Avenue Tucson, Arizona 85717
2	Dr. David Medved Electro-Optical Systems, Inc. 300 North Halstead Pasadena, California 91107
	Elliot C. Morris U.S. Geological Center Flagstaff, Arizona 86001
2	Dr. George E. Mueller, M Associate Administrator for Manned Space Flight National Aeronautics and Space Administration Washington, D.C. 20546
2	Mr. Kenneth M. Nagler Chief, Operations Support Division Grammax Building Room 1415 U.S. Weather Bureau Washington, D.C. 20689

DISTRIBUTION LIST - Continued

Number of copies	Addressees
2	Dr. John E. Naugle, SS Deputy Associate Administrator (Sciences) Office of Space Science and Applications National Aeronautics and Space Administration Washington, D.C. 20546
2	Dr. William Neuman University of Rochester Rochester, New York 14627
2	Dr. Homer E. Newell, S Associate Administrator for Space Science and Applications National Aeronautics and Space Administration Washington, D.C. 20546
2	Dr. Edward P. Ney School of Physics and Astronomy Institute of Minnesota Minneapolis, Minnesota 55455
10	Mr. David Novick, RNV National Aeronautics and Space Administration Washington, D.C. 20546
2	Dr. Hugh Odishaw National Academy of Sciences 2101 Constitution Avenue Washington, D.C. 20418
2	Mr. J. P. T. Pearman National Academy of Sciences 2101 Constitution Avenue Washington, D.C. 20418
2	Dr. Max Peterson Department of Aeronautics and Astronautics Instrumentation Laboratory 68 Albany Street Cambridge, Massachusetts 02139

DISTRIBUTION LIST - Continued

Number of copies	Addressees
2	Professor Courtland D. Perkins Chairman, Department of Aerospace and Mechanical Sciences Princeton University Princeton, New Jersey 08540
2	Dr. Martin A. Pomerantz Director, Bartol Research Foundation Swarthmore, Pennsylvania 19081
2	Dr. Richard W. Porter Space Science Board National Academy of Sciences 2101 Constitution Avenue Washington, D.C. 20418
10	Dr. Leonard Reiffel, MA National Aeronautics and Space Administration Washington, D.C. 20546
2	Dr. Bruno B. Rossi Laboratory for Nuclear Science Massachusetts Institute of Technology Cambridge, Massachusetts 02139
2	Miss Rita C. Sagalyn Hqs Air Force Cambridge Research Laboratories Laurence G. Hanscom Field Bedford, Massachusetts 07130
2	Dr. F. Saiedy Meteorological Office Damascus, Syria
2	Professor Leonard I. Schiff Executive Head, Department of Physics Stanford University Stanford, California 94305

DISTRIBUTION LIST - Continued

Number of copies	Addressees
2	Mr. Lyle C. Schroeder Instrument Research Division Langley Research Center National Aeronautics and Space Administration Langley Station Hampton, Virginia 23365
2	Mr. M. Shapiro Superintendent Nucleonics Division (Code 7200) U.S. Naval Research Laboratory Washington, D.C. 20390
2	Dr. William G. Shepherd Vice President Academic Department 200 Morrill Hall University of Minnesota Minneapolis, Minnesota 55455
2	Dr. H. G. Shepler National Academy of Sciences 2101 Constitution Avenue Washington, D.C. 20418
2	Dr. William Shockley Stanford University Palo Alto, California 94305
3	Mr. Thomas Shopple Naval Air Development Center Johnsville-Warmister, Pennsylvania 18974
2	Dr. John A. Simpson Laboratory of Astrophysics and Space Research Enrico Fermi Institute for Nuclear Studies The University of Chicago Chicago, Illinois 60637

DISTRIBUTION LIST - Continued

Number of copies	Addressees
1	Mr. Stanley Soules U.S. Department of Commerce U.S. Weather Bureau Suitland, Maryland 20689
2	Donald Smith, 210-9 Ames Research Center Moffett Field, California 94035
2	Dr. William H. Sweet Massachusetts General Hospital Boston, Massachusetts 02114
2	Dr. Charles H. Townes Provost, Massachusetts Institute of Technology Cambridge, Massachusetts 02139
2	Dr. James A. Van Allen Head, Department of Physics and Astronomy University of Iowa Iowa City, Iowa 52440
10	Dr. Sherman P. Vinograd, MM National Aeronautics and Space Administration Washington, D.C. 20546
2	Dr. John R. Whinnery Department of Electrical Engineering Cory Hall University of California Berkley, California 94720
2	Dr. George P. Woolard Director, Hawaii Institute of Geophysics University of Hawaii Honolulu, Hawaii 96822

DISTRIBUTION LIST - Continued

Number of copies	Addressees
2	Dr. Richard S. Young Bio-Satelite Division NASA Ames Research Center Moffett Field, California 94035
3	Mr. Samuel H. Hubbard, MGO National Aeronautics and Space Administration Washington, D.C. 20546
MANNED SPACECRAFT CENTER:	
2	AA/Dr. Robert R. Gilruth
1	BL/J. R. Brinkmann
1	BL/Richard Underwood
3	BM5/E. F. Meade
10	BM6/MSC Library
2	CB2/John Peterson
10	CB/Astronaut Library
2	CF/Helmut Kuehnel
2	EA/Warren Gillespie
1	EC7/W. J. Young
1	EC/R. S. Johnston
1	EG26/C. Manry
2	FA3/R. G. Rose
1	FC/J. Bates

DISTRIBUTION LIST - Continued

Number of copies	Addressees
3	AP/Paul Haney
1	AP3/Matt Story
1	TA/Wilmot N. Hess
1	TA/Robert O. Piland
1	TA/Paul R. Penrod
3	TE/Bruce Jackson
3	TF/N. G. Foster
1	TF3/B. R. Hand
1	TG/J. Modisette
1	TG/P. B. Burbank
1	TG4/J. Lintott
1	TG4/J. Shafer
1	TG4/R. Stokes
1	TG5/D. Womack
1	TG5/J. Lill
1	TG53/R. Lindsey
1	TG53/J. Marback
1	TH4/R. L. Jones
10	ZR1/AFSC Field Office

DISTRIBUTION LIST - Concluded

Number of copies	Addressees
1	FC/M. Lowe
1	FC/C. Kouitz
2	GM/W. Nesbitt
2	KA/R. F. Thompson
10	RL/W. E. Davidson
Balance	TF2/James Campbell